REPUBLIC OF TURKEY
ACIBADEM MEHMET ALİ AYDINLAR UNIVERSITY
INSTITUTE OF SCIENCE

WIRELESS fNIRS WITH SPATIALLY RESOLVED SHORT SEPARATION APPROACH FOR IMPROVED SNR

SERHAT ILGAZ YÖNER

MASTER THESIS

DEPARTMENT OF MEDICAL ENGINEERING

SUPERVISOR
Prof. Dr. Ata Akın

SECOND SUPERVISOR
Assist. Prof. Dr. Gökhan Ertaş

İSTANBUL – 2018

BEYAN

Bu tez çalışmasının kendi çalışmam olduğunu, tezin planlanmasından yazımına kadar bütün aşamalarda etik dışı davranışımın olmadığını, bu tezdeki bütün bilgileri akademik ve etik kurallar içinde elde ettiğimi, bu tez çalışmasıyla elde edilmeyen bütün bilgi ve yorumlara kaynak gösterdiğimi ve bu kaynakları da kaynaklar listesine aldığımı, yine bu tezin çalışılması ve yazımı sırasında patent ve telif haklarını ihlal edici bir davranışımın olmadığı beyan ederim.

5/6/2018

Serhat Ilgaz Yöner

TABLE OF CONTENTS

LIST OF FIGURES

LIST OF TABLES

LIST OF SYMBOLS

cm	Centimeter
dB	Decibel
GHz	Gigahertz
gr	Gram
H_2O	Water
Hb	De-oxyhemoglobin
HbO_2	Oxyhemoglobin
kg	Kilogram
mA	Milliamps
MHz	Megahertz
mm	Millimeter
nm	Nanometer
pH	Potential of Hydrogen
TotHb	Total Hemoglobin
V	Volts
Ω	Ohm

LIST OF ABBREVIATIONS

ADC	Analog-to-Digital Converter
BCI	Brain – Computer Interface
BOLD	Blood Oxygen Level Dependent
CBF	Cerebral Blood Flow
CBV	Cerebral Blood Volume
CPS	Complex Partial Seizures
EEG	Electroencephalography
exe	Executable
fMRI	Functional Magnetic Resonance Imaging
fNIRS	Functional Near Infrared Spectroscopy
GUI	Graphical User Interface
I^2C	Inter-Integrated Circuit
IC	Integrated Circuit
LED	Light Emitting Diode
MCU	Microcontroller Unit
MDT	Mirror Drawing Task

MRI	Magnetic Resonance Imaging
NIR	Near Infrared
OI	Optical Imaging
OP-AMP	Operational-Amplifier
PCB	Printed Circuit Board
PFC	Prefrontal Cortex
RC	Ruler-Catching
RCPS	Rapidly Secondarily Complex Partial Seizures
RNG	Random Number Generation
rTMS	Repetitive Transcranial Magnetic Stimulation
SCR	Skin Conductance Response
SFT	Sequential Finger-to-Thumb
SNR	Signal-to-Noise Ratio
SPECT	Single-Photon Emission Computed Tomography
TBI	Traumatic Brain Injury
VFT	Verbal Fluency Task

ACKNOWLEDGEMENT

I would like to thank to my thesis supervisors Dr. Akın and Dr. Ertaş for their offer of support and guidance throughout this project. I also would like to thank to Dr. Ademoğlu and Dr. Erdoğan for their time and remark. This project was financially aided by Acıbadem University Scientific Research Projects Commission.

Lastly I would like to quote someone who triggered my ambition on understanding the laws of nature;

"Nothing is too wonderful to be true, if it be consistent with the laws of nature."
M. Faraday

ABSTRACT

In this project, “Vega Vision” a wearable wireless functional near infrared spectroscopy (fNIRS) device was developed with a unique probe geometry. A spatially resolved high signal-to-noise ratio (SNR) device was designed by utilization of far/short detector probe (3/1.5cm separation) geometry and oversampling technique. Measurements were taken from non-smoking and smoking individuals during a head-tilt maneuver protocol. Total hemoglobin (TotHb) changes from resting to head down and from head down to up showed statistically different values: deviation of delta TotHb down between non-smokers and smokers was 33.2% (P=0.040) for the right half of brain and 35.4% (P=0.008) for the 4^{th} channel from left end side, meanwhile deviation of delta TotHb up between non-smokers and smokers was 30.0% (P=0.040) for the right half of brain and 30.8% (P=0.015) for the 4^{th} channel from left end side. In overall, the device designed proved to be a safe, affordable and easy-to-use fNIRS device suitable for clinical deployment.

ÖZET

Bu projede, özgün prob geometrisi ile giyilebilir kablosuz bir fNIRS cihazı olan "Vega Vision" geliştirilmiştir. Cihaz uzamsal olarak çözümlenmiş yüksek sinyal-gürültü oranına sahip bir şekilde, uzak/yakın detektör prob (3/1.5cm aralık) geometrisi ve aşırı örnekleme tekniği kullanılarak tasarlanmıştır. Sigara içen ve sigara içmeyen kişilerden, kafa eğme manevrası protokolüne uygun şekilde ölçümler alınmıştır. Dik duruştan öne eğik pozisyona geçişte ve öne eğik pozisyondan dik duruşa geri geçişte toplam hemoglobin değişimleri iki grup arasında istatistiksel olarak: sigara içmeyen ve sigara içenler arasında delta TotHb down'daki sapma beynin sağ yarım küresi için 33.2% (P=0.040), soldan 4. kanal için 35.4% (P=0.008) olarak hesaplanmıştır. Sigara içmeyen ve sigara içenler arasında delta TotHb up'daki sapma beynin sağ yarım küresi için 30% (P=0.040), soldan 4. kanal için 30.8% (P=0.015) olarak hesaplanmıştır. Genel anlamıyla, tasarlanan cihaz güvenilirliği, düşük maliyeti ve kolay kullanımı ile klinik kullanıma hazır bir fNIRS cihazı olduğunu kanıtlamıştır.

INTRODUCTION

In the 21th century, most notable advancements of science comprise biomedical engineering, which promoted a deeper and more detailed understanding of human form. In biomedical engineering, biomedical instrumentation holds major importance. A variety of biomedical instruments are being utilized by healthcare professionals from all around the world towards; monitoring, diagnosing and treating patients especially with brain diseases. As a non-invasive imaging technique, optical imaging (OI) plays a great role in all three steps. However, one of the key information that has to be known is optical characteristics of target tissues/molecules, otherwise raw measurements won't mean anything without proper data conversions. Most basic and fundamental parts of a typical OI device consist of light emitters and light detectors. Regarding feasibility, OI devices most commonly utilize one of two operation modes: reflective mode or transmissive mode. In this field, fNIRS technology emerged with the aim of monitoring and assessing neuronal activities of human brain.

First studies of fNIRS were conducted by M. Ferrari in 1985. In the following times, fNIRS studies kept expanding with contributions of R. Barbour, B. Chance, A. Villringer, M. Cope, DT. Delpy, E. Gratton and others. As a low cost non-invasive OI modality, fNIRS technology monitors neuronal activities of the human brain indirectly, from measurements of oxyhemoglobin (HbO_2) and de-oxyhemoglobin (Hb) molecules (hemodynamic changes). Generally, device consists of multiple wavelength light emitting diodes (LEDs) (around 730nm and 850nm) and photodiodes with a high response at a large spectrum (between 600nm and 1050nm). Some of the light emitted by an LED at a specific wavelength is absorbed by HbO_2 while others are reflected by Hb, which are all found in the arterial red blood cells of living tissues. Since technology utilizes reflective mode, reflected portion of the light is sensed by photodiodes and then transformed into electrical signals. Collected raw data are then transformed into hemoglobin values with the implementation of Beer-Lambert Law. Although fNIRS technology is a promising one, some problems are encountered in practical applications. Since near infrared light waves are emitted by

LEDs right at the surface of forehead skin, a portion of light waves travel through layers of skin and skull, prior to being absorbed by the capillary arteries of the cortex. The unabsorbed portion of the light waves is reflected from the same layers and sensed by photodiodes positioned on the head probe. Hemodynamic changes that may occur on these layers are mixed with changes in the cortex. This phenomenon causes the accuracy, precision and specificity of measurements to drop, which affects overall measurement quality.

In this thesis, a wearable wireless fNIRS device, “Vega Vision” has been developed to provide high measurement accuracy and precision. All the steps of design and development processes have been explained in details complemented with technical drawings and schematics. Most saliently, an untraditional far/short detector probe geometry suitable for data subtractions and oversampling technique have been utilized to achieve high signal-to-noise ratio. Moreover, a unique calibration algorithm has been developed with future studies in mind (i.e. phantom development). To further prove the reliability of the device, excessive performance tests have been done. An experimental protocol is structured and plenty of sample measurements are taken from non-smoking and smoking individuals using the protocol. After the conversion of raw data into hemoglobin values, mathematical analyses of measured data are carried out. All the major questions that may arise from results analysis are answered and recommendations for future works are made while possible sources of measurement errors are acknowledged in details.

1. BACKGROUND

1.1. Optical Imaging

OI is a non-invasive imaging technique, which uses light waves towards taking measurements from target tissues/molecules. In this manner, optical characteristics of target biological tissues and molecules are highly important. Optical microscopy, spectroscopy, endoscopy, scanning laser ophthalmoscopy and optical coherence tomography are a number of examples for OI techniques. An optical sensor and sometimes a light emitting source are two of the major parts of an OI system. Regarding the target tissue/molecule, a specific wavelength of external light source may be required to excite endogenous or exogenous chromophores within a volume of interest in the measurement environment. This requirement can be met by using a light emitting source. Basically, all kinds molecules that are found in biologic tissues with the ability to interact with light waves are called “chromophores”. As mentioned above, optical characteristics of target tissues are tremendously important in OI, as a result of light – tissue interactions a number of optical phenomena may take place such as; absorption, scattering, reflection or refraction of light waves (1-5). To further expand;

1. Absorption: The light energy penetrates the incident object, followed by the conversion of light waves into heat energy.
2. Scattering: Irregularities that may be found on the surface of the incident object results in bouncing of light waves in many different directions.
3. Reflection: Smooth and shiny surfaces habitually result in bouncing of light waves at the same angle they hit.
4. Refraction: When light waves travel from a medium to another they tend to bend.

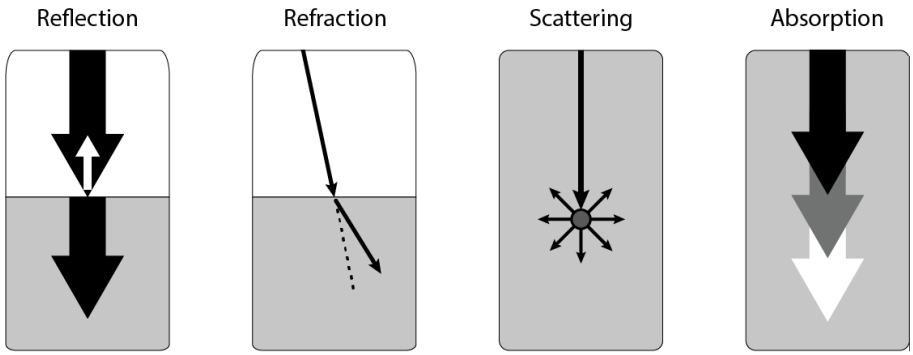

Figure 1: Visual explanation of optical phenomena (6).

Drawings of these optical phenomena are given above, in figure 1. These optical phenomena form foundations of OI technique known as spectroscopy. The most common chromophores are hemoglobin, water, and lipids. For a better understanding, OI excitation can be thought of as a group of photons hitting a target tissue/molecule which then a portion of it is scattered all around that tissue/molecule while others are absorbed by that tissue/molecule (7).

1.1.1. Operating Domains of Optical Imaging

There are three major implementation methods of OI; time domain, frequency domain and continuous wave. Time domain systems use pulses to excite tissues. Width of these pulses can be set in a wide range from picoseconds to milliseconds regarding the needs of application and physiology. If the tissue-specific absorption coefficients are known from previous analysis, it is possible to calculate the amount of target molecules. Detection of these pulses can be achieved in various ways. Photons can be counted one by one with their time delay for the highest accuracy, or a simple photodetector can be used to sense light waves that can be converted into corresponding level of electrical signals, later on. Time domain systems are known to provide high spatial and depth resolution with high accuracy. An evident downside of time domain systems is their slow response to changes in the signal.

Frequency domain systems use intensity-modulated signals to excite chromophores. Unlike time domain systems, photons are not counted. Instead, demodulations and phase shifts are measured to calculate absorption and scattering coefficients. Signals sent to excite chromophores can be thought as continuous electromagnetic waves. At the moment of impact with chromophores; intensity, frequency and phase properties of these electromagnetic waves are altered. These alterations are detected with the use of proper hardware, which is called "demodulation". Modulation frequencies as low as 100MHz and as high as 1GHz are widely used. Although there is a bandwidth for modulation frequencies, a selected fixed frequency is used to excite target tissues/molecules. Then, excitation frequencies are stepped up one level and the whole measurement process is repeated. The measurement process is repeated again and again until the last exciting frequency is reached. Other than the multiple single-frequency signal usage, this technique is highly similar with magnetic resonance spectroscopy that utilizes a broadband radiofrequency. Compared to systems utilizing other domains, frequency domain systems are known to provide high spatial and depth resolution in a less expensive and much faster way, but with low accuracy.

Continuous wave systems use light sources in the near infrared (NIR) region of the spectrum to emit light waves, non-stop. Then the average attenuation coefficient of the transmitted light is calculated as a combination of absorption and scattering coefficients. Continuous wave systems are a lot cheaper and faster than time domain and frequency domain systems, making it convenient to use plenty of sources and detectors (8).

1.1.2. Techniques in Optical Imaging

Although diffuse optical spectroscopy does not render images, it is the most established OI technique there is (9-15). Primary principle of this technique relies on hemoglobin and blood oxygen saturation measurements from the target tissue/molecule (see figure 2). A well calibrated diffuse optical spectroscopy device is capable of providing highly accurate measurements.

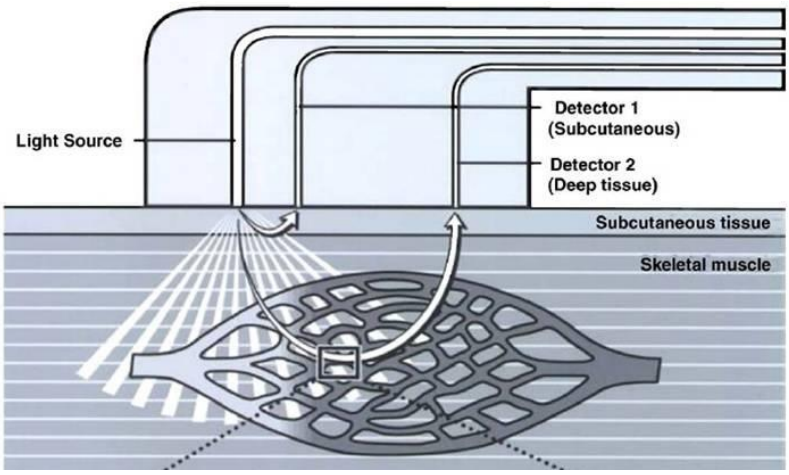

Figure 2: Basic engineering design behind diffuse optical spectroscopy (16).

Another technique which is based on diffuse optical spectroscopy is the diffuse OI. Diffuse OI is highly complex when compared to diffuse optical spectroscopy, to be able to handle image reconstruction and provide 2D or 3D images; it needs multiple sources – detector pairs. The technique is repeated for all the voxels of the imaging plane and provides a colorimetric map for visualization and analysis purposes (17).

Fluorescence emissions of endogenous fluorophores and exogenous contrast agents are used in fluorescence optical tomography. Special chromophores in human body are known to emit light just like fluorine, which gave them the name "fluorophore". Charge coupled cameras are used to detect excitation lights which are then used for normalization. Due to its SNR and operational simplicity, continuous-waves are widely used in fluorescence bio distribution measurements (18).

Perturbations can be applied in photoacoustic imaging to trigger and detect responses from target tissues. In this way, system is thought as a black box model and the primary aim is to understand the biochemical composition of this model. The key point of this technique is to exploit potential differential behavior of compounds that are sensitive to perturbation. Visible and NIR lights are used in these systems for both perturbation and detection. High spatial resolution from deep tissues is an upside of photoacoustic imaging over fluorescence imaging (2,19-21). Vibrational status of target chromophores is enhanced by exciting photons, resulting in increased local temperature. This phenomenon is similar to another one in magnetic resonance

imaging (MRI). In MRI during spin-lattice relaxation, radiofrequency coils absorb the energy which is then transferred to the lattice in the form of heat. Thermal expansion is triggered by sudden temperature increase which is approximately between 0.0001-0.1000 celcius, corresponding to a pressure of 0.01-0.10 kilopascal. Array of ultrasonic transducers are used, capable of detecting even tiny changes in magnitude. Afterwards, acoustic waves with different intensities are formed from differential heating. Then, different absorption properties of target tissues are used in determining the image contrast. Ultrasonic waves make it possible to explore deep tissues due to its higher penetrance when compared to visible light or NIR lights. Nevertheless, the main principle of light propagation in tissues for excitation of chromophores is a limiting factor when it comes to deep tissue imaging. A spatial resolution of 0.15mm at a 3cm depth is possible with modern devices (22). Image reconstruction algorithms are run in photoacoustic tomography. The system consists of a pulsed laser and sensitive microphones or piezo-transducers. It is appropriate to use lasers with wavelengths of somewhere between 500-600nm in hemoglobin rich tissue measurements. Exogenous contrast agents such as cyanine dyes can be used to for absorption in NIR range (23-25). Table 1 lists the main characteristics of the OI techniques inspired.

Table 1: Main characteristics of major optical imaging techniques (6).

Technique	**Output and Measured Parameters**	**Endogenous Contrast**	**Resolution**	**Depth**
Diffuse optical spectroscopy	Absorption coefficient Scattering coefficient	Total hemoglobin, lipid, water, collagen, cell nuclei diameter	Not Available	Not Available
Diffuse optical imaging	Absorption coefficient Scattering coefficient	Total hemoglobin, lipid, water, collagen, cell nuclei diameter	10mm	Up to 10cm
Photoacoustic imaging	Ultrasound Intensity	Hemoglobin, melanin, water	0.15mm at 3cm of depth	Up to 3cm
Fluorescence optical tomography	NIR fluorescence intensity and lifetime	Amino acids, tissue environment such as pH and temperature	0.5mm	Up to 1cm

1.2. Functional Near Infrared Spectroscopy

fNIRS is a low cost, non-invasive medical imaging technique which takes advantage of optical properties of the tissues to detect hemodynamic changes as an outcome of neural activities in brain (26-27). The optical structure of fNIRS devices generally consist of multiple wavelength LEDs (around 730nm and 850nm) and photodetectors with a high response at a large spectrum (between 600nm and 1050nm). A portion of the emitted light at a specific wavelength by an LED is absorbed by HbO_2 while others are reflected by Hb, which are all found in the arterial red blood cells of living tissues. Reflected portion of the light is sensed by photodetectors and then transformed into electrical signals. Calculating the initial HbO_2 percentage from these electrical signals indirectly is possible (28). Although fNIRS technology is a promising one, some problems are encountered in practical applications.

1.2.1. Principles of fNIRS

Optical properties of tissues are influenced by their own functional states. Environmental stimuli cause the human brain to undergo a number of physiological changes such as blood levels and electrochemical activity. These changes affect optical properties of tissues that can be measured in means of functional optical imaging which uses near-infrared light waves (29). Two events that is associated with the brain activity can be assessed. During neural activity, the membrane potential is influenced by ionic fluxes across cell's membrane. When neurons are activated synchronously, magnetic and electrical fields all around the body are affected at a level that can be assessed using electroencephalography (EEG) or magnetoencephalography. Since the neuronal activity is fueled by glucose metabolism, there is a positive correlation between neuronal activity and glucose – oxygen consumption from the local capillary bed. Local arteriolar vasodilation is increased as a result of stimulation of brain caused by the reduction in local glucose and oxygen. In turn, the local arteriolar vasodilation increases local cerebral blood flow (CBF) and cerebral blood volume (CBV) (30). In about only several seconds,

glucose and oxygen are transported to the region with CBF, which is achieved via HbO_2 found in CBF. Local neuronal rate of oxygen utilization is exceeded by increased oxygen transportation to the region, which causes overabundance of cerebral blood oxygenation in the active region (31). As oxygen is withdrawn from the hemoglobin for use in the metabolization of glucose, Hb molecules found in the capillary bed is increased as a result of initial increase in neural activity.

Since HbO_2 and Hb both have their own characteristic optical properties, optical methods can be used to measure molecular concentrations in visible and near-infrared regions during neurovascular coupling phase (32-33). The most commonly used method of fNIRS is based on measuring the initial ratio of HbO_2 to Hb. Since hemoglobin absorption and H_2O absorption are small between 700-1000nm (see figure 3), most biological tissues can be considered as transparent in this region. Whereas, in this region at specific wavelengths, HbO_2 and Hb have high reflection coefficients which is why this region is called “the optical window” of human brain (29). A portion of photons scattered by LEDs follow banana- shaped paths back to the surface, which can be then measured with the help of photodetectors (see figure 4) (35). Since there is a linear correlation between the chromophore concentration and reflected light intensity, detected light waves can be quantified using a modified version of Beer-Lambert law (37-38). If two or more wavelengths are applied to target tissues, absorbance and reflectance differences can be used towards calculating relative concentrations of these chromophores.

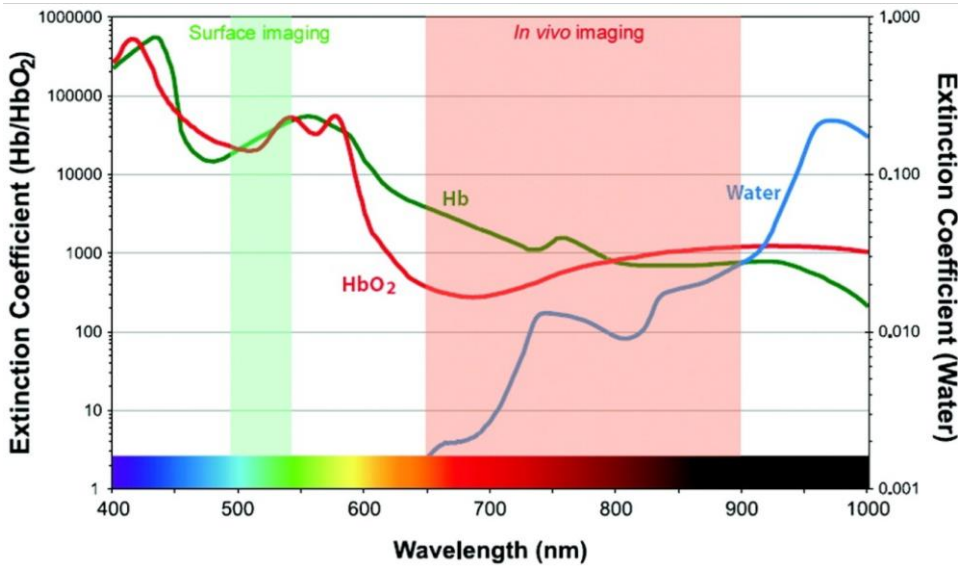

Figure 3: Absorption characteristics of Hb, HbO_2 and H_2O in the visible and near – infrared region of the electromagnetic spectrum (34).

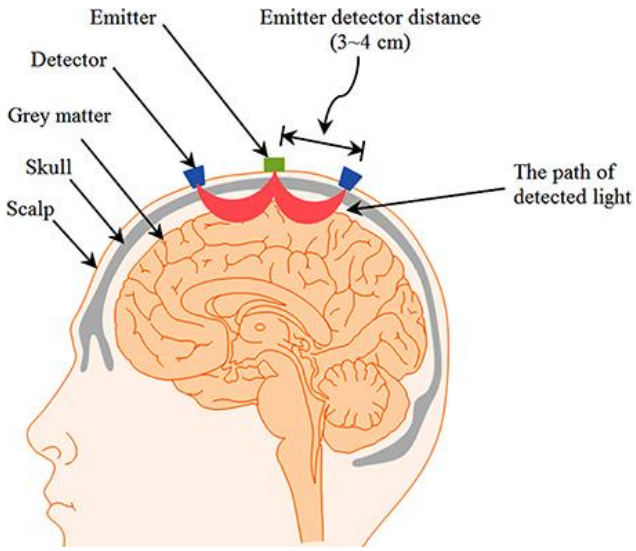

Figure 4: Emitter – detector pairs showing the banana-shaped paths of light in fNIRS (36).

The head probe part of a typical fNIRS device consists of LEDs (used for transmitting near-infrared signals) and photodetectors (used to collect data from tissues) (see figure 5).

Figure 5: Head probe part of a commercial fNIRS device (Artinis OctaMon) (39).

The ideal LED – photodetector distance is from 2 to 7cm. Reason for this wide range is a trade-off between covered region and signal strength. As the distance increases, detected light waves are mostly from deep tissues which follow longer paths resulting in weakening of signals. Conversely as the distance decreases, detected light waves are mostly from superficial tissues which follow shorter paths resulting in strong signals. A distance of 4cm results in high sensitivity of the system to hemodynamic changes within the top 2-3mm of the cortex (40-41). Previous studies show that inter-optode distances from 2 to 2.5cm are ideal for collecting data from grey matter (40-42). By this technique, brain activities such as motor activity, visual activation, auditory stimulation and cognitive task performance can be tracked (34).

There are several commercially available fNIRS devices with different operating domains, each one of them with different advantages and disadvantages on source, detector and other electronic parts. Since operating domains of OI systems are previously explained in detail, it is unnecessary to repeat this for fNIRS devices with different domains. Same advantages and disadvantages are valid for fNIRS devices with different operating domains.

fNIRS technology is a great way to measure cognitive workloads in complex tasks and to create a link between the operator and operational environments (43). fNIRS technology plays an important role in the study of neonatal cerebral hemodynamics (44). Imaging of the solid tumors of the breast with fNIRS technology is reported to offer exceptional advantages (45-46). During acute heart

failure treatment, fNIRS has success in detecting critically low oxygen levels resulting in improved cerebral oxygen saturation (47). fNIRS is an easy to customize technology due to its basic hardware needs. A great example for this; with Hematoscope (InfraScan Inc., PA, USA), it is possible for army medics to make critical analysis on the scene which makes this a low cost and high benefit situation. Immediate on-site applicability of the technology makes it indispensable especially in the field of neuropsychology. This adaptability of fNIRS technology to both clinical and research applications is probably the best aspect of it.

fNIRS still has a long way to go towards being the gold standard. Problems and limitations in spatial resolution, cranial reference points, signal attenuation by extracerebral matter, data comparisons between individuals, influence of skin color on signal strength and absolute baseline determination (for Hb and HbO_2) effect the reliability of fNIRS devices tremendously (48-49). Improved sensor designs and wireless systems are being developed towards increasing the comfort and flexibility of the devices for the subjects. On the order hand, fNIRS is still at its early stages when compared to functional magnetic resonance imaging, making it hard for the health community to embrace for use in practical clinical applications. Also, the incorrectly interpreted concept of “high tech” implies “low touch” by some individuals in the field of health community makes it hard for fNIRS to be accepted.

In overall, extensive researches should be carried out to improve the fNIRS technology to provide continuous measurements of neurobiological signals within variable environmental conditions (50). Systematic, informatics-driven modifications of clinical databases on standardized and normative data are heightened with the advent of a portable technology.

1.2.2. Comparison of fNIRS with fMRI

Functional magnetic resonance imaging (fMRI) is a well-established imaging technique for measuring brain activations by offering a safe non-invasive approach with better spatial resolution. This makes fMRI a great reference point on how fNIRS should be (51). fMRI enables acquisition of blood oxygen level dependent

(BOLD) signal. As mentioned early, increased CBF results in a decreased amount Hb concentration in the subject tissue. While the magnetic susceptibility of HbO_2 is only a little different than H_2O and other tissues, magnetic susceptibility of Hb is evidently different. High paramagnetic property of Hb makes it a natural contrast agent (52). fMRI measures neuronal activities indirectly just like fNIRS. It assesses concentration changes of Hb in subject tissues. Changes in blood flow, blood volume and local oxygen tension all effect the fMRI signals in such a complex way that, a simple correlation cannot be found.

Since typical fNIRS devices measure relative changes in concentrations of Hb, it carries similarities with the BOLD-based signal fMRI technique such as indirect measurement of neuronal activities. Just like fMRI, fNIRS is another non-invasive safe OI technique with a level of spatial resolution. Also, regarding its physics it is safe to use fNIRS on the same subject repeatedly. A level of repeated stimulation must be used in both OI techniques due to their SNR. Other than mentioned above, a number of major differences between fMRI and fNIRS technologies are present.

Towards neurophysiological assessment, it is difficult for fNIRS to surpass fMRI. One of two major reasons for this inadequacy is the superior spatial resolution obtained with fMRI when compared to fNIRS. The second reason is the imaging limitations of fNIRS against fMRI. fMRI has the capacity of imaging entire brain, on the other hand fNIRS is limited to a couple of cm in depth due to weak source signals with low tissue penetration capability. Although a large hemorrhage such as thalamus can be imaged with an fNIRS device, cognitive or emotional events induce much weaker signals that, it is not likely for an fNIRS device to detect these neuronal activities. In this context, fNIRS technology comes up short.

Since fMRI requires subject to lie inside a magnet, it may not be applicable to subjects with significant symptoms. Also some protocols of fMRI are unfeasible due to their resulting loud noise. Another disadvantage of fMRI is the high sensitivity of the system to subject movements during imaging resulting in artifacts (53-54). Because of huge magnetic fields created by the magnets of MRI device, any metal with magnetic susceptibility must be kept far away to ensure patient and operator

safety. Last but not least, fMRI technology is considerably expensive when compared to fNIRS technology.

On the other hand, fNIRS has a lot of unique potential when it comes to measuring the hemodynamic changes in cortex. fNIRS calculates neuronal activities indirectly, through HbO_2 and Hb measurements. Technique itself allows subjects to sit, stand, walk or even engage in mild athletic activities during the measurement process, making it unchallengeable by fMRI to this end (55). The portable and spacious design of fNIRS systems make it preferable by children and some adults with claustrophobic emotions. Also, fNIRS devices run quietly thereby comfortably in the eyes of subjects. fNIRS is already in use with the combination of EEG (see figure 6) and/or transcranial magnetic stimulation systems most notably.

Figure 6: A model of Artinis brand fNIRS device with combination of EEG (56).

Emerging technologies must be validated by comparing with other well established technologies, before they can be used safely in clinics. In this manner, fNIRS must be compared with other validated neuroimaging technologies such as fMRI. To this end, device specifications such as sensitivity, accuracy and reliability must be tested with various experiments (34, 49, 57). There are already some studies done towards this end. A study done showed that there are high temporal correlations between BOLD signals in fMRI and Hb concentrations in fNIRS on a motor task (58). In another study, fNIRS and BOLD fMRI data were acquired simultaneously while a simple motor task was being performed (28). This helped characterize the amplitude correspondences between fNIRS and fMRI by comparing delta signals of fMRI to changes in Hb, HbO_2 and TotHb concentrations of fNIRS. Strong correlations were found between fMRI and fNIRS measurements after systematic

errors were counted out of the equation. These findings were valid even with skin effects included. Also, cross-validative comparisons were made on patient from all ages with a hemiparetic stroke, cerebral ischemia (59-61). Studies showed that when it comes to motor tasks, fNIRS provided direct information about neuronal activity-associated changes in cerebral parameters while fMRI didn't (62). Another study suggests great correspondence between BOLD response and Hb under an event-related finger-tapping task experiment during fMRI and fNIRS measurements (63). This event-related finger-tapping task evoked activities in both primary motor and sensory cortices, also a significant correlation was seen across all participants between Delta signals and Hb responses. Similar results were obtained in another study which used a simple visual stimulation task (64). As a result, hemodynamic activity was invoked in the visual cortex bilaterally and a high correlation between changes in BOLD signal and Hb were obtained. A lower correlation between changes in BOLD signal and HbO_2 were obtained, same correlation for TotHb was valid. Also, repeated measurements within-subjects under simple visual stimuli showed good reliability and repeatability with high precision (65). However, result comparisons between participants were less reliable. In another study, fNIRS and fMRI measurements were taken during a variety of tasks. Under visual stimulation and a response inhibition task, results from both modalities showed a significant concordance, demonstrating the ability of fNIRS to distinguish between motor and premotor responses of a go/no-go task (57). Briefly, biological signals detected by both modalities indicated high consistency. Also, a general concordance was found between fNIRS and fMRI measurements under a breath-holding experiment, however a considerable difference was seen between BOLD and fNIRS signal levels (66). Another study imparted concordance between fNIRS and fMRI again, but this time it was a face-recognition task (67-69).

Ecological validity of fNIRS technology has been also examined. Both fNIRS and fMRI were used while subjects took on an apple-peeling task. Prior results were found to be valid for this task as well, indicating a congruity between the two modalities for brain areas providing motoric, visual and cognitive aspects of the task (70). After the actual apple-peeling task, subjects took on a mock apple-peeling task. This time, there were inconsistent results in the spatial localization data. fMRI data

during mock apple-peeling did not show an activation observed by fNIRS in the prefrontal cortex during actual apple-peeling task. Although further researches are required, these findings indicate that as an emerging technology fNIRS is a promising one, especially during ecologically valid paradigms. Still, cross-validation should be carried out towards comparing fNIRS with other neuroimaging modalities.

In a study carried out at Drexel University and the University of Pennsylvania, scientists attempted to indirectly validate an fNIRS device of their own. A series of fNIRS and fMRI experiments using identical tasks on different sets of participants involved self-face recognition and social cognition processes. The results show that self-face recognition activates right frontal lobe while social cognition activates both right and medial frontal lobe. A statistical parametric fMRI activation map for 12 participants is shown in figure 7.

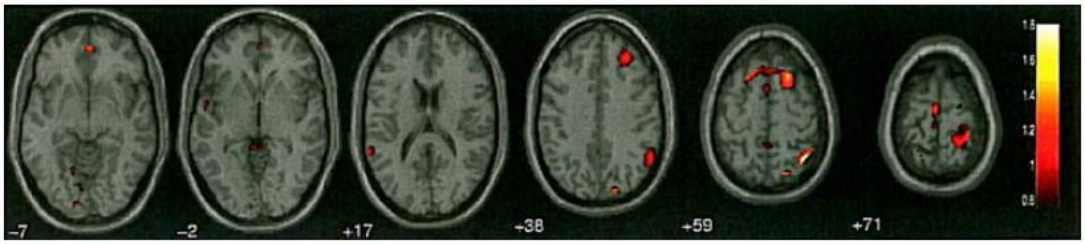

Figure 7: Right prefrontal localization associated with the contrast self-ace familiar-face ($p < 0.001$; 8 voxel cluster level) (71).

Preliminary studies showed that, fMRI and fNIRS signals are consistent not only in simple motoric responses but also in paradigms requiring more complex cognitive and physiological activities. Still, more detailed and deeper researches should be conducted on congruence between fNIRS and fMRI to help fNIRS establish a more concrete reputation as a reliable modality. However, studies done so far have proved that fNIRS has a great potential towards examining various neurological and psychiatric disorders.

1.2.3. Tracking Neurological Conditions and Psychiatric Disorders with fNIRS

A study foresaw that operating rooms, intensive care units for patients who are undergoing operations with significant risk of reversible cerebral ischemia, patients with severe head injuries or strokes and individuals at risk of for intracranial hemorrhage are major fields of fNIRS as neuro-monitoring (72). In a large sample of patients, S.P. Gopinath carried out a series of examinations while fNIRS measurements were taken to detect the development of late hematomas in a large sample of patients (73). Results showed 16% of total patients developed a type of late hematoma: Intracerebral hematoma in 8 patients, extracerebral hematoma in 6 patients and postoperative hematoma in 13 patients. Of the late hematomas listed above, 18 of them appeared between the first 2 to 72 hours after admission to hospital. These hematomas had significant mass effects and surgeries were required. Most of these patient's subject tissues had increased light absorption characteristics, before other symptoms such as increased intracranial pressure, changes on neurological examination, and changes on computed tomography scans. At patients with late hematomas, 67% of them had positive outcomes.

fNIRS is already employed in studies on patients with subarachnoid hemorrhage and traumatic brain injuries (TBI). Similarities between local oxygen pressure in brain white matter and local HbO_2 saturation were evaluated by A. Brawanski and colleagues by using frequency-based methods (74). In more than 90% of data sets a significant correlation was found on frequencies for coherence and overall density distribution. Also, A. Kampfl and colleagues demonstrated that fNIRS may be used as an additional diagnostic tool on non-invasive evaluation of impaired cerebral microcirculation in patients with increased intracranial pressure (75). Towards investigating the pathophysiology of severe TBIs on kids, P.D. Adelson and colleagues used fNIRS technology (76). Optodes were placed over the frontal-parietal region of kids to be able to monitor continuously with fNIRS. The comparisons of relative HbO_2, Hb, TotHb were made with intracranial pressure, mean arterial pressure, electroencephalography. Results showed that changes in cerebral hemodynamics in children can be made reliably with fNIRS technology.

Also, further understanding of etiology of the diffuse cerebral swelling could be done. All these researches point out to the fact that understanding primary and secondary responses to brain injuries in patients of all ages is possible with fNIRS. Although some studies questioned validity of fNIRS in detecting cerebral ischemia due to concern about a lack of correlation with changes in jugular venous blood oxygen saturation, with accurate probe placement fNIRS is proved to be much more sensitive than jugular venous saturation (77-78).

fNIRS technology is also used to monitor brains of patients with epileptic seizures. A study held by E. Watanabe on epileptic seizures showed that the regional cerebral blood volume on focus side increased consistently for about 30-60 seconds after the seizure onset (79). This study showed that, with the use of fNIRS technology CBV can be monitored continuously during seizures. Another more up to date study concluded that, ictal single photon emission computed tomography (SPECT) can be combined with fNIRS to form a more enhanced reliable non-invasive method towards diagnosing epilepsy (80).

Patients with spontaneously occurring complex-partial seizures (CPS) are also examined with fNIRS (81). Measurements taken during these seizures showed extreme increases in both blood volume and HbO_2 concentration, thereby proving how valuable fNIRS could be on assessing brain functions at bedside. Another study done on adults with CPS and rapidly secondarily generalized CPS (RCPS) investigated the capability of fNIRS technology (82). Results showed the capabilities of fNIRS technology. Measurements taken on subclinical seizures showed increased cerebral oxygenation for CPS and decreased for RCPS but no change in cerebral oximetry was seen. This study indicated that fNIRS can be used towards distinguishing cerebral oxygenation patterns between CPS and RCPS in adults. BJ. Steinhoff and colleagues presented preliminary results stating the simplicity, cost-effectiveness and non-invasiveness of fNIRS and thereby emphasizing the potential of this technology as an additional method to lateralize the primary epileptogenic zone in temporal lobe epilepsy (83).

Furthermore, a study on pathophysiology of seizures in childhood epilepsy was done by K. Haginoya and colleagues with fNIRS. Research was done on children ranging between ages of 1.5 months and 16 years. A total of 6 series of tonic spasms and 67 isolated seizures were recorded. Findings stated the existence of several pathophysiological processes whereby a relationship between convulsive seizures and remarkable increases in CBV was found. Another relationship between absence seizures and mild decreases or no changes in blood volume of the frontal cortex were found. Also in some types of convulsive seizures, an initial transient decrease in blood volume was observed. An ictal decrease in the course of tonic status epilepticus was triggered by an ictal increase in blood volume. Furthermore, in patients with West syndrome, heterogeneity was observed in the changes during tonic spasms which are epileptic syndromes.

Studies done by C. Hock and colleagues on the feasibility of fNIRS technology towards Alzheimer's disease (AD) monitored changes in the HbO_2 in the frontal cortex of human brain using NIRO 500 NIRS system. Patients with probable AD were asked to perform a verbal fluency task (VFT) (84). Test results showed increase in local concentrations of HbO_2 and TotHb at elderly healthy subjects, in contrast a rapid decrease in these parameters at subjects with Alzheimer's disease. This effect was not so clear in the frontal cortex while it was at parietal cortex. Authors found a relation between the neurodegeneration and regional reduction in oxygen supply during the activation of brain function. Also they stated that due to alterations in functional brain organization, a reduction in hemoglobin oxygenation during cognitive tasks might be seen in degenerating brain areas resulting in favor of healthier brain regions. Furthermore, the coupling mechanism between brain cell activity and blood flow or a change in the optical properties of the brain had alterations. Towards investigating changes in prefrontal activation in patients with AD, AJ. Fallgatter and colleagues employed VFT (85). As a result, a significant interaction between hemispheric effects and participant diagnosis was found, indicating a relationship between good performance on VFT and predominance of left hemispheric activation. Patients with AD had a low number of correct responses which is related to the loss of asymmetric activation pattern. Even though both

patients and controls performed better for semantic fluency, the metabolic effects were significantly less pronounced when compared to one in phonemic fluency.

Consequently, the examination of a disease that could give way to neurodegeneration or increases in severity over time can be done by continuous brain monitoring via fNIRS technology. When compared with other available neuroimaging technologies, it is a huge advantage of fNIRS in continuous monitoring of hemodynamic activity over extended periods of time in ecologically valid settings. Sometimes transporting the patient to a modality may be difficult or even impossible (ex: elderly, multimorbid, etc.), in this case fNIRS could be the best choice. With its portability, it can be brought to patient side thereby eliminating the need of patient transport.

Since motion artifacts are not a huge problem in fNIRS technology, it is also promising in neurobehavioral investigations of Parkinson's disease (PD). A study investigated direct stimulation induced cerebral blood oxygenation changes in the frontal lobe at patient with PD or essential tremor (86-87). When neural activation took place in the frontal lobe, HbO_2 and TotHb were increased, while behavior of Hb varied for different cases. During globus pallidus stimulation Hb was decreased in two cases. During low-frequency stimulation of the thalamus Hb was increased in four cases. Especially in HbO_2, fNIRS detected neural activation-induced patterns of cerebral blood oxygenation. Furthermore, authors claimed that in some cases, fMRI based on the BOLD contrast may be insufficient in detecting areas of neural activation, pointing out to the potential of fNIRS. In a study done by K. Sakatani and colleagues, electrical stimulation of these brain regions triggered cerebral blood oxygenation changes in the frontal lobe (similar to ones found during cognitive tasks) (87). Also, they suggested complex neuronal circuits in the frontal lobe might be the source of the multiplicity of the cerebral oxygenation changes in the frontal lobe.

Since available functional neuroimaging techniques come up short in detecting movement disorders artifact freely, fNIRS technology is relevant with its invulnerability to such parameter. Other studies done so far on fNIRS, remark it as a

potential modality in surgical treatment interventions, too. Still, fNIRS technology should be further enhanced by decreasing motion artifacts to attain a higher level of measurement reliability in PD and other movement disorder.

Schizophrenia is the number one neuropsychiatric condition utilized in fNIRS technology's capability studies. After decades of investigations done on schizophrenia, the necessary information required to fully understand the disorder itself, is still lacking. F. Okada and colleagues investigated disturbance in interhemispheric integration of brain oxygen metabolism and hemodynamics with a multi-channel fNIRS device (88). For this investigation, a mirror drawing task (MDT) was utilized. During the MDT, controls showed distinct and well-integrated patterns of changes in HbO_2, Hb, and total blood volume. At half of the patients with schizophrenia, no parallelity was found between increases in HbO_2 and decreases in Hb in frontal regions between hemispheres. Thus, a connection between problems in interhemispheric integration and certain symptoms of schizophrenia was found.

Similarly, during the execution of a continuous performance test AJ. Fallgatter and colleagues examined the relationship between lateralized frontal fNIRS activation patterns, no (89). In their cohort, no overall or hemispheric activation effects were found. Whereas, group differences were found with a lack of lateralized activation in schizophrenia in comparison to healthy controls. Also in subjects with schizophrenia, at resting state and during activation a trend towards higher left relative to right HbO_2 and Hb ratios were observed. As a result, authors claimed that, based on a left hemisphere functional deficit in schizophrenia, there may be a reduced specific lateralized frontal reactivity. In another investigation, random number generation (RNG), ruler-catching (RC), and sequential finger-to-thumb (SFT) tasks (which are frontally based tasks) were utilized towards proving the existence of task-dependent functional abnormalities frontal brain metabolism in schizophrenia (90). In schizophrenic patients although the responses were significantly smaller, TotHb and HbO_2 concentrations increased while Hb decreased especially during RNG tasks. In contrast to most of the control subjects, HbO_2 in patients with schizophrenia had a tendency to decrease during RC tasks. During the SFT task in the whole group, no difference was observed.

In schizophrenia, to help clarify the nature of language-related problems, VFTs have been utilized. In studies done by Y. Kubota and colleagues, subjects with schizophrenia showed more compromised performance in semantic VFTs compared to the phonemic VFTs while healthy subjects performed the same in both types of VFTs (91). As a result of fNIRS measurements taken from healthy subjects, compared to semantic VFT a greater prefrontal cortex (PFC) activation was found in phonemic VFT. This points out to a more prominent PFC involvement in phonemic-cued retrieval. Semantic mode of lexical access might impose greater cognitive demands on the PFC, since subjects with schizophrenia showed the opposite pattern of activation.

All of these fNIRS-based investigations provided valuable information on abnormal patterns of frontal activation in schizophrenia in response to cognitive demands. Also, studies done on schizophrenia prove that there is a strong analogy between findings from fNIRS-based studies and findings from other established neuroimaging studies, thereby acting as a source of motivation for further work involving non-invasive and continuous explorations of cortical activation patterns in schizophrenia. Since schizophrenia is a type of frontally based dysfunction, fNIRS holds a priority on investigations of the disorder. Also, ease of administration of fNIRS technology stands invaluable in some situations. For example, schizophrenic patients going through psychotic episodes may get disturbed by being inactive in stuffy environments, therefore cannot participate in these kind of research studies. However, with its portability, fNIRS may overcome these problems that might occur during fMRI or MRI sessions. Instead of enduring rigid protocols required in fMRI sessions, if fNIRS can be used in real time lengthy measurements it can monitor cortex involvements in delusional and hallucinatory states, comfortably. This would provide first pieces of information on delusional and hallucinatory states in real-world environments. However, if fNIRS is intended to be the gold standard on such studies, it still has a long way to go. As time goes by, current limitations of the technology must be surpassed, so that it can be reconsidered as the best choice against modalities such as fMRI or MRI on schizophrenia studies.

Mood disorders like depression and bipolar disorder are recently taken into investigation with the fNIRS modality. Just like studies done on schizophrenia, hemispheric activation patterns are investigated with the use of MDT (92). As a result, a non-dominant response pattern was triggered at almost half of the patients with major depression, which was not found in healthy controls. Based on the handedness, all of this corresponds to an increase in TotHb to a markedly lesser level in the dominant (left) hemisphere than in the non-dominant (right) hemisphere. Other half of patients had comparable levels of TotHb, HbO_2 and Hb in their both hemispheres. A correlation may be found between the course of depression and the response patterns based on the shifts in the response patterns related to the course of depression. When data are examined a gender related difference is seen, there is a high chance for women to show the bilateral response pattern, while show of dominant hemisphere response pattern is higher for men. Continuous monitoring of cerebral activation for long periods of time, allowed scientists to discover effects of both course-related changes and influence of gender.

Another study was carried out to have a deeper understanding of the neurobiological basis of the hypofrontality. In the left frontal region of a group of elderly patients with depression who were diagnosed after the age of 50, K. Matsuo and colleagues ran an examination consisted of VFT, verbal repetition, hyperventilation and paper-bag breathing tasks (93). During the VFT, control subjects had a significant increase in their HbO_2 and decrease in their Hb values while depressed patients had no significant quantity change of their chromophores. However, during hyperventilation in both groups, a significant decrease in HbO_2 and increase in Hb were observed. In contrary to the vascular depression hypothesis, findings suggested that the functional hypofrontality in elderly depression is not due to altered vasodilator response associated with cerebral arteriosclerosis. Since previous study consisted of a small sample size with imprecise statistical analysis, towards conducting a more thorough investigation of the neurobiological basis of hypofrontality in mood disorders a larger study was done using the same paradigm (94). The sample group included patients with major depressive disorder and bipolar disorder. Findings pointed out to an increase in HbO_2 during the VFT which resulted in activation of the left dorsolateral prefrontal cortex. However, this activation of the

left dorsolateral prefrontal cortex was lower in the depressed and bipolar groups when compared to the controls. Also, the decrease of HbO_2 during hyperventilation was significantly smaller in the depressed, too. Regarding these findings, authors concluded that there may be an association between the hypofrontality on mood disorders and a poor response in the cerebral blood vessels to neuronal and chemical stimuli.

Use of fNIRS is not permitted to only course and cerebral activation patterns in depression, fields of fNIRS can be broadened by adapting it to modalities such as repetitive transcranial magnetic stimulation (rTMS) and electroconvulsive therapy. An evaluation done by GW. Eschweiler and colleagues on the clinical status and the hemodynamic response of the PFC before therapeutic rTMS to treat depression utilized fNIRS (95). fNIRS measurements of hemodynamic changes taken during a 10Hz rTMS to the left dorsolateral PFC indicated a decrease in depression levels after 5 days of active stimulation compared to no change after sham stimulation. Patient's clinical response to treatment with rTMS was significantly predicted by an absence of a task-related increase of TotHb concentrations at the stimulation site before the first active rTMS. Authors stated that, low local hemodynamic responses and provided support for the idea of activation-dependent targeting of rTMS location can be used to predict the clinical benefits of rTMS.

Anxiety related disorders such as panic disorder and posttraumatic stress disorder (PTSD) are also investigated with fNIRS. In a group characterized as having both negative emotions and avoidance withdrawal behavior, J. Akiyoshi and colleagues took measurements regarding the frontal activation in patients with panic disorder without depression (96). fNIRS measurements and recordings were taken from patients and controls in the thee different conditions: Confrontation at rest with neutral stimuli (e.g. mushroom), anxiety-relevant stimuli (e.g. spider and snake) and anxiety-irrelevant but emotionally relevant stimuli (e.g. erotic picture). With anxiety-relevant or anxiety-irrelevant but not emotionally relevant stimuli, left frontal HbO_2 of patients was significantly lower when compared to control subjects'. As a result of this study, no evidence was attained related to frontal brain asymmetry during stimuli observations. This study provided biological evidence for disturbed cortical

processing in panic disorder by building a connection between great decreases in the activation of a left frontal avoidance-withdrawal system and negative valences.

Another study carried out by K. Matsuo and colleagues utilized fNIRS to assess the psychophysiological effects of PTSD on victims of the 1995 Tokyo subway attack (97). During stimulation via trauma-related video presentations, a multi-channel fNIRS was used to measure the hemodynamic responses of prefrontal cortex and skin conductance responses (SCR). While trauma-related images were being viewed, a significant elevation of HbO_2 in the PFC was measured from both subjects with and without PTSD. Although, amount of HbO_2 and TotHb increase differed between subjects with PTSD and without PTSD, subjects with PTSD showed a smaller increase in HbO_2 with enhanced SCR. A consistency was found between previous studies (which utilized other measurement techniques such as pulse, blood pressure, SCR, electromyogram, etc.) and long lasting psychophysiological response to trauma-related stimuli. This consistency is bound to the increase of HbO_2 (which lasts at least three minutes) which took place after the trauma-related stimuli. Towards achieving the psychophysiological assessment of PTSD, utilization of fNIRS in cerebral hemodynamic response measurements is crucial. Due to movement causing emotional activations encountered in participants, assessment of PTSD non-invasively via fNIRS holds great advantage over other physically restraining functional neuroimaging procedures. Convenience of fNIRS to motion artifact filtration, may allow even patients that are unable to maintain a normal body position during measurements to be assessed, since the technology allows examination of salient variables of PTSD (55). Last but not least, the real time use of fNIRS towards monitoring cortical activity may be used as part of biofeedback mechanisms to enhance treatment of these patients.

1.2.4. Brain – Computer Interface

A brain-computer interface (BCI) system provides its users with control channels that are independent from the brain's output channels (98). People suffering from motor function disorders can utilize BCI for communications and also towards restoring these motor functions. These motor function disorders include amyotrophic

lateral sclerosis and spinal cord injury, and/or people in the persistent locked-in state. A typical BCI system consists of five stages: Brain-signal acquisition, preprocessing, feature extraction and selection, classification, and application interface.

1.2.5. Well-Recognized fNIRS Devices

There are various fNIRS devices with different specifications commercially available on market. All of these fNIRS devices are designed with different priorities in mind, regarding specific measurement needs. The well-recognized ones are explained as next.

1.2.5.a. OctaMon

OctaMon (Artinis Medical Systems, The Holland) is a 10Hz, 8-channel, fully portable fNIRS device (see figure 5). It utilizes continuous wave domain towards achieving low-cost and high portability. This 8-channel design consists of two sources (4-channels for each source), four detectors are positioned around each source at the same distance (3.5cm) on the imaginary corners of a square. Even though device has only two sources, these sources are dual wavelength LEDs meaning that both 760 and 850nm wavelengths are found in each source. This dual wavelength design allows calculations of HbO_2, Hb and TotHb concentration changes. Device is designed in such a way that combining it with other modalities such as EEG and EMG is also feasible. Collected data are sent wirelessly with the use of Bluetooth communication protocol. Also, measurements can be made offline by just turning off the Bluetooth module. Analysis of the collected data can be achieved easily and rapidly with its unique analysis software “Oxysoft”. System can operate with its battery for six hours straight. With its lightweight (230gr) and portable design, OctaMon is suitable for use during sports activities, brain oxygenation monitoring, functional studies, cerebral studies and hyper scanning (99).

1.2.5.b. fNIRS103P

fNIRS103P (Biopac Systems Inc., CA, USA) is an fNIRS solution pack, which consists of wireless pediatric imager 2000W/1200 with a sampling rate of 4Hz and one of the head probes RXFNIR-PED or RXFNIR-4, regarding customer's choice (see figure 8). System is a portable one like most of the modern fNIRS systems and uses continuous wave domain. 2000W/1200 is a wireless fNIRS box that can communicate with any computer that utilizes Windows 7, 8 or 10 operating systems (Microsoft Corporation, Washington DC, USA). Data analysis is achieved with its unique software "fNIRSSoft Standard and COBI", with ease. RXFNIR-4 is an adult head probe with a split sensor design; head probe is split into 2 pieces, each piece containing 2 channels. The source – detector distance of this head probe is 2.5cm. RXFNIR-PED is another head probe designed with pediatrics in mind; it is a 2 channel system with a source – detector distance of 2.0cm. Both of these head probes' sensor parts have selection options regarding measurement needs, also source parts are dual wavelength LEDs with 730 and 850nm (100).

Figure 8: Biopac fNIRS103P with FNIR-PED head probe (101).

1.2.5.c. NIRO-200NX

NIRO-200NX (Hamamatsu, Japan) is a multi-purpose near infrared tissue oxygenation monitoring system which utilizes low levels of light waves towards high level of patient safety (see figure 9). System is designed to be used in both brain and muscle measurements. Two different measurement techniques; modified Beer Lambert law and spatially resolved spectroscopy runs independently of each other.

Also, combining these two provides local hemodynamic information as well as improved data reliability, in general. NIRO-200NX has a wide field of application as listed below;

1. Brain oxygenation monitoring during heart surgery and other procedures.
2. Patient monitoring in emergency rooms.
3. Patient monitoring in intensive care units, coronary care units, neonatal intensive care units.
4. Clinical studies related to oxygenation levels and blood metabolism in the brain.
5. Studies of muscle tissue oxygenation for sports medicine, rehabilitation and similar applications.
6. Suitable for use on emergency carts.
7. Suitable for use on rescue helicopters.

NIRO-200NX utilizes LED technology with a triple wavelength model (730, 810 and 850nm). Device's battery operated lightweight (6kg) design eliminates the need for a power line, thereby enhancing portability. With its data storing feature, retrieval of the previous measurements for patient counselling and research purposes is also feasible (102).

Figure 9: Hamamatsu NIRO-200NX fNIRS device (103).

1.2.5.d. ETG-4000

ETG-4000 (Hitachi Ltd, Japan) is a bulky (130kg) non-portable 3D topographic image display system which combines results of fNIRS with MRI images to generate a sophisticated 3 dimensional and dynamic model (see figure 10). Device utilizes the laser diode technology and capable of measuring HbO_2, Hb and TotHb concentration changes. Two separate head probe configurations allow ETG-4000 to be used with 24 or 48 (52 with 3x11 probe holder) channels. Programmable feature of system allows it to be used at a sampling rate up to 10 Hz. Dual wavelength laser diodes of the device operate at 695 and 850nm. Device can communicate and share data with other nearby device through local network. ETG-4000 is considered as the ideal tool in cognitive neuroscience, stroke rehabilitation, etc. (104-105). Major specifications of the fNIRS devices are listed in table 2.

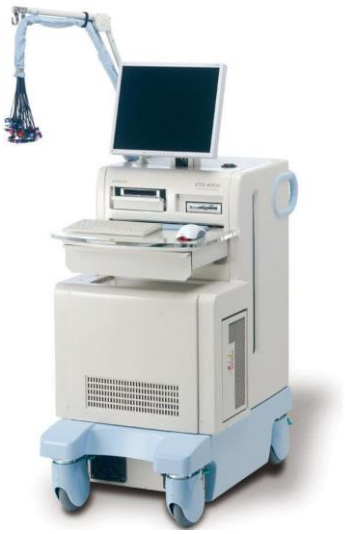

Figure 10: Hitachi ETG-4000 fNIRS device (106).

Table 2: Major specifications of top fNIRS devices.

Producer	Model	Sampling Rate	# of Channels	Wireless	Wavelengths
Artinis	OctaMon	10Hz	8	Yes	760 and 850nm
Biopac	fNIR103P	4Hz	2 or 4	Yes	730 and 850nm
Hamamatsu	NIRO-200NX	Up to 20Hz	-	No	735, 810 and 850nm
Hitachi	ETG-4000	Up to 10Hz	24 or 48/52	No	695 and 830nm
Hitachi	WOT-100	5Hz	16	Yes	705 and 830nm
ISS	Imagent	Up to 50Hz	Up to 512	No	690 and 830nm
NIRX	NIRSport	62.5Hz	8	Yes	760 and 850nm
Device Developed	Vega Vision	5Hz	8	Yes	730 and 850nm

2. MATERIALS AND METHODS

In this study, an 18V battery powered continuous wave domain 4-channel wireless fNIRS device called Vega Vision, with 5Hz sampling frequency was designed and tested for use in frontal lobe measurements. Also, short separation approach was utilized towards eliminating the skin effect. Although, the number of channels is 8 in reality, due to short separation approach, data received from 4 of these channels are subtracted from the other 4. Therefore, after the signal processing procedure the final information is a 4-channel subtracted fNIRS data with improved SNR. All the schematic drawings, circuit simulations, printed circuit board (PCB) designs were done with Proteus 8.6 Professional while embedded coding was done with Proton Integrated Development Environment. Also, a Bluetooth data receiving computer program with a user interface was written in MATLAB R2016a. Vega Vision is split into three major parts; main circuit board, head probe and a computerized control system. Data is carried in between main circuit board and head probe via insulation-displacement connectors and a flat cable.

2.1. Main Circuit Board

The main circuit board consists of a three step regulator part, an operational amplifier (OP-AMP) based constant current source, an analog switch, a digital potentiometer, a Bluetooth module and two microcontroller units (MCU) (see figures 11, 12 and 13).

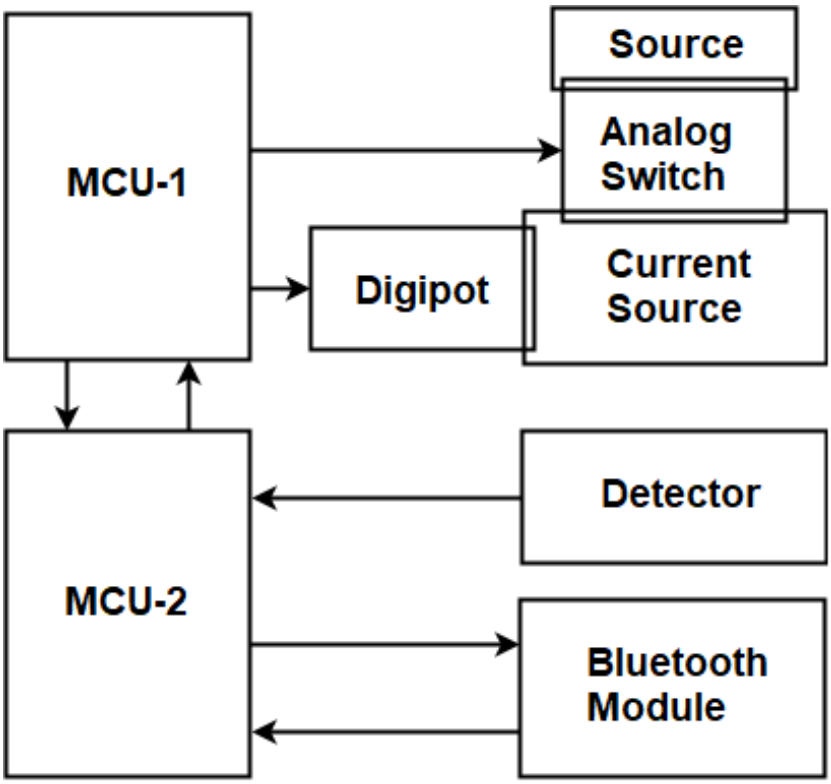

Figure 11: Block diagram of the developed device.

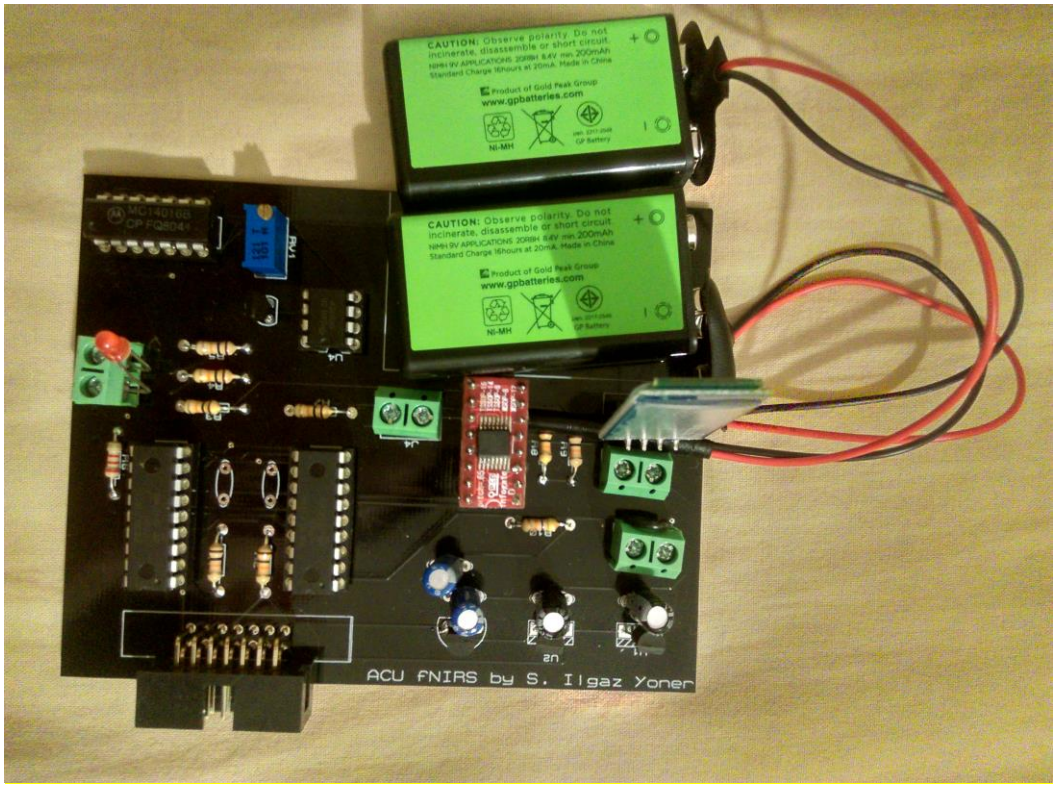

Figure 12: Photograph of the main circuit board.

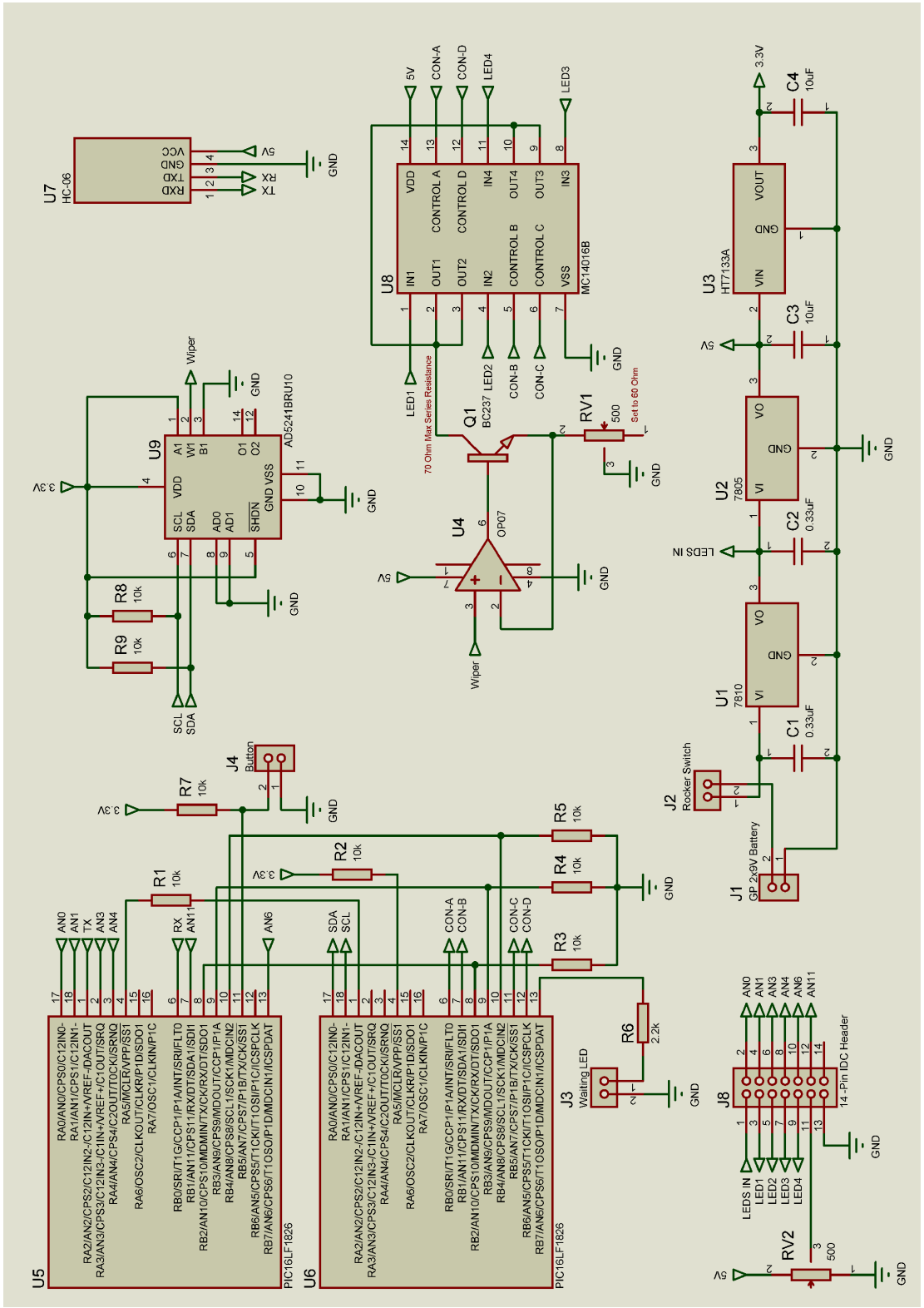

Figure 13: Schematic diagram of the main circuit board.

2.1.1. Voltage Regulator Unit

Vega Vision is comprised of components which run on different voltage levels; therefore different levels of regulated voltage outputs are required for proper operation. To meet these requirements, three regulators are used in series with their noise filtering capacitors (see figure 14);

1. L78L10CZ (STMicroelectronics, Switzerland): A fixed positive voltage regulator that outputs +10Vdc with 100mA current delivery limit. This output feeds the LEDs of the device.

2. L7805CZ (STMicroelectronics, Switzerland): A fixed positive voltage regulator that outputs +5Vdc with 100mA current limit. This output feeds the analog switch and the Bluetooth module.

3. HT7133A (HOLTEK Semiconductor Inc., Taiwan), A fixed positive voltage regulator that outputs +3.3Vdc with 30mA typical current delivery. This output feeds the rest of the electronic circuits in the device.

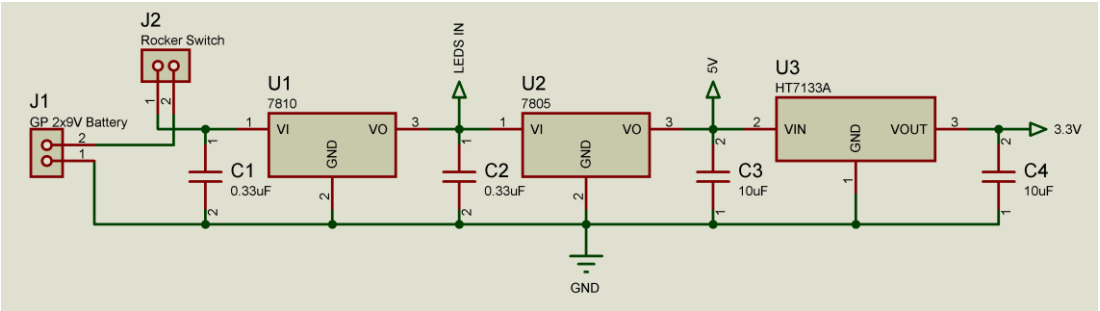

Figure 14: Schematic diagram of the voltage regulator unit.

2.1.2. Constant Current Source Unit

In an OI system such as fNIRS, if the transmitted signal is not stable enough, accurate calculation of a parameter such as tissue oxygenation would not be possible. Therefore, stability of the transmitted light holds major importance. In electronics, feeding a circuit with a plain and simple voltage source lacks the desired level of

stability. For the highest current stability possible, circuits are fed with currents via constant current sources (107).

The constant current source unit of the device developed houses an NPN type bipolar junction transistor, BC237 (Fairchild Semiconductor, CA, USA) and an ultra-low offset voltage operational amplifier, OP07 (Analog Devices ink, MA, USA). As shown in figure 15, a typical OP-AMP based constant current source is obtained by connecting the OP-AMP's output to transistor's base terminal and OP-AMP's negative input to transistor's emitter terminal. Also, OP-AMP's positive input was connected to a voltage source through a voltage divider potentiometer. Connecting a 500Ω trimpot between the emitter terminal of the transistor and the ground allows circuit to be calibrated by the user, later on. The desired load must be connected between the collector terminal of the transistor and the feeding voltage. When the feeding voltage of the load is above a certain minimum level, voltage across the load settles down and the excess voltage is held between the transistor's collector – base terminals. Also, the current across the load can be manipulated by adjusting the sense resistor (see figure 15). Thereby, in a stable temperature environment a constant current source keeps the current across a desired load constant, if the implementation is applied in the right way.

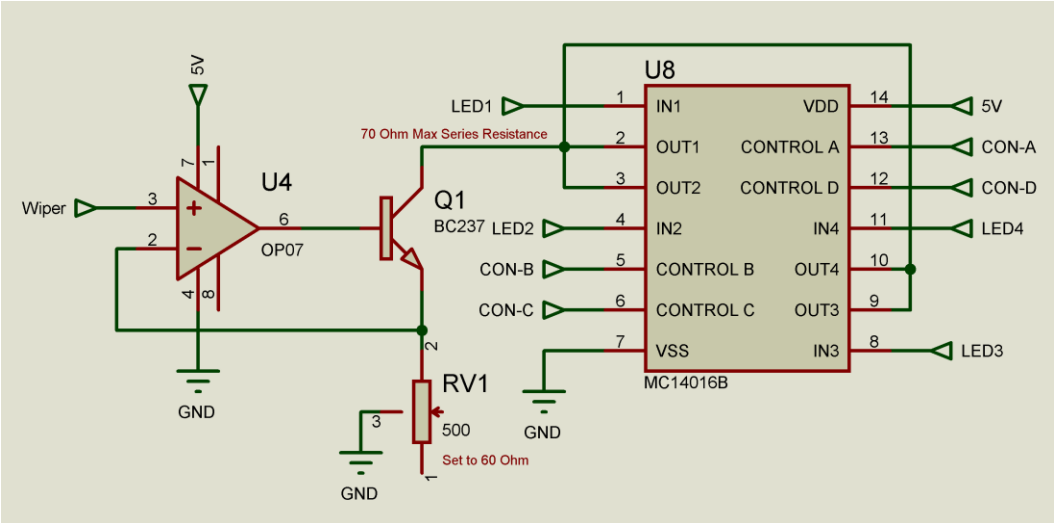

Figure 15: Schematic diagram of the constant current source unit.

2.1.3. Bilateral Switch

When more than one LED is used, an analog switch eliminates the necessity for multiple current sources. In the current design a complementary metal-oxide semiconductor quad bilateral switch, MC14016B, (ON Semiconductor, AZ, USA) has been used. With its low on resistance, MC14016B is ideal for use in series with a current source, furthermore logic control inputs allow for rapid and sudden LED switching. Regarding the datasheet of MC14016B, +5V operating voltage was found to be ideal for a +3.3V logic control level. Therefore, voltage supply pin of MC14016B was supplied with +5V and logic control inputs were controlled by a +3.3V MCU.

2.1.4. Digital Potentiometer

In optical measurement systems, it is crucial to run optical units at optimal power levels towards achieving optimal measurement sensitivity. Since biological tissues have different absorption characteristics towards different wavelengths, 730nm and 850nm LEDs must be run at different power levels. Conventionally, control of the voltage across positive input of OP-AMP is achieved with an analog potentiometer.

Thanks to current technological advances, with a digital potentiometer Vega Vision has real time control capability over LED luminations. AD5241BRU10 (Analog Devices Inc., MA, USA) is an I^2C compatible 8-bit 10KΩ digital potentiometer (see figure 16). On the order of microseconds, AD5241BRU10 can communicate with an I2C compatible MCU, thereby it can be controlled by a busy MCU in between tasks rapidly and repeatedly. AD5241BRU10 was used as a voltage divider by connecting its one end to +3.3V, other end to ground line and wiper pin to the positive input of OP-AMP.

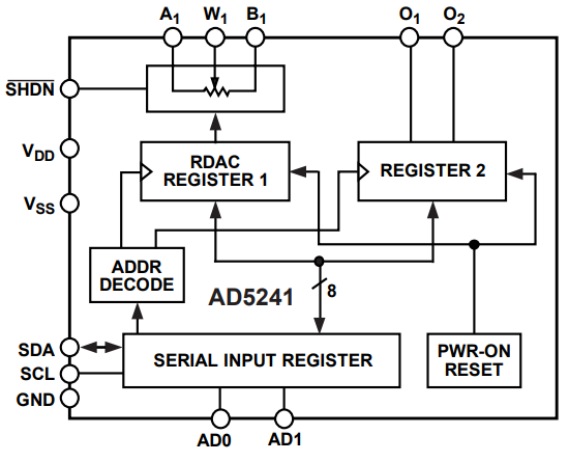

Figure 16: Block diagram of AD5241BRU10 (108).

2.1.5. Bluetooth Module

For a portable and wireless fNIRS system, Bluetooth communication protocol was utilized with HC-06 (Olimex Ltd., Bulgaria). HC-06 can communicate with other digital units through universal asynchronous receiver transmitter and transceives data at 2.4GHz with Bluetooth 2.0 technology. In this project, HC-06 was used in pair with computer's internal Bluetooth module (see figure 17).

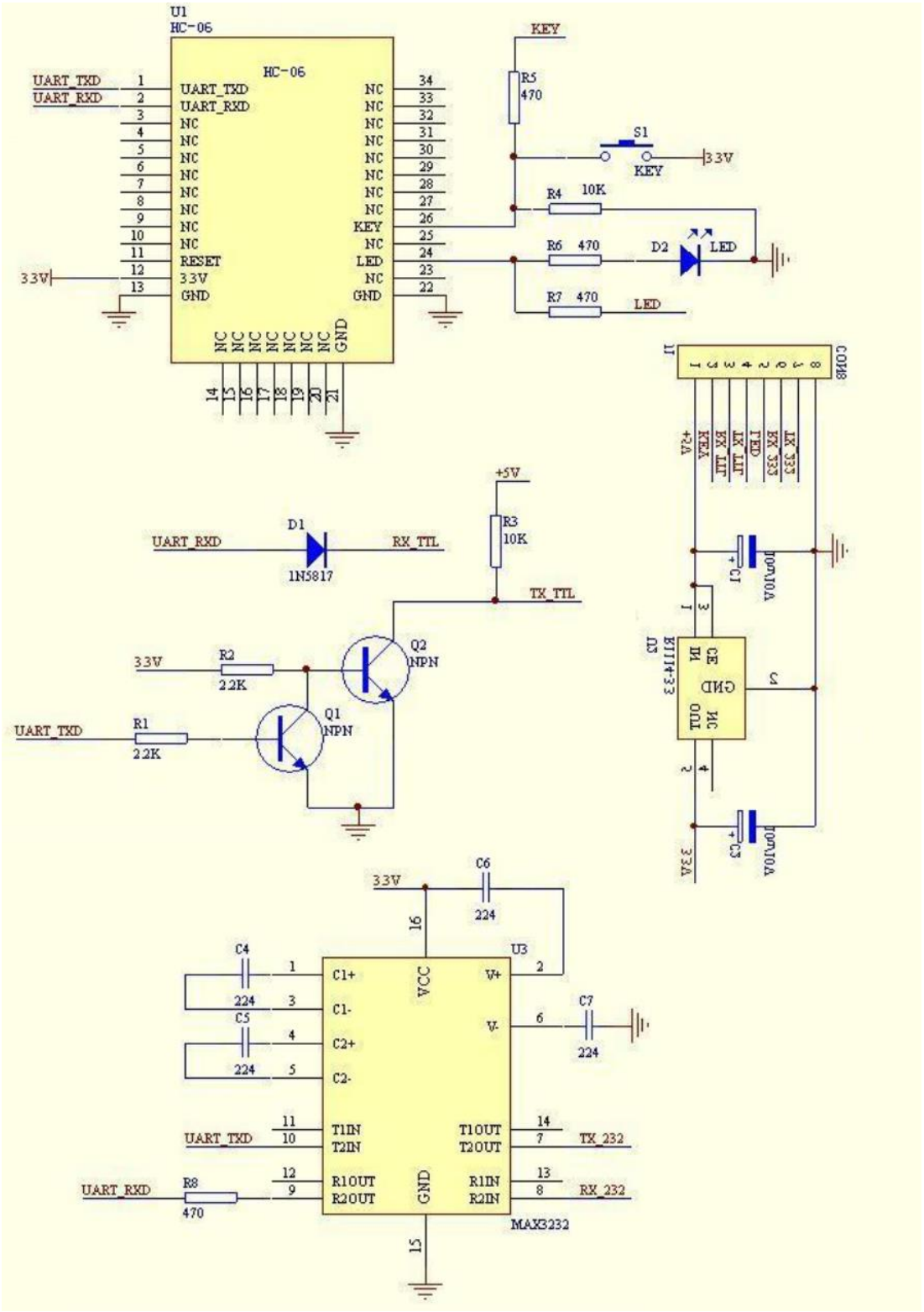

Figure 17: Block diagram of HC-06 (109).

2.1.6. Microcontroller Units

PIC16LF1826 (Microchip Technology Inc., USA) is an 18-pin FLASH MCU with nano watt extreme low power technology. PIC16LF1826 has a software selectable internal oscillator block that can provide clock speeds up to 32MHz precisely. Due to high noise levels present in measurement environments, it is not possible to benefit from full potential of a high resolution ADC system. Also, high resolution ADC systems require a lot of time for precise calculations of voltage levels. In this case, it was wise to utilize a relatively lower resolution ADC system and use it with a high sampling frequency, than average measurements for a period of time. For this manner, 10-bit, 12-channel analog-to-digital converter (ADC) module of PIC16LF1826 was utilized. With its stable fixed voltage reference, ADC conversions can be easily made with high accuracy. Serial peripheral interface and inter-integrated circuit (I^2C) communication protocols can be utilized with its enhanced universal synchronous asynchronous receiver transmitter module. Block diagram of the MCU is shown in figure 18.

PIC16LF1826 is a single core MCU, meaning that it can run only one task at a time. In a continuous wave domain fNIRS system, accurate timing of source switching holds major importance. In this study an 8-channel, 5Hz, dual wavelength fNIRS system is designed, which corresponds to 50ms on time for each wavelength from each LED (see figure 19).

In the current design, two MCU units are used: one (MCU-1) for switching the LEDs and another one (MCU-2) for ADC, mathematical calculations, data storing, Bluetooth communications. To avoid unnecessary load on MCU-1, MCU-2 receives data from and transceives data to Bluetooth device. Still, MCU-1 and MCU-2 communicates from time to time by pulling each other's inputs to high or low states for a synchronous operation. While MCU-1 is switching LEDs, it informs MCU-2 on which LED is active. Regarding this LED information, MCU-2 executes ADCs from 4 related channels. MCU-2 stores result of these ADC in corresponding float variables. Throughout this 50ms time interval, MCU-2 adds ADC results over the previous results from same channels and also counts the number of ADC

measurements. When this 50ms time interval is over, MCU-2 calculates the average of each channel and sends the required data to computer end byte by byte via Bluetooth module. Flowcharts for the MCU-1's and MCU-2's embedded codes are as seen in Figures 20-21.

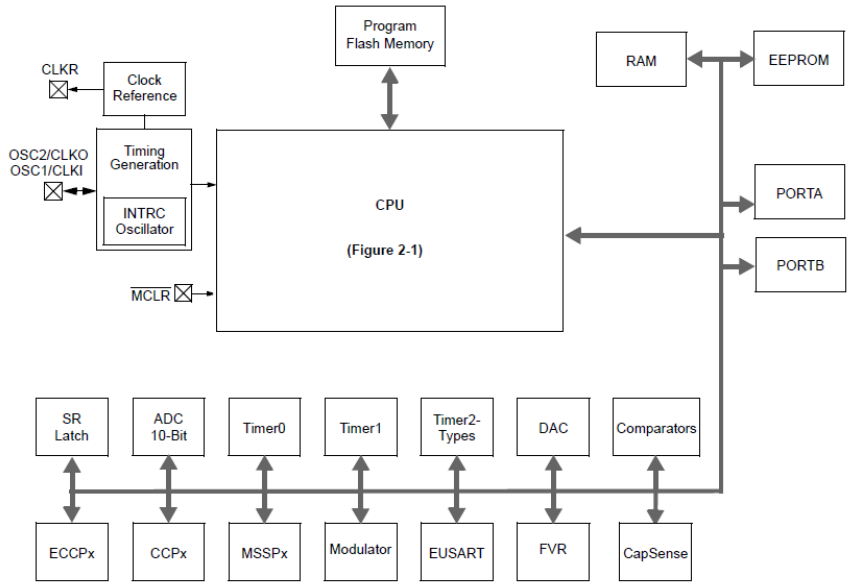

Figure 18: Block diagram of PIC16LF1826 (110).

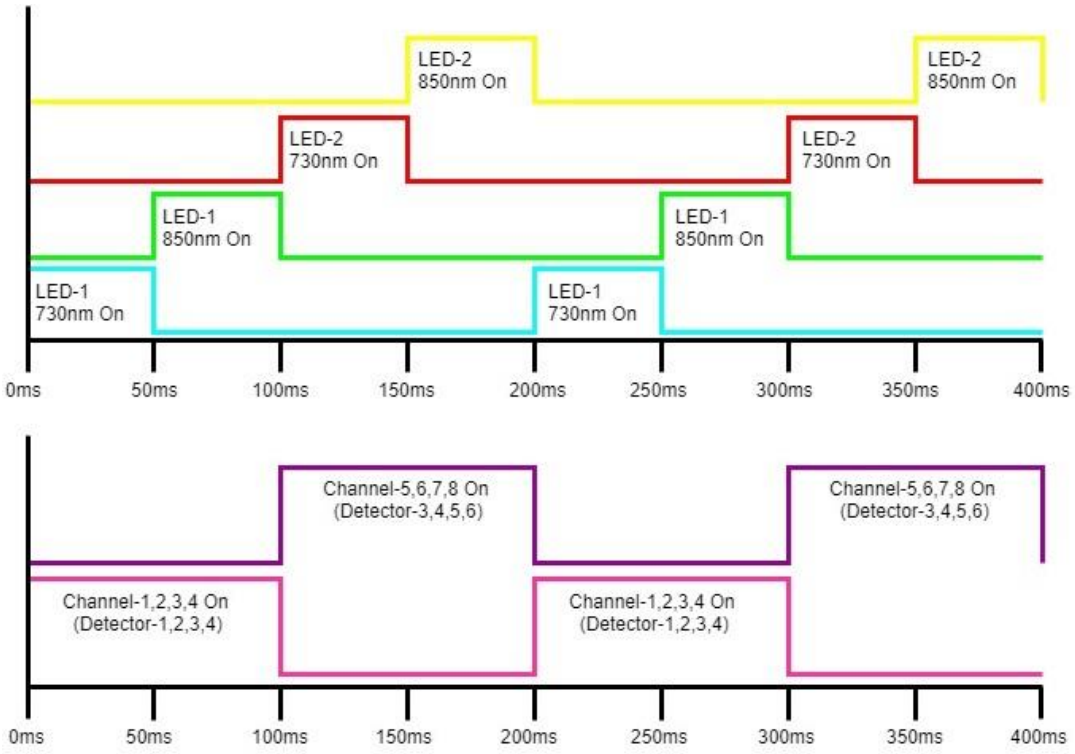

Figure 19: LEDs and detectors switching timing.

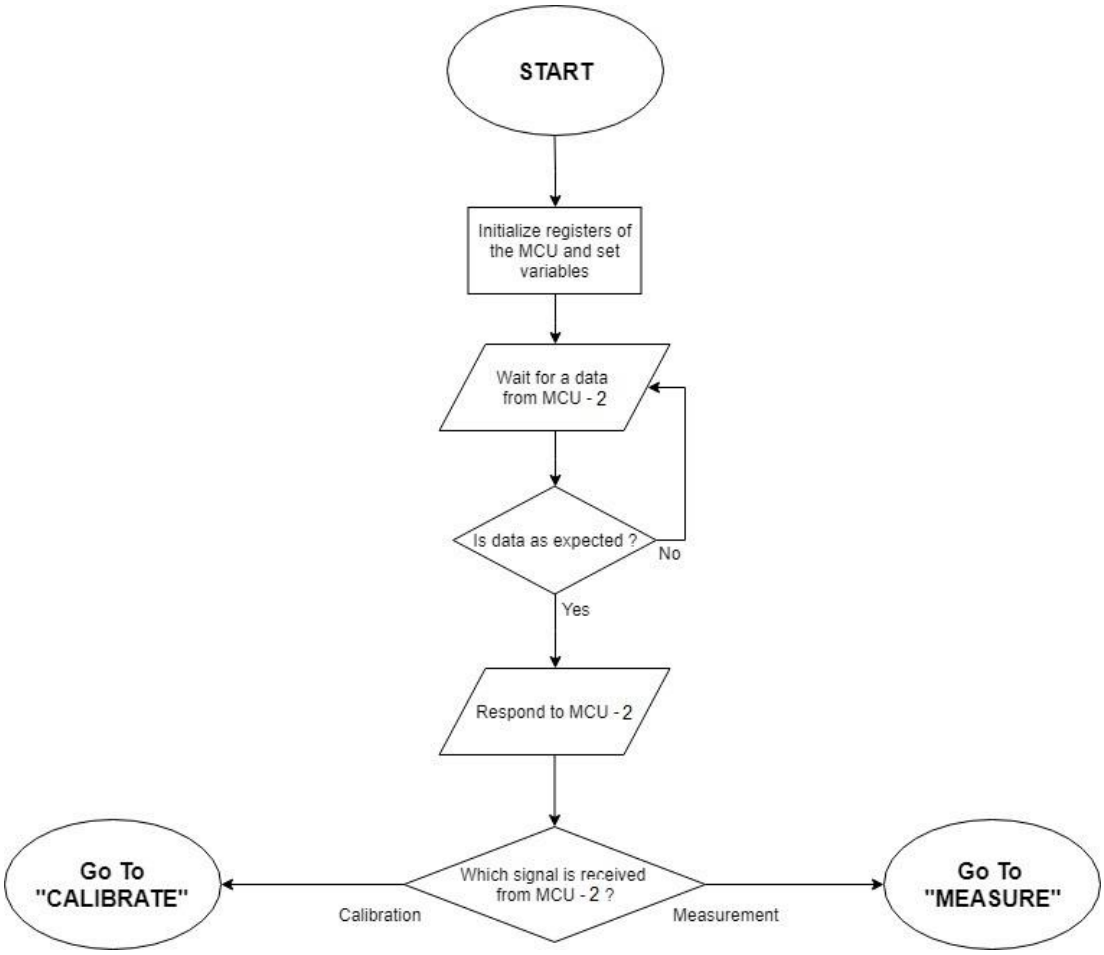
START
Initialize registers of the MCU and set variables
Wait for a data from MCU - 2
Is data as expected ?
No
Yes
Respond to MCU - 2
Which signal is received from MCU - 2 ?
Calibration
Measurement
Go To "CALIBRATE"
Go To "MEASURE"

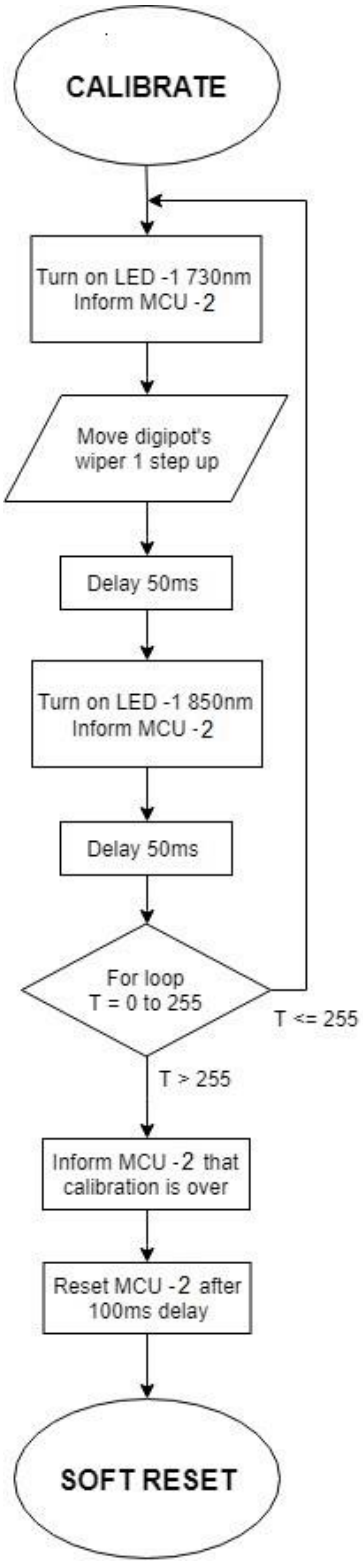
CALIBRATE
Turn on LED -1 730nm
Inform MCU -2
Move digipot's
wiper 1 step up
Delay 50ms
Turn on LED -1 850nm
Inform MCU -2
Delay 50ms
For loop
T = 0 to 255
T <= 255
T > 255
Inform MCU -2 that
calibration is over
Reset MCU -2 after
100ms delay
SOFT RESET

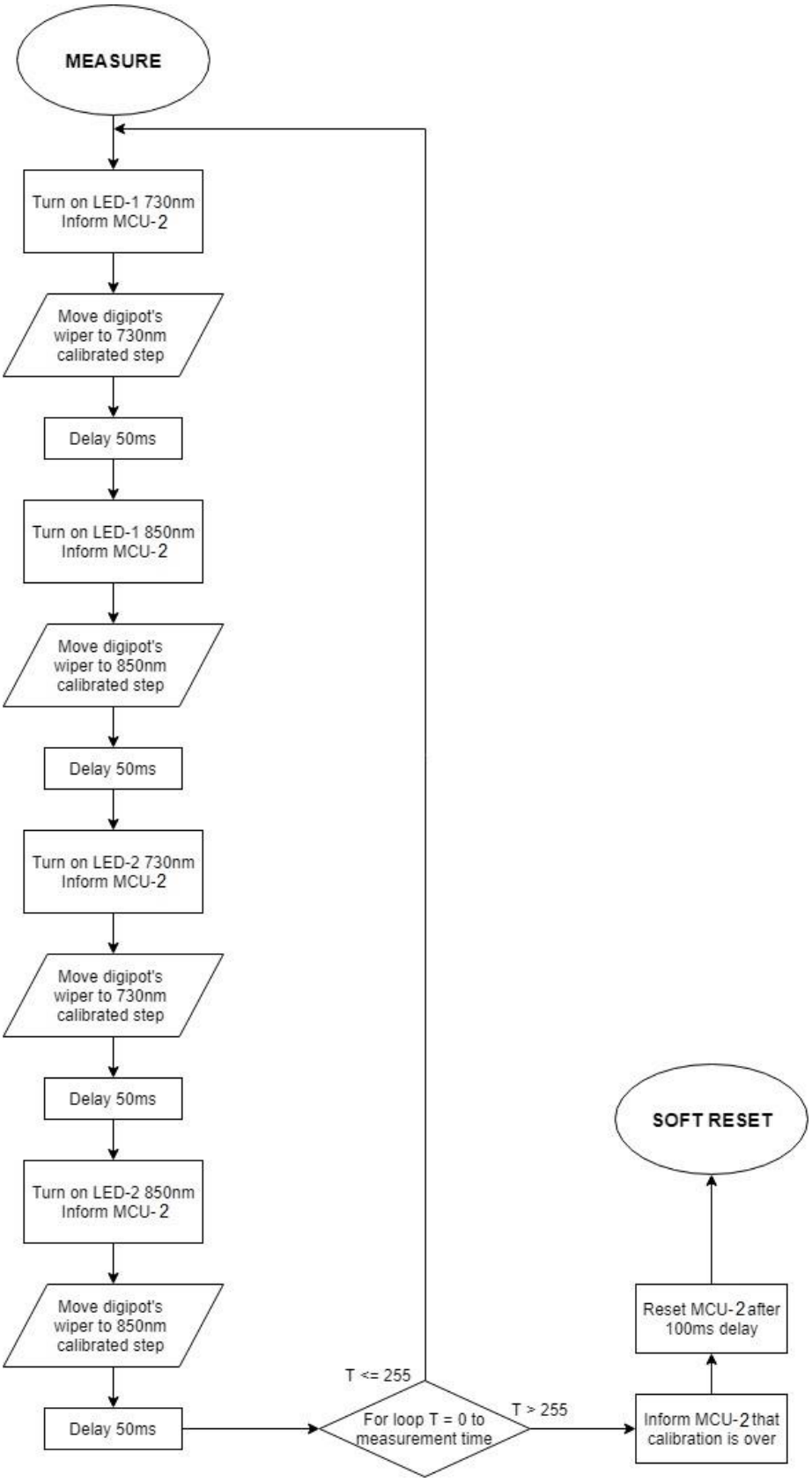

Figure 20: Flowchart of MCU-1's embedded code.

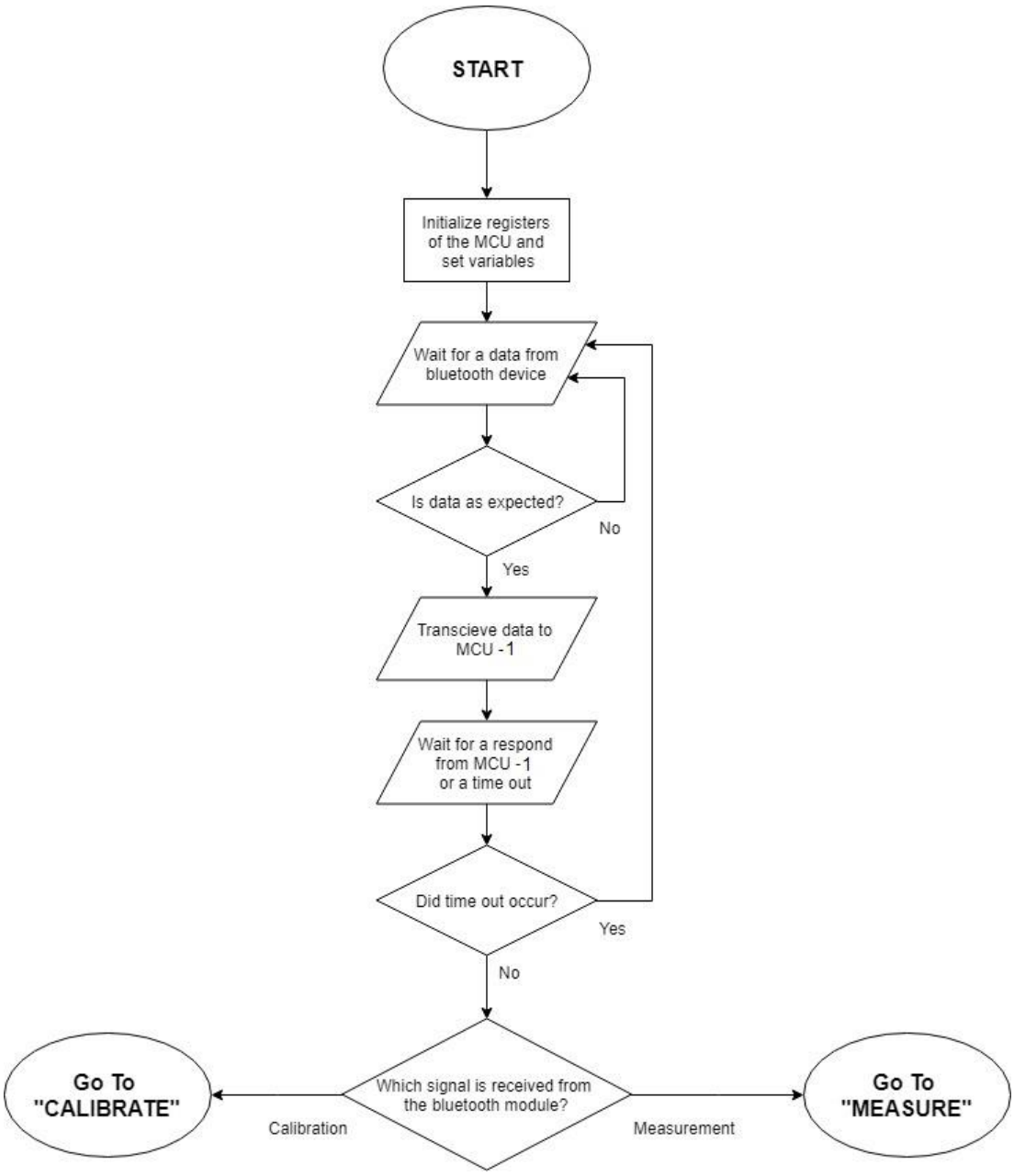
START
Initialize registers of the MCU and set variables
Wait for a data from bluetooth device
Is data as expected?
No
Yes
Transcieve data to MCU -1
Wait for a respond from MCU -1 or a time out
Did time out occur?
Yes
No
Which signal is received from the bluetooth module?
Calibration
Measurement
Go To "CALIBRATE"
Go To "MEASURE"

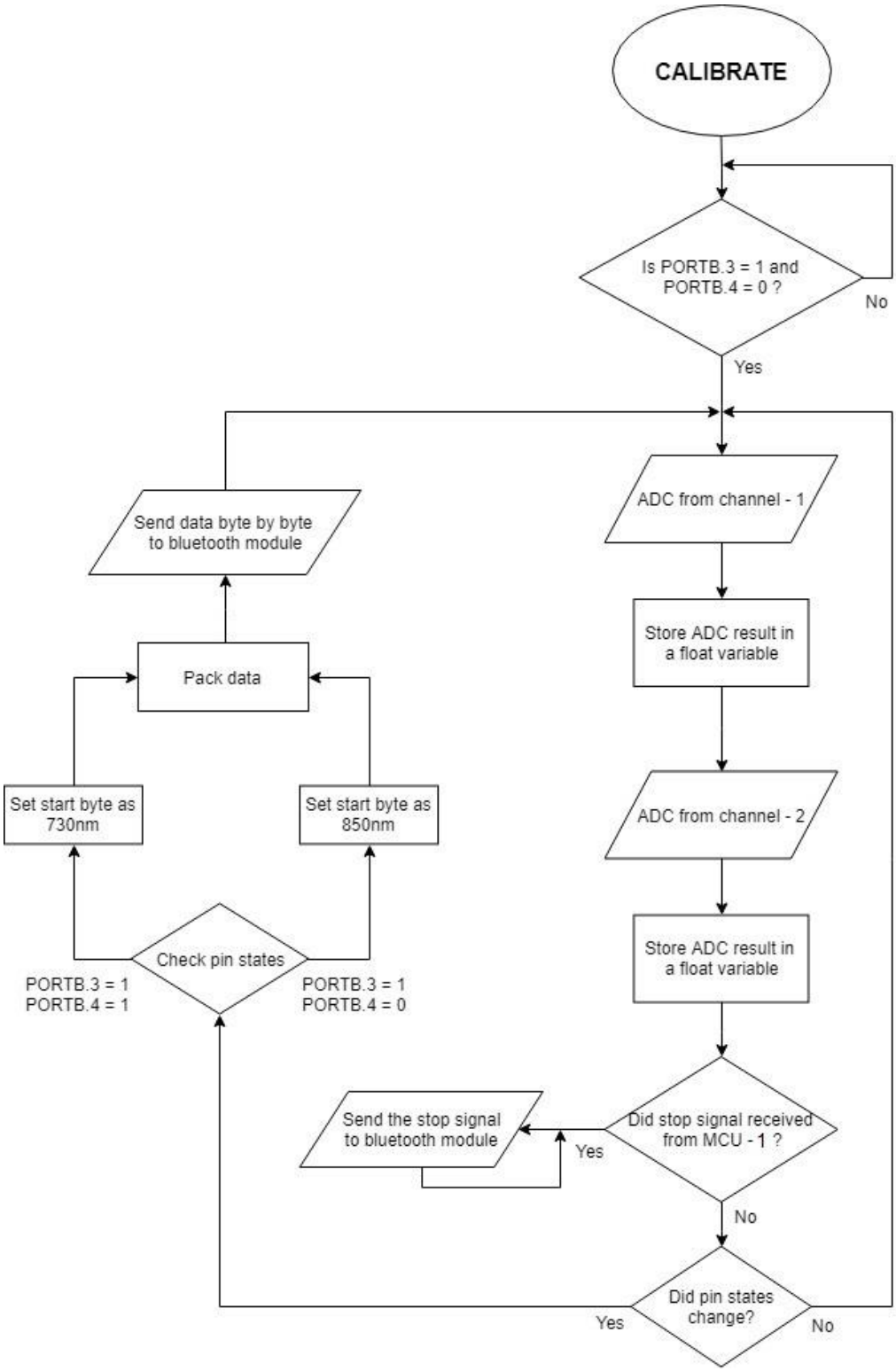
CALIBRATE
Is PORTB.3 = 1 and PORTB.4 = 0 ?
No
Yes
ADC from channel - 1
Store ADC result in a float variable
ADC from channel - 2
Store ADC result in a float variable
Did stop signal received from MCU - 1 ?
Yes
Send the stop signal to bluetooth module
No
Did pin states change?
Yes
No
Check pin states
PORTB.3 = 1
PORTB.4 = 1
PORTB.3 = 1
PORTB.4 = 0
Set start byte as 730nm
Set start byte as 850nm
Pack data
Send data byte by byte to bluetooth module

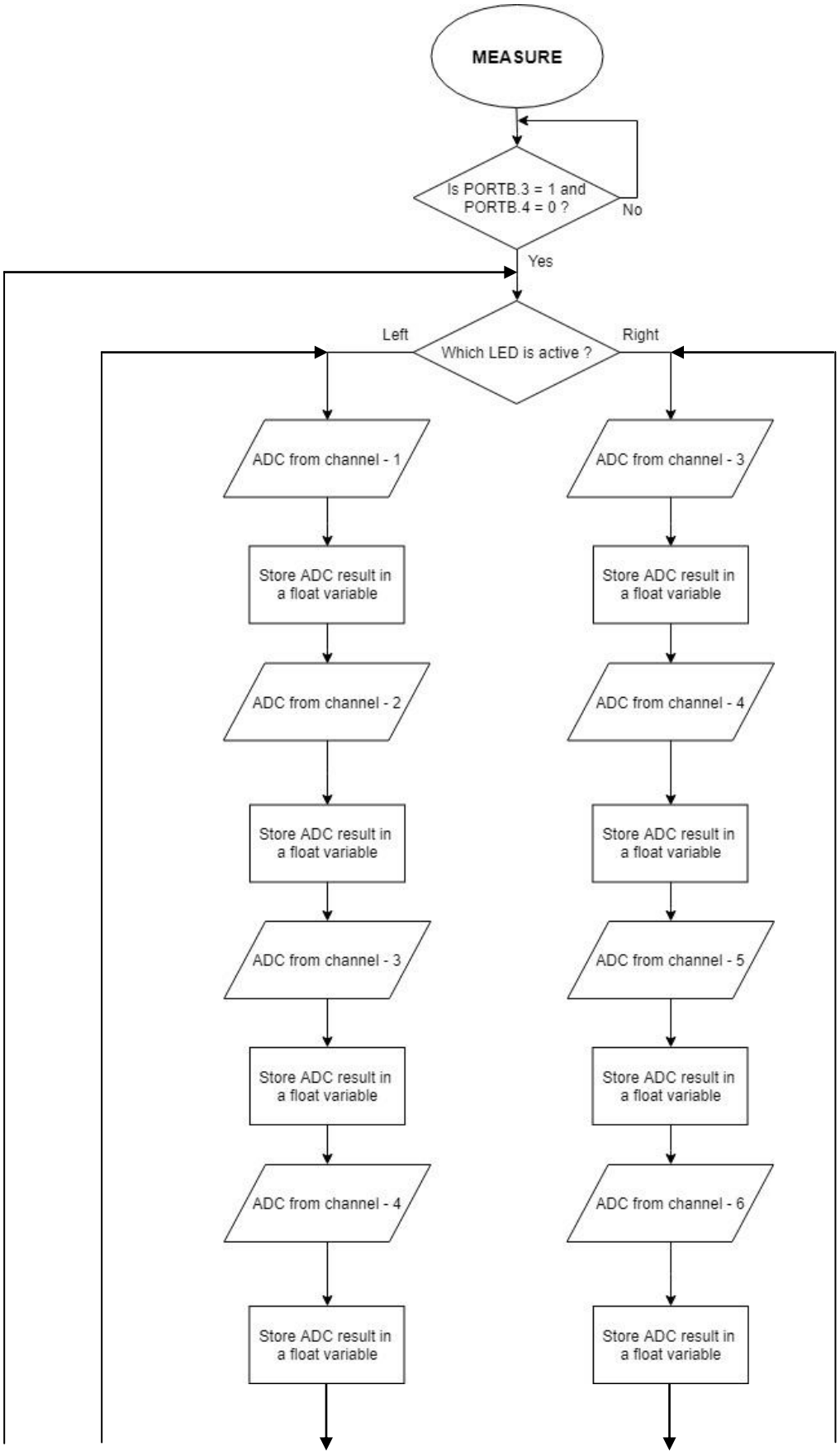
MEASURE
Is PORTB.3 = 1 and PORTB.4 = 0 ?
No
Yes
Left
Which LED is active ?
Right
ADC from channel - 1
Store ADC result in a float variable
ADC from channel - 2
Store ADC result in a float variable
ADC from channel - 3
Store ADC result in a float variable
ADC from channel - 4
Store ADC result in a float variable
ADC from channel - 3
Store ADC result in a float variable
ADC from channel - 4
Store ADC result in a float variable
ADC from channel - 5
Store ADC result in a float variable
ADC from channel - 6
Store ADC result in a float variable

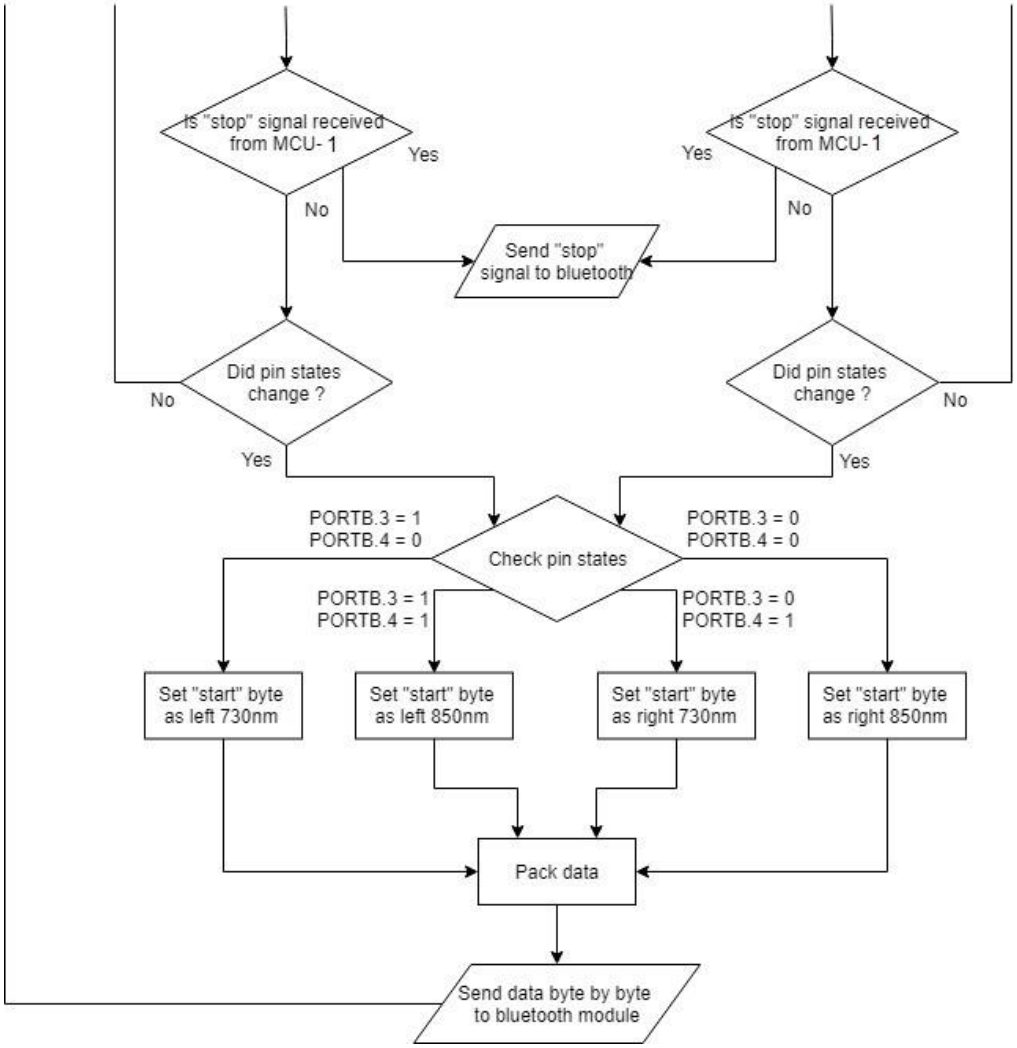

Figure 21: Flowchart of MCU-2's embedded code.

2.2. Head Probe

The head probe of Vega Vision consists of specially designed triple wavelength LED sources and photodetector integrated circuits (see figure 22). Light sources (S) and the detectors corresponding far (FC)/short (SC) channels are seen with the same colors in figure 23.

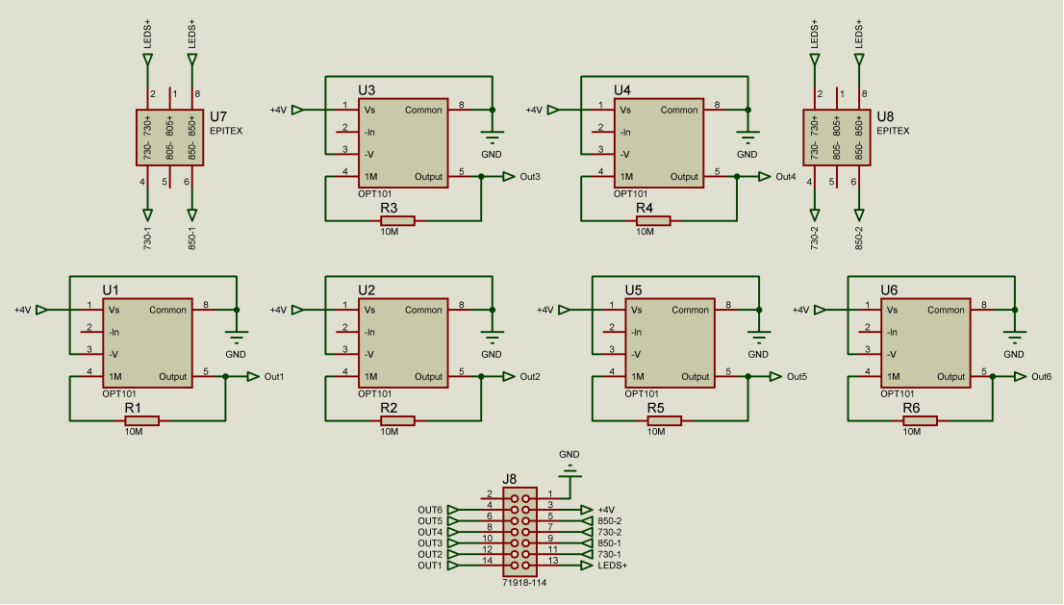

Figure 22: Schematic diagram of the head probe.

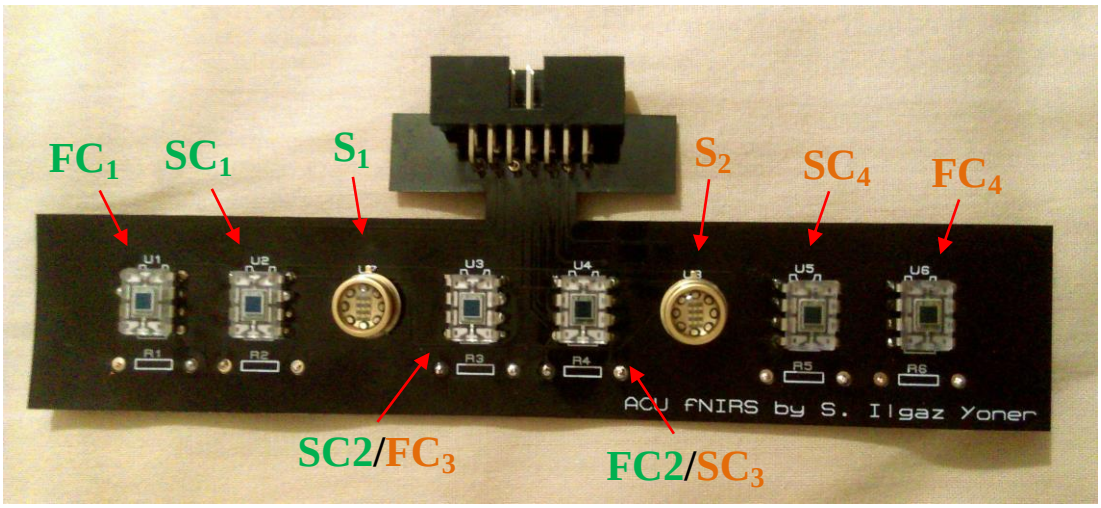

Figure 23: Front view of the head probe.

2.2.1. Light Sources

In the current design, L4*730/4*850/4*850-40Q96-1 (Marubeni, Japan) triple wavelength high power LEDs have been utilized. L4*730/4*850/4*850-40Q96-1 consists of 12 chips made of aluminum gallium arsenide material. These LEDs are mounted with aluminum nitride heat sink pedestal on TO-5 stems and sealed with flat glass cans. With its 730, 805 and 850nm wavelength LEDs, it is specifically designed for use in medical applications. Some fNIRS designs prefer the utilization of 805nm as the third wavelength, which is the exact point for equal extinction coefficients of Hb and HbO_2 in the electromagnetic spectrum. This third wavelength is considered as optional and was unnecessary in our design, therefore was not utilized. Regarding the datasheet of L4*730/4*850/4*850-40Q96-1, for proper operations 730 and 850nm LEDs require 7.6V and 5.6V at minimum, respectively. Since LEDs were fed via a constant current source, 10V supply voltage was found to be sufficient.

2.2.2. Light Detectors

OPT101 (Texas Instruments, TX, USA) monolithic photodiode and single-supply trans-impedance amplifier IC was chosen as the photo detecting solution. Six detectors were utilized for this 8 channel design. With its wide operating voltage bandwidth and internal amplification stage, OPT101 was the ideal choice for use in this head probe design. Internal amplification eliminates the external amplification requirement, thereby saving space and eliminating the chance of extra noise formation. Nevertheless, IC supports external amplification when needed. In this design, 10MΩ resistors were combined with 1MΩ internal resistors of the OPT101 to have a gain value of 11. Also, OPT101 is highly sensitive to electromagnetic waves in the near-infrared region of the spectrum which holds major importance in our design (see figure 24).

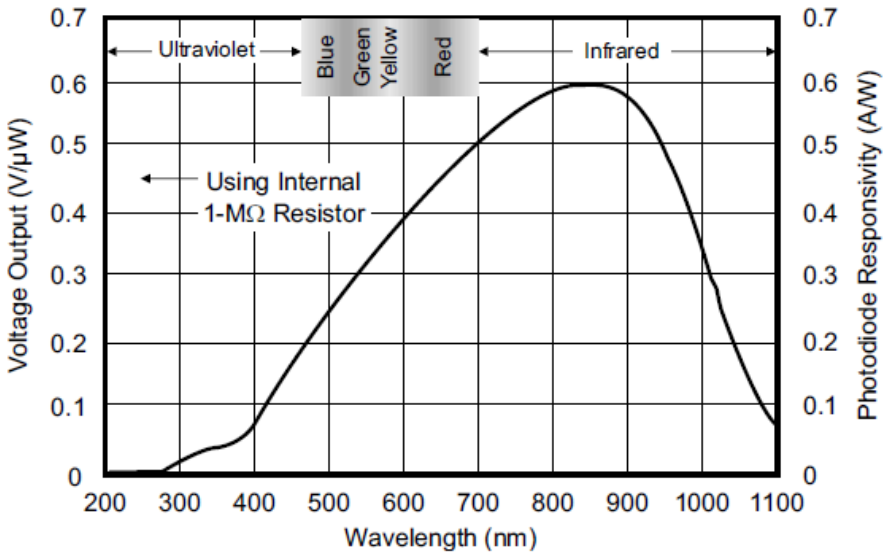

Figure 24: Spectral sensitivity of OPT101 (111).

2.3. Computerized Control System

To enhance the portability and comfort of the device, data transceiving is performed via Bluetooth technology and all calculations and data analysis have been handled by a computerized system. Almost all the modern day laptops are equipped with a Bluetooth module, which can be utilized to communicate with other electronic devices. Towards this approach, a software program is written in MATLAB R2016a for wireless control of the device.

MATLAB R2016a introduces a new tool called the “App Designer”. With the “App Designer”, graphical user interfaces (GUI) can be developed and integrated with codes written in MATLAB. After the completion of development stage, program must be compiled to have an executable (exe) file. With this exe in hand, MATLAB is no longer needed to control the fNIRS device. In short, any modern day laptop can be used to control the developed fNIRS device with the only requirement of a 13 megabyte sized small program. Developed GUI is shown in figure 25.

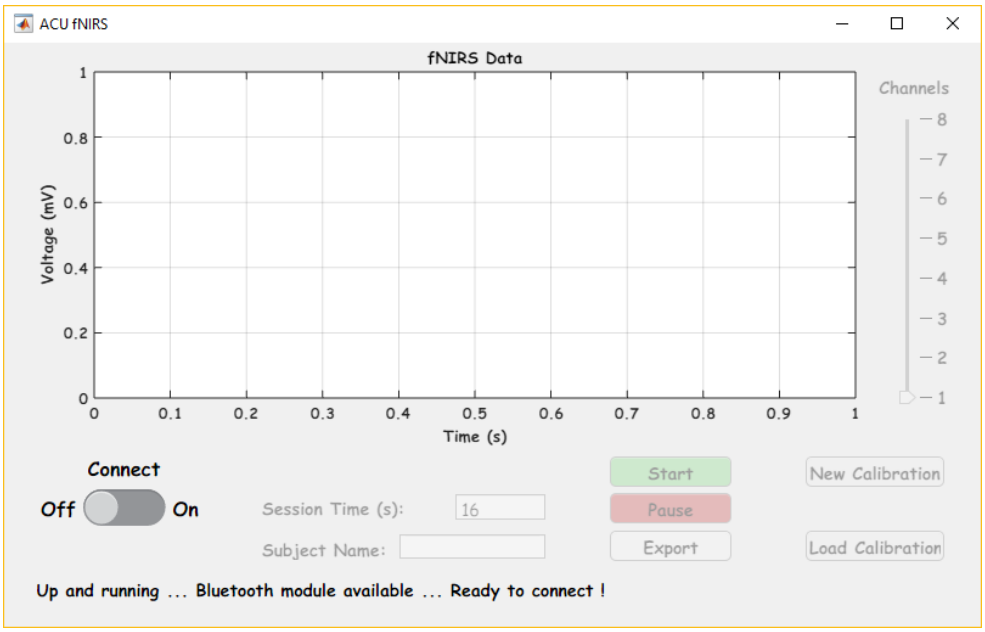

Figure 25: GUI of the developed program.

The computer program developed has the ability to start and pause a measurement session. Results of the latest measurement session can be exported to an Excel file for further investigations. Right after a measurements session, 730 and 850nm raw data measurements from channel 1 are automatically plotted in the chart field, the slider bar in the right hand side can be used to scroll through measurements for each channel. Although there is no developed phantom for calibrations, a calibration algorithm was also developed for use with a phantom. With an appropriate phantom, this calibration algorithm can be utilized to calibrate the device specifically for each subject. Subject-specific calibrating is in importance when skin color differences are taken into account (With this, quality of the measurements can be set as equal between an afro American and an Asian subject). Since the calibration is done for each wavelength separately, 730 and 850nm LEDs can run on different power levels thereby obtaining closer SNR values.

2.4. Printed Circuit Board

For a low noise hardware system rather than utilizing prototyping boards, PCBs were designed. This helps limit the amount of connections and solders required, thereby reducing the unwanted added impedance. Since black surfaces are known to

absorb light waves at their maximum compared other colors, with the optic measurements in mind PCBs were designed in black. Also, regarding the requirements of the project, main circuit board was chosen as a 1.6mm rigid PCB while the head probe was chosen as a .4mm flexible PCB. PCB drawings of the main board and the head probe are given in figure 26 and figure 27 respectively.

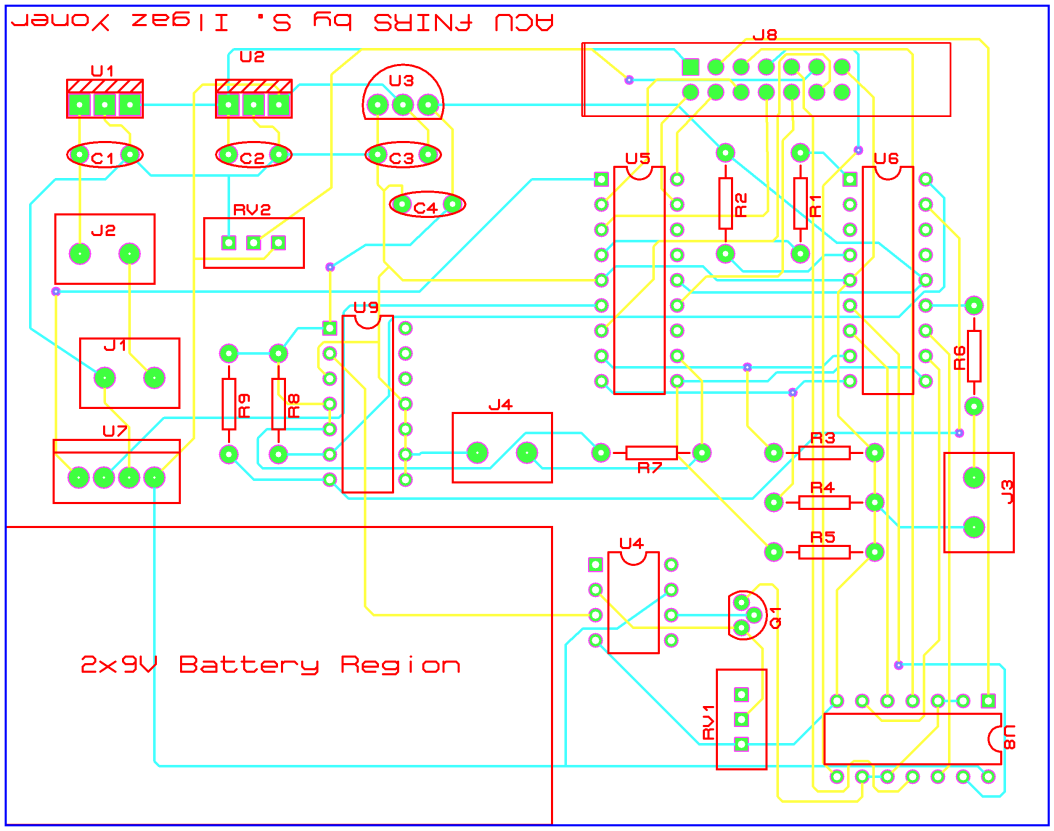

Figure 26: PCB design of the main board.

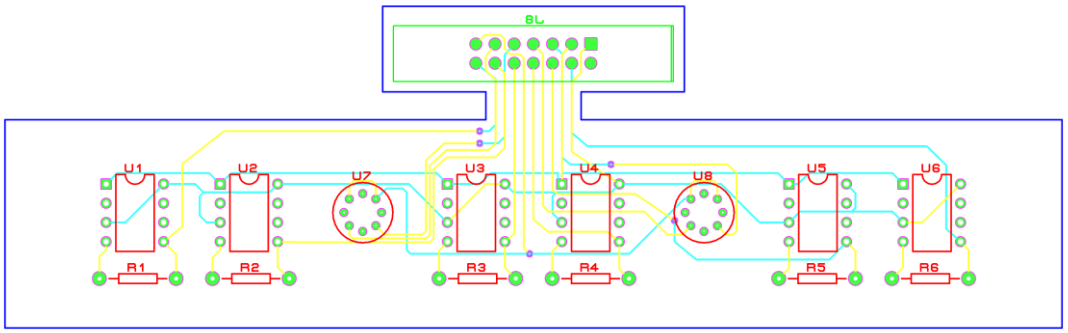

Figure 27: PCB design of the head probe.

2.5. Protective Case and Shield

Both rigid and flexible PCBs had to be electrically insulated and protected from environmental conditions. During the design process, Fusion 360 (Autodesk, CA, USA) was utilized. After the design process, M200 (Zortrax, Poland) 3D printer was utilized to manufacture the design. For the rigid PCB, a protective case design was manufactured from z-ultrat material (see figure 28). For the flexible PCB, a soft sponge-like material was cut and used as a simple shield (see figure 28).

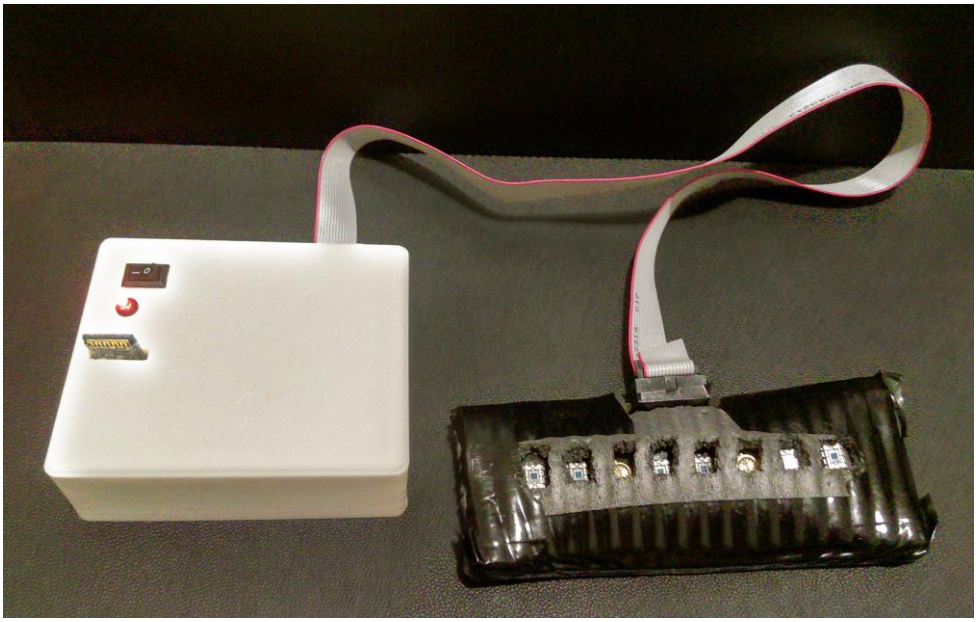

Figure 28: Designed fNIRS device with its protective case and head probe.

2.6. System Performance

To ensure the reliability of Vega Vision, a sample dark measurement was taken. For this measurement, all the sensors of the head probe were covered with a plain black material to make sure that no light is sensed by the sensory system. With this test, dark current of OPT101 sensors were measured while LEDs were turned off. Measurement results varied between 6 and 10mV. When referred to the electrical characteristics section in the datasheet of OPT101, it is clearly stated that output voltage may vary between 5 and 10mV as a cumulative result of dark error sources. Measurements for channel-1 are shown in figure 29.

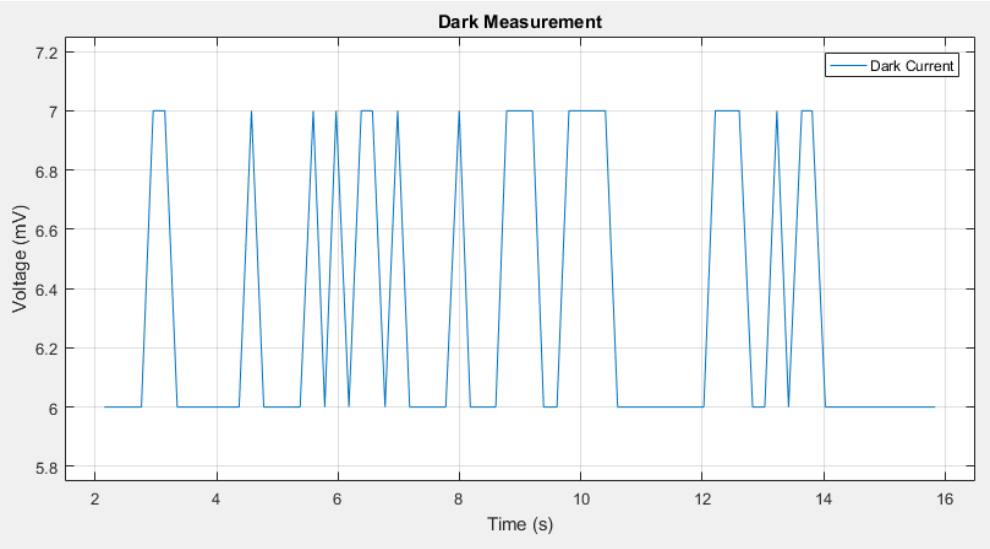

Figure 29: A sample measurement taken in a dark environment.

SNR values for all the sensors were calculated for the dark measurement test. Results were shown in table 3.

Table 3: Calculated mean values, standard deviations and coefficient of variations for dark current.

	FAR-1	SHORT-1	SHORT-2	FAR-2	FAR-3	SHORT-3	SHORT-4	FAR-4
MEAN:	6.31	6.04	6.00	6.81	6.00	9.00	6.00	6.79
STANDARD DEVIATION:	0.46	0.20	0.00	0.39	0.00	0.17	0.00	0.40
COEFFICIENT OF VARIATION:	7.38%	3.37%	0.00%	5.74%	0.00%	1.89%	0.00%	5.92%
SIGNAL TO NOISE RATIO (dB):	22.64	29.43	-	24.82	-	34.46	-	24.55

2.7. Experimental Protocol

Testing of Vega Vision was done via the head down test, which is the standard test used for verification of fNIRS systems. The test starts with the subject sitting on a chair in an upright position. After the first 20 seconds, subject is asked to bend over. In this period, one important thing is to execute the bending movement from torso, instead of neck. After proper execution, subject stays still in this bend over position for 30 seconds. With this 30 second period over, subject returns to the upright position and waits for another 80 seconds. The whole purpose of this head

down test is to force blood into and out of arterial capillaries of the frontal lobe with the help of gravitational pull. When the blood is forced into arterial capillaries, Hb and HbO_2 are also forced and a blood pool is formed in the region. Due to measurement principals of fNIRS technology, track of these hemodynamic changes is well possible. Timing diagram of the head down test and a sample measurement are shown in figure 30-31 respectively. A subject photo during test is shown in figure 32.

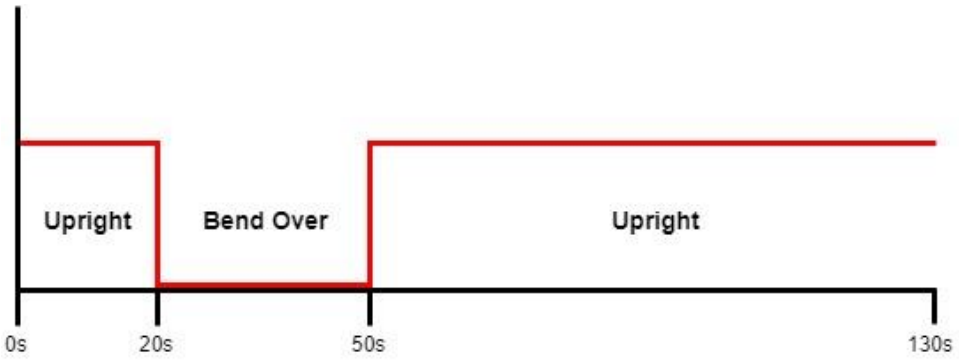

Figure 30: Head down test timing diagram.

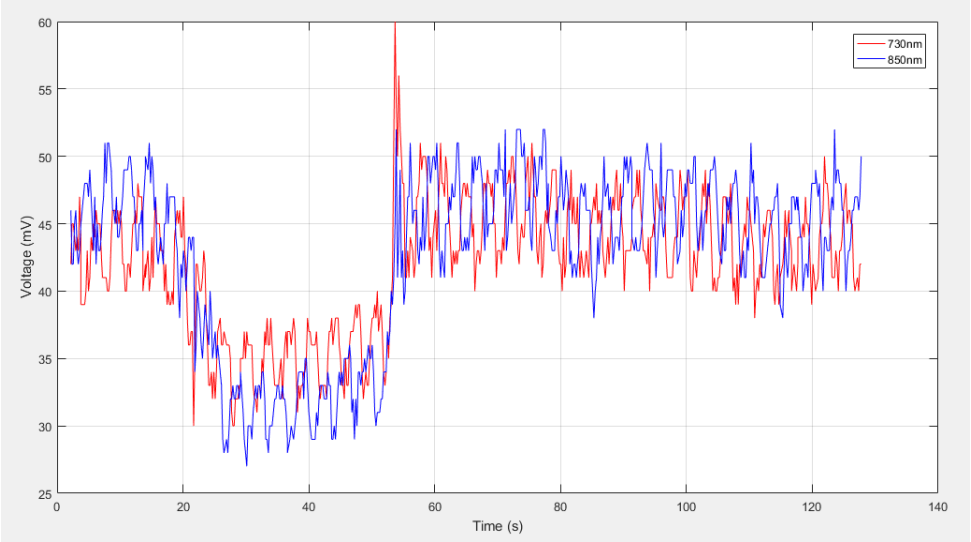

Figure 31: One channel sample data during the head down test.

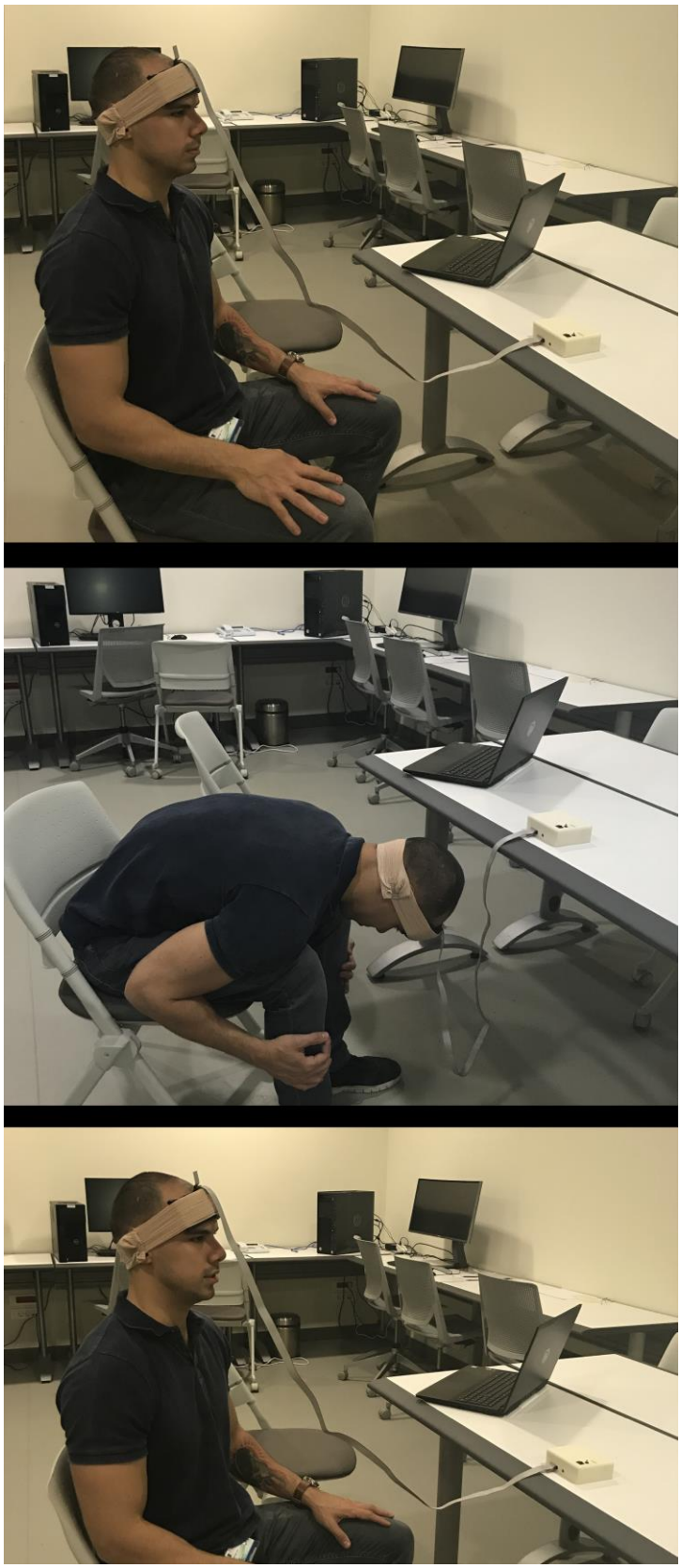

Figure 32: A subject during the head down test.

2.8. Data Conversion

To convert raw data into meaningful Hb and HbO_2 values, light absorption rates for both 730nm and 850nm wavelengths must be calculated with Eq.1.

$$\Delta OD^{\lambda_i} = \ln\left(\frac{I_o}{I}\right) = \varepsilon_{Hb,HbO_2}^{\lambda_i} \Delta C_{Hb,HbO_2} L \qquad \text{(Eq.1)}$$

ΔOD (optical density) represents the ratio of transitive light to emitted light, λ_i represents applied wavelength, $\varepsilon_{Hb,HbO_2}^{\lambda_i}$ represents molar absorption coefficients of different chromophores and $\Delta C_{Hb,HbO_2} L$ represents absolute change quantities of chromophores regarding the values of initial light waves. eq.1 must be adapted for Hb and HbO_2 separately as shown in eq.2 and eq.3.

$$\Delta[Hb] = \frac{\varepsilon_{HbO_2}^{\lambda_2} \Delta OD^{\lambda_1} - \varepsilon_{HbO_2}^{\lambda_1} \Delta OD^{\lambda_2}}{\left(\varepsilon_{Hb}^{\lambda_1} \varepsilon_{HbO_2}^{\lambda_2} - \varepsilon_{Hb}^{\lambda_2} \varepsilon_{HbO_2}^{\lambda_1}\right) L} \qquad \text{(Eq.2)}$$

$$\Delta[HbO_2] = \frac{\varepsilon_{Hb}^{\lambda_1} \Delta OD^{\lambda_2} - \varepsilon_{Hb}^{\lambda_2} \Delta OD^{\lambda_1}}{\left(\varepsilon_{Hb}^{\lambda_1} \varepsilon_{HbO_2}^{\lambda_2} - \varepsilon_{Hb}^{\lambda_2} \varepsilon_{HbO_2}^{\lambda_1}\right) L} \qquad \text{(Eq.3)}$$

With the Beer-Lambert Law (eq.2, eq.3), raw data have been converted into hemoglobin values and then filtered with a band pass (0.003-0.08Hz) Butterworth filter (figure 36).

2.9. Data Analysis

In total, 24 test subjects (ages with a mean of 24.8 and a standard deviation of ±4.1, 10 females in total) attended the head down test (see figure 32). Out of these 24 subjects, 11 of them were smokers while 13 were non-smokers. 8-channel raw data (4-channel far, 4-channel short sensors), collected from one of the healthy subjects is shown in figure 34 and figure 35 respectively. For detailed analysis of these measurements, Beer-Lambert law was utilized towards converting the raw data into hemoglobin values. After the hemoglobin values were obtained, a software based

filtering via Butterworth filter was applied. Converted and filtered values are shown in figure 36 under the results section. Simple analysis was made on all the measurements for two specific time periods. The first period (delta down) (see figure 33) was between times 20s and 50s (Head down period). For this period, differences between maximum and minimum values were calculated for all 8-channels. Times regarding all the measurements are well known. So, a simple code can easily look for maximum and minimum points for any time interval and calculate the absolute differences. Same operation was repeated for the second region (delta up) (see figure 33) which was times between 50s and 130s. Lastly, t-test was done on all the subjects for a better comparison between non-smokers and smokers. For a better understanding of all these calculations, two tables (table A.2 and table A.3 under appendix section) were made for two different time periods and subjects were categorized as non-smokers and smokers. Brief information is given in table 4 under results section.

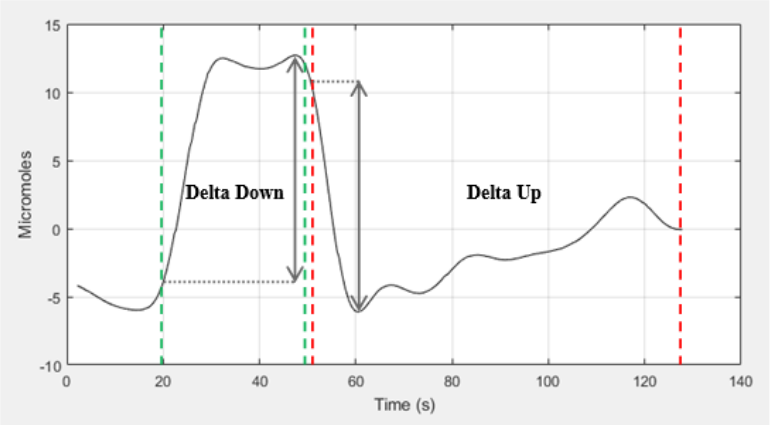

Figure 33: Delta down and delta up periods.

2.10. Statistical Analysis

Since two groups (non-smokers and smokers) had unequal variances and delta values for smokers were smaller in all cases (distribution in one side); 1 tail, type 3 t-test has been chosen. T-tests for non-smokers and smokers were calculated for both deltas down (table A.2) and delta up (table A.3) regions. Also, t-tests between contralateral channels were calculated for both groups and periods.

3. RESULTS

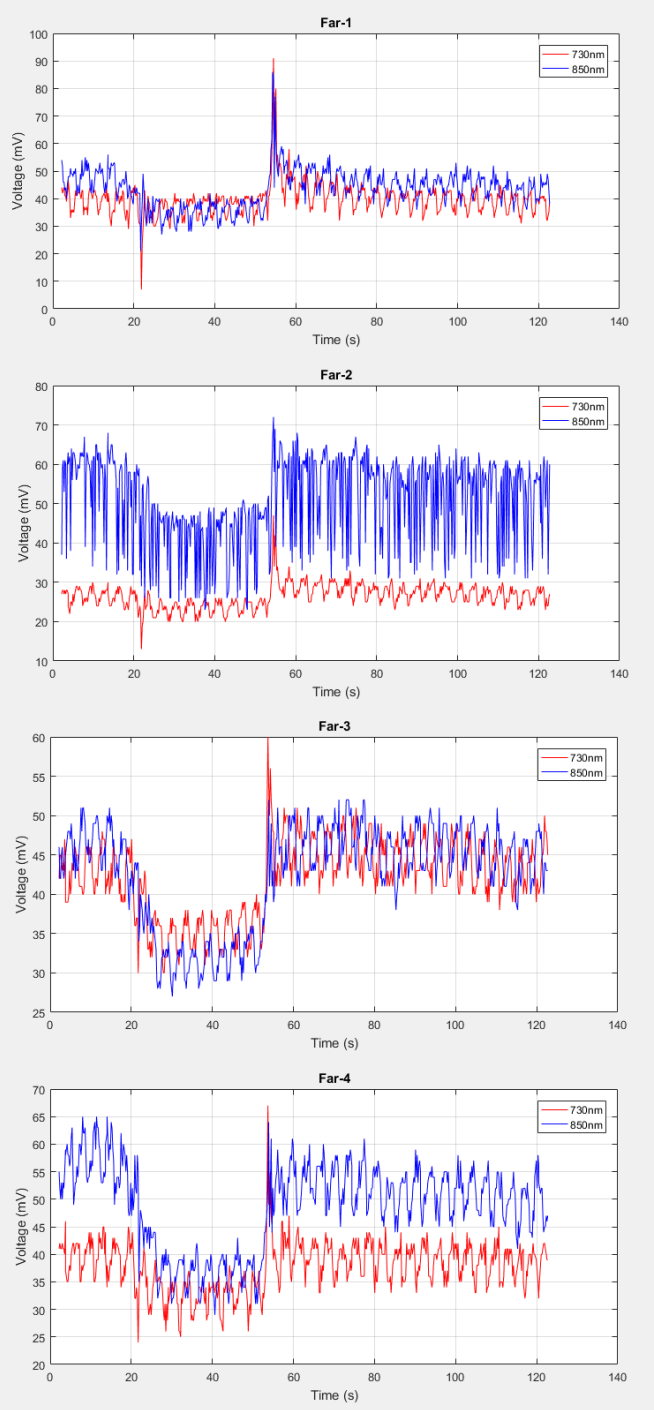

Figure 34: Far-channel raw data of a healthy subject.

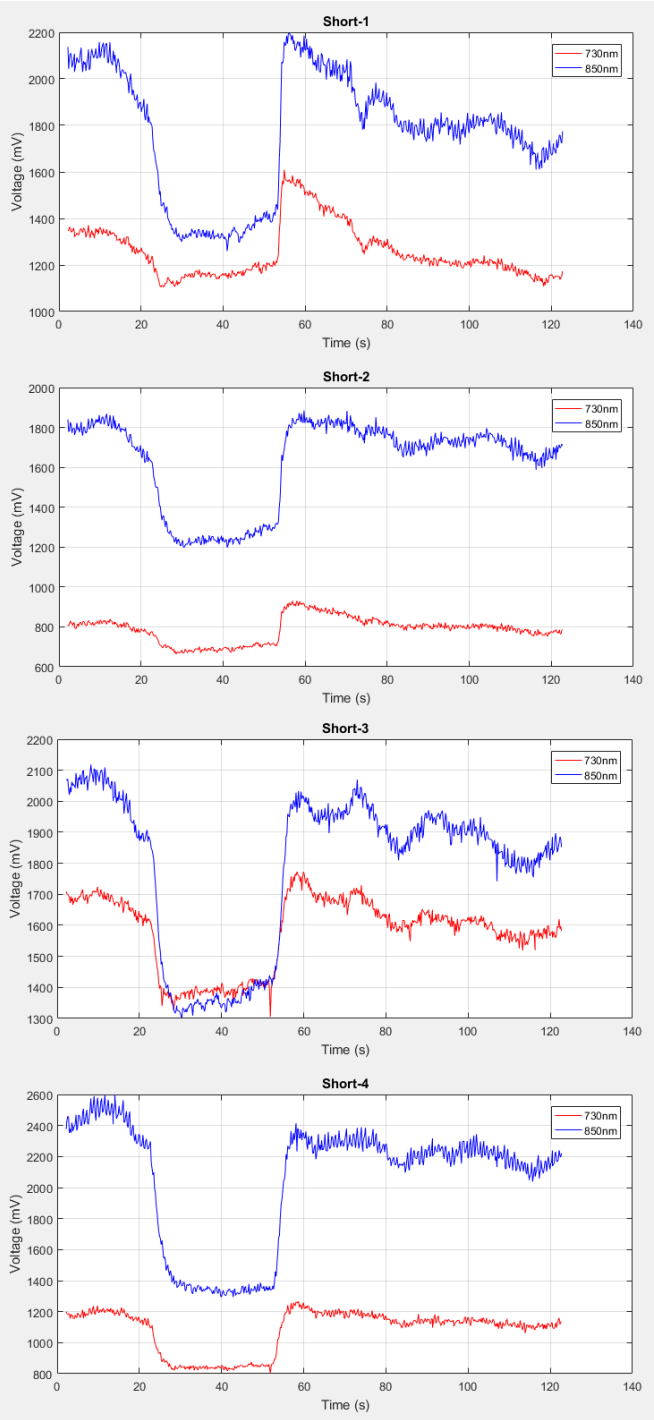

Figure 35: Short-channel raw data of a healthy subject.

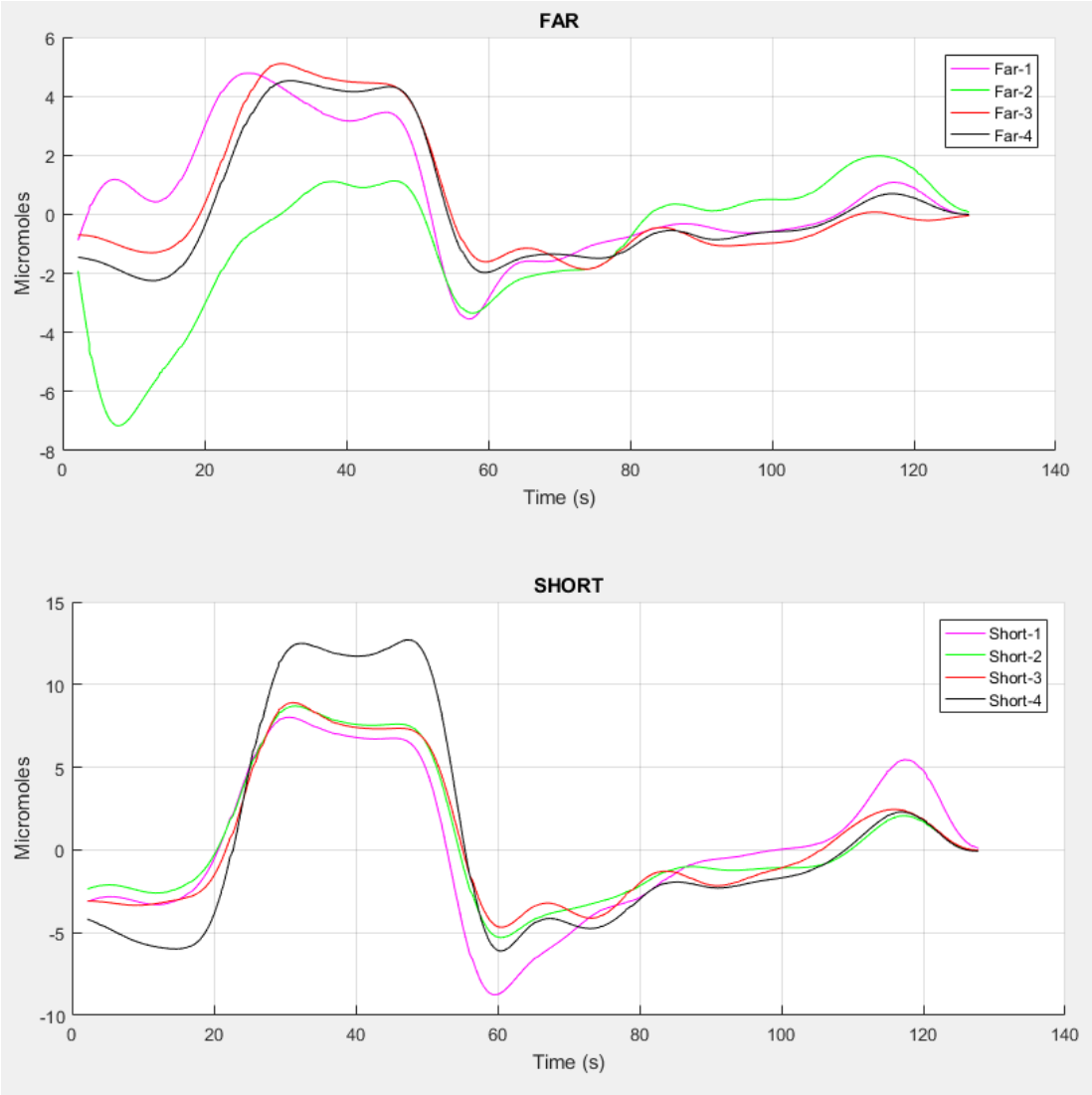

Figure 36: Converted and software based low pass filtered values of a healthy subject.

Table 4: Calculated mean values, standard deviations and t-tests for head down period.

▲Down	FAR-1	SHORT-1	SHORT-2	FAR-2	FAR-3	SHORT-3	SHORT-4	FAR-4
NON-SMOKERS								
MEAN:	2,88	9,09	10,57	6,18	5,96	17,85	16,85	3,39
STANDARD DEVIATION:	1,40	6,66	8,41	2,14	2,66	10,19	10,24	1,19
SMOKERS								
MEAN:	2,96	8,16	8,98	3,99	4,27	11,88	9,98	2,35
STANDARD DEVIATION:	2,02	6,62	6,37	1,79	1,79	5,37	7,76	1,13
P VALUES:	**0.458**	**0.374**	**0.310**	**0.008**	**0.046**	**0.048**	**0.044**	**0.024**

Table 5: Calculated mean values, standard deviations and t-tests for head up period.

▲Up	FAR-1	SHORT-1	SHORT-2	FAR-2	FAR-3	SHORT-3	SHORT-4	FAR-4
NON-SMOKERS								
MEAN:	3,17	11,04	11,19	6,13	5,88	17,18	16,51	3,60
STANDARD DEVIATION:	1,02	6,89	8,55	2,22	2,22	10,23	9,27	0,79
SMOKERS								
MEAN:	3,39	9,16	9,40	4,24	4,52	10,73	10,55	2,76
STANDARD DEVIATION:	1,89	6,21	6,67	1,58	1,66	4,58	7,53	0,83
P VALUES:	**0.376**	**0.254**	**0.293**	**0.015**	**0.059**	**0.033**	**0.055**	**0.013**

Table 6: T-test results between contralateral channels calculated separately for non-smokers and smokers.

	FAR-1/FAR-4	SHORT-1/SHORT-4	SHORT-2/SHORT-3	FAR-2/FAR-3
NON-SMOKERS ▲DOWN P VALUES:	**0.17**	**0.01**	**0.03**	**0.41**
SMOKERS ▲DOWN P VALUES:	**0.21**	**0.28**	**0.10**	**0.36**
NON-SMOKERS ▲UP P VALUES:	**0.13**	**0.05**	**0.06**	**0.38**
SMOKERS ▲UP P VALUES:	**0.17**	**0.32**	**0.30**	**0.35**

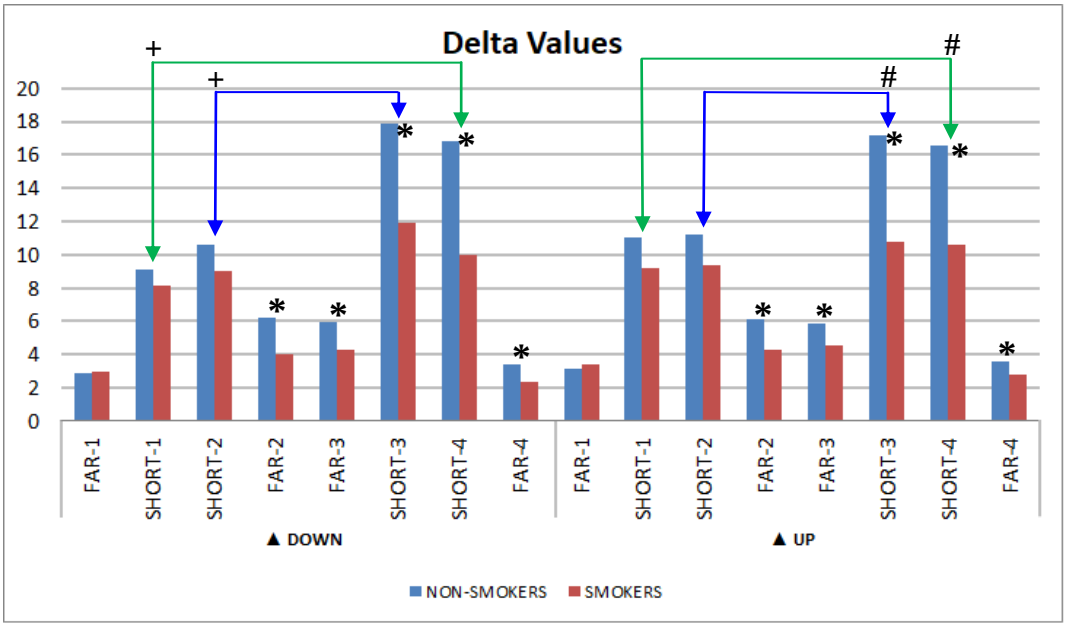

Figure 37: Delta values for both groups per channel as graphical bar representation (*smokers vs. non-smokers, # and + for contralateral comparisons).

4. DISCUSSION

From electronics design aspect, Vega Vision has a lot of room for improvement. For starters, one of the major goals of the project was to develop an fNIRS device suitable for use in sports activities and such. Towards achieving this goal, system was designed with batteries in mind. Two 9-volt carbon zinc batteries (18 volts in total) were utilized to power the device. Due to their chemical structure and technological limitations, 9-volt carbon zinc rechargeable batteries come with a battery life of 200 milliamps-hour at their best. For a longer battery life, lithium polymer batteries may be utilized instead of carbon zinc ones. Lithium polymer batteries have both higher current life and higher voltage compared to carbon zinc. In this case, one downside would be the extra space requirement related to increased battery size. Also, a simple low battery level indicating LED must be added to the device, so that the user can acknowledge this and charge the batteries before a measurement session. Currently, device runs on a sampling frequency of 5Hz which is acceptable for an fNIRS system. Still, sampling frequency could be increased so that any sudden hemodynamic change can be detected by the system and monitored by the operator. To be able to run two separate tasks at a time, two single core MCUs were utilized. With current technology, multiple core MCUs are available which has the ability to run multiple tasks at a time. A dual core MCU could be utilized in place of two separate single core MCUs. Although dual core MCUs are a more advanced technology, when compared to single core MCUs they are considerably expensive. For LED switching, MC14016B was utilized. At 25^{o}C, MC14016B has an approximate on resistance of 15Ω between any two circuits. Another analog switch with a lower on resistance value and a shorter switching time could be utilized to ensure desired performance. Wireless communication was achieved via HC-06 Bluetooth module. HC-06 uses Bluetooth version 2.0, which is not the most up to date version but the most commonly used one. Any of the higher versions of Bluetooth could be utilized for lower power consumption and higher communication speed. Instead of flat cables which are known to break easily and also cause signal interferences, connection between the main board and the head probe can be

achieved with circular multi-core cables. The program developed in MATLAB to control the fNIRS device was more than enough for an academic study. Still, one problem with the developed program was the lengthy start up time. To get rid of this issue, a similar program could be developed with a lower level language such as C for a lower program load. One huge problem was encountered during the design process of the head probe. A flexible PCB was designed and manufactured, so that the head probe can fit any individual's head firmly. Problem with this design was that flexible PCBs can endure only slight bending. If bent too much, copper traces can easily break, which was the case. A more original head probe design is absolutely necessary to ensure a long life for Vega Vision. Also, head down test should be repeated with a flat static white surfaced object to observe and thereby ensure that system does not produce any motion related artifacts. A slow but repetitive oscillation was observed in all channels of all the subjects with an approximate fixed frequency of 0.3Hz. This oscillation is most probably linked to respiration, which is also known to have a frequency of 0.2-0.3Hz in adults.

On the other hand, when compared to commercial fNIRS devices such as OctaMon, fNIRS103P, WOT-100 and NIRSport, Vega Vision has a couple of major advantages. Short/far detector head probe design allowed acquiring a higher SNR via channel subtraction methods. None of these devices are designed with a probe geometry that is suitable to such application. Furthermore, before channel subtraction methods were applied, SNR values of all the channels were over 20 decibel (dB) during dark measurement (table 3). Since systems resolution is limited to 1mV, probable oscillations at some channels lower than this limit were not detected. Therefore, standard deviations were computed as zero and SNR values were theoretically infinite. An SNR of 20 dB and over is considered more than acceptable. The utilized digital potentiometer allowed the user to run LEDs at different power levels. Throughout the testing process and afterwards, this feature proved its usefulness. With some subjects, sensors seem to saturate when LEDs were run at high power levels. To prevent sensors from saturating, LEDs were adjusted to run at lower power levels. This feature is found in neither of these devices. Also, Vega Vision is far cheaper than any of these devices with a cost of 330$, including unexpected expenses. Also Vega Vision is a lightweight device just like these other

devices mentioned above. Vega Vision is specially designed for applications such as sports activity, therefore easily wearable.

When results were examined, p values for far-2, far-3, far-4, short-3 and short-4 channels were around or lower than 0.05 for both regions indicating clear differences between two groups.

Results suggest less arterial vasodilation in smokers when compared to non-smokers. Physiologically, there is a known correlation between amount of smooth muscle cells found in arterial walls and vasodilation capability of arteries. Healthy smooth muscle cells are known to control vasodilation and vasoconstriction by relaxation and contraction. As in fluid mechanics, increased radius of a pipe leads to decreased pressure difference between two ends of that pipe. Blood vessels can be thought as equivalent of these pipes and same laws would apply. In a study done, tobacco constituents were found to have mitogenic effects on arterial smooth muscle cells which result in excessive number of smooth muscle cells in the region. Thereby decreased elastic property caused by thickening of arterial walls (112). A study done on rats revealed that chronic nicotine exposure decreases cerebral blood flow (113). Physically, increased blood flow results in increased pressure against arterial walls. This physical phenomenon leads to a physiological phenomenon; increased arterial wall pressure (hypertension) triggers vasodilation. Vasodilation abnormalities of smokers compared to non-smokers may be also affected by reduced cerebral blood flow, thereby less arterial wall pressure followed by less vasodilation. In a study done by Zhang JY and colleagues, lipid soluble smoke particles were used to incubate human middle cerebral arteries. After some time, the procedure resulted in swelling and detaching of endothelium from underlying structures which impaired endothelium dependent dilatation (114). Another study showed that cigarette smoking causes in increased elastic modulus and wall thickness in mouse coronary arteries (115). Briefly, there are plenty of solid findings in science literature pointing out to harming effects of acute, short term and long term smoking.

P values for far-1, short-1 and short-2 channels were higher than .05 indicating insufficient differences between two groups. Vega Vision's system performance tests proved proper operations of its sensory systems. Therefore, these measurement results can only be explained with possibility of anatomical and/or physiological hemispheric asymmetries of the human brain. Although a detailed research was carried out to bring a physiological explanation to this phenomenon, no related academic study was found on internet. One explanation for this may be an unknown cerebral blood flow asymmetry between left and right carotid arteries. If the blood flow of right carotid artery is slower compared to its left counterpart, this may also decrease vasodilation through reduced arterial wall tension. Another explanation may be related to smooth muscle cells found in arterial walls. Mitogenic effects of tobacco constituents on smooth muscle cells may be much more dominant in the right hemispheric arteries as a result of structural and functional nature of human brain. As RB Panerai stated in his study; metabolites and chemical mediators responsible for vasomotor control of the cerebral circulation require some time to affect. Therefore, any sudden change in arterial blood pressure undesirably influences cerebral blood flow until the effects of these metabolites and chemicals kick in. However, when they do kick in, cerebral blood flow returns to its original level (116). Also, results of a study done with Valsalva maneuvers found that a 5 to 8 second delayed response is present autoregulation mechanism (117). Findings of a study done by BL Edlow showed that healthy aging alters the magnitude of changes in frontal cortical HbO_2 (118).

To further investigate whether an asymmetrical vasodilation exists in human brain, t-tests between contralateral channels were calculated for non-smokers and smokers for both periods (table 6). For both periods, non-smokers' short-1 vs. short-4 and short-2 vs. short-3 t-test results were lower than 0.05 pointing out to the existence of such an asymmetrical behavior. Since this huge difference between contralateral regions of human brain were observed with short channels, this asymmetrical behavior may only be valid for capillary arteries found under skin but not brain capillaries. When it comes to far channels, results suggested a much more symmetrical behavior. This difference may be due to rapid response of peripheral arteries which results in immediate vasodilation, while pressure changes in capillary

arteries just under the skin are much smaller and actualize with latency. Still, existence of such an asymmetric behavior remains to be investigated and verified with other methodologies (i.e. laser blood flow systems).

5. CONCLUSION

Main goal of this thesis project was to develop an accurate wearable wireless fNIRS device with a minimal probe configuration consisting of short and far detectors. As of today, no such integration of methodologies exists in fNIRS devices. In overall, developed wireless fNIRS device "Vega Vision" was a success. Vega Vision's head probe geometry, lightweight wearable design, unique calibration algorithm, high data acquisition rate (5Hz) and power mode optimization are its distinctive features. Control of the device is achieved through a user interface.

Vega Vision's clinical utility is investigated with a head-tilt maneuver. Preliminary results from non-smokers and smoker reveal statistically significant differences proposing that Vega Vision is a safe, low-cost and easy-to-use fNIRS device that has a potential for use in a clinical setting.

Future Work:

Only major drawback of Vega Vision was its carbon zinc batteries which had short current life. For long measurement sessions, another type of battery must be utilized. An accelerometer may be added to sense motion related artifacts and eliminate these artifacts with means of software. To have much more accurate results, steps explained in the experimental protocol section (such as bend over – straighten up angles and times) must be applied by subjects with precision. Also, test subjects must be handpicked according to test criteria such as age, height, weight, gender, hunger level, caffeine intake, years of smoking and subject's last time of smoking. Applying the testing protocol on more strictly formed test groups (non-smokers/smokers) would definitely generate much more solid results. Still, results of the testing protocol from both non-smokers and smokers had its significance. With time, a better understanding of human brain physiology may help interpret fNIRS results in a much more detailed manner. To continue to prove the reliability of Vega Vision, more complex tests such as cognitive tests should be held with the device. To this end, just like single-photon emission computed tomography (SPECT) and MRI, combining fNIRS technology with other well established ones such as EEG may

provide right answers. Instead of all the difficulties of fNIRS technology, in time, small but prominent advancements may help technology take its place in clinics.

APPENDIX A.

Table A.1: Measurement results, calculated mean values, standard deviations and coefficient of variations for dark current.

Time (s)	FAR-1	SHORT-1	SHORT-2	FAR-2	FAR-3	SHORT-3	SHORT-4	FAR-4
2.15	6	6	6	6	6	9	6	7
2.35	6	6	6	7	6	9	6	7
2.56	6	6	6	7	6	9	6	7
2.76	6	6	6	7	6	9	6	7
2.96	7	6	6	7	6	9	6	7
3.15	7	6	6	7	6	9	6	7
3.35	6	6	6	7	6	9	6	7
3.57	6	6	6	7	6	9	6	7
3.77	6	6	6	7	6	9	6	7
3.95	6	6	6	7	6	9	6	6
4.18	6	6	6	6	6	9	6	6
4.37	6	6	6	6	6	9	6	7
4.57	7	6	6	7	6	9	6	6
4.78	6	6	6	7	6	9	6	6
4.98	6	6	6	6	6	10	6	7
5.18	6	6	6	6	6	9	6	7
5.38	6	6	6	7	6	8	6	7
5.59	7	6	6	7	6	9	6	7
5.78	6	6	6	7	6	9	6	6
5.97	7	6	6	7	6	9	6	6
6.18	6	6	6	7	6	9	6	7
6.38	7	6	6	7	6	9	6	7
6.57	7	6	6	7	6	9	6	7
6.78	6	6	6	6	6	9	6	7
6.98	7	6	6	7	6	9	6	7
7.18	6	6	6	6	6	9	6	6
7.38	6	6	6	7	6	9	6	6
7.57	6	7	6	6	6	9	6	7
7.78	6	6	6	7	6	9	6	7
8.00	7	6	6	7	6	9	6	7
8.18	6	6	6	7	6	9	6	7
8.42	6	6	6	7	6	9	6	7
8.60	6	6	6	7	6	9	6	7
8.78	7	6	6	7	6	9	6	7
9.00	7	6	6	7	6	9	6	7
9.21	7	6	6	6	6	9	6	7

9.39	6	6	6	7	6	9	6	7
9.61	6	6	6	7	6	9	6	6
9.81	7	6	6	7	6	9	6	7
10.00	7	7	6	7	6	9	6	6
10.22	7	6	6	7	6	9	6	7
10.41	7	6	6	7	6	9	6	6
10.61	6	6	6	7	6	9	6	7
10.80	6	6	6	7	6	9	6	7
11.00	6	6	6	7	6	9	6	7
11.21	6	6	6	7	6	9	6	7
11.41	6	6	6	7	6	9	6	7
11.61	6	6	6	7	6	9	6	7
11.83	6	6	6	7	6	9	6	7
12.03	6	6	6	7	6	9	6	7
12.22	7	6	6	7	6	9	6	7
12.43	7	6	6	7	6	9	6	6
12.61	7	6	6	6	6	9	6	7
12.83	6	6	6	7	6	9	6	7
13.03	6	6	6	7	6	9	6	7
13.23	7	6	6	7	6	9	6	6
13.42	6	6	6	6	6	9	6	7
13.65	7	6	6	6	6	9	6	7
13.81	7	6	6	7	6	9	6	7
14.03	6	6	6	7	6	9	6	6
14.22	6	6	6	7	6	9	6	7
14.44	6	6	6	7	6	9	6	7
14.63	6	6	6	7	6	9	6	7
14.82	6	6	6	7	6	9	6	7
15.04	6	7	6	7	6	9	6	7
15.24	6	6	6	6	6	9	6	7
15.45	6	6	6	7	6	9	6	7
15.65	6	6	6	7	6	9	6	7
15.84	6	6	6	7	6	9	6	7
MEAN:	**6.32**	**6.04**	**6.00**	**6.81**	**6.00**	**9.00**	**6.00**	**6.80**
STANDARD DEVIATION:	**0.47**	**0.20**	**0.00**	**0.39**	**0.00**	**0.17**	**0.00**	**0.40**
COEFFICIENT OF VARIATION:	**7.38%**	**3.37%**	**0.00%**	**5.74%**	**0.00%**	**1.89%**	**0.00%**	**5.92%**
SIGNAL TO NOISE RATIO (dB):	**22.65**	**29.44**	**-**	**24.82**	**-**	**34.46**	**-**	**24.56**

Table A.2: Calculated differences between maximum and minimum values for head down period.

▲Down	FAR-1	SHORT-1	SHORT-2	FAR-2	FAR-3	SHORT-3	SHORT-4	FAR-4
NON-SMOKERS:								
SUBJECT-1	5,01	4,00	8,80	5,07	6,47	9,86	9,36	5,12
SUBJECT-2	1,90	4,89	6,64	7,26	9,40	14,50	10,77	2,49
SUBJECT-3	5,20	10,78	10,10	8,34	7,88	20,27	46,09	6,01
SUBJECT-4	1,93	4,23	8,02	4,55	2,66	6,40	13,69	2,81
SUBJECT-5	5,16	8,47	12,28	3,50	5,48	21,25	12,63	2,63
SUBJECT-6	3,72	27,16	38,46	9,78	12,25	46,74	32,20	4,21
SUBJECT-7	3,00	12,81	11,19	5,45	5,06	11,67	15,25	2,30
SUBJECT-8	1,10	4,89	4,15	5,98	3,95	11,94	8,98	2,70
SUBJECT-9	2,33	5,23	3,60	9,28	7,65	19,83	10,09	3,04
SUBJECT-10	1,70	2,88	7,75	8,82	5,83	26,84	14,53	3,20
SUBJECT-11	1,84	5,91	6,88	4,11	3,15	10,11	10,88	2,13
SUBJECT-12	3,00	8,52	8,96	4,15	4,72	10,40	16,52	4,88
SUBJECT-13	1,50	18,35	10,54	4,034	3,01	22,26	18,08	2,58
SMOKERS:								
SUBJECT-14	1,62	4,79	5,75	3,70	4,07	13,31	6,34	1,40
SUBJECT-15	4,60	5,66	7,43	6,91	6,89	14,81	8,26	4,07
SUBJECT-16	1,67	1,48	4,22	4,53	4,59	13,62	5,71	1,44
SUBJECT-17	1,34	7,47	9,00	4,18	3,07	12,98	7,06	1,81
SUBJECT-18	5,74	7,55	6,78	3,80	4,35	5,37	8,75	4,38
SUBJECT-19	7,21	13,27	12,45	6,23	7,56	18,19	10,44	3,91
SUBJECT-20	2,11	14,35	12,81	4,35	5,29	14,47	14,42	2,24
SUBJECT-21	4,17	25,02	26,81	5,54	4,83	21,04	32,93	2,35
SUBJECT-22	0,81	2,25	4,01	1,70	1,74	6,64	3,37	1,30
SUBJECT-23	1,40	3,51	3,83	2,07	2,97	7,47	6,78	1,56
SUBJECT-24	1,88	4,37	5,71	0,86	1,66	2,74	5,74	1,421
P VALUES (T-TEST):	**0.458**	**0.374**	**0.310**	**0.008**	**0.046**	**0.048**	**0.044**	**0.024**

Table A.3: Calculated differences between maximum and minimum values for head up period.

▲Up	FAR-1	SHORT-1	SHORT-2	FAR-2	FAR-3	SHORT-3	SHORT-4	FAR-4
NON-SMOKERS:								
SUBJECT-1	3,70	4,67	7,20	3,76	5,23	7,14	10,91	4,47
SUBJECT-2	2,16	5,23	7,10	8,26	8,43	14,68	9,75	2,73
SUBJECT-3	4,13	11,18	10,86	6,47	6,02	15,61	41,22	3,85
SUBJECT-4	2,18	7,10	9,16	4,79	3,64	8,18	15,39	4,03
SUBJECT-5	3,40	10,62	14,72	6,66	6,62	20,78	13,67	3,26
SUBJECT-6	4,46	29,83	39,06	10,39	12,20	48,56	31,67	4,58
SUBJECT-7	3,28	11,01	9,54	4,56	5,32	12,39	13,98	2,94
SUBJECT-8	2,59	7,40	5,61	4,72	4,82	12,07	9,46	3,34
SUBJECT-9	1,70	6,05	4,31	9,96	6,64	17,30	8,95	2,43
SUBJECT-10	2,77	8,54	7,51	7,50	4,43	20,34	12,70	3,16
SUBJECT-11	3,61	6,62	5,95	3,42	3,96	11,39	9,39	3,06
SUBJECT-12	5,31	14,21	11,65	5,32	5,22	11,13	17,58	5,33
SUBJECT-13	2,01	21,12	12,86	3,98	3,93	23,90	20,03	3,65
SMOKERS:								
SUBJECT-14	1,63	5,80	7,88	5,01	4,80	12,02	8,84	2,15
SUBJECT-15	4,02	4,61	6,07	4,67	5,77	13,36	6,95	3,38
SUBJECT-16	1,56	2,58	4,45	5,40	4,50	13,30	7,18	1,84
SUBJECT-17	4,39	8,94	10,36	5,92	6,08	12,22	7,39	3,98
SUBJECT-18	3,05	9,41	7,02	2,11	1,88	5,11	9,05	2,28
SUBJECT-19	8,15	14,46	12,63	7,15	7,23	14,77	10,11	3,57
SUBJECT-20	2,91	10,62	8,47	2,70	3,39	9,22	9,08	2,80
SUBJECT-21	5,00	25,99	28,78	5,29	6,52	19,73	34,13	3,67
SUBJECT-22	3,34	8,42	2,57	3,02	3,41	9,60	9,45	2,95
SUBJECT-23	1,50	4,77	5,99	2,55	4,05	5,15	6,41	1,09
SUBJECT-24	1,79	5,19	9,20	2,90	2,19	3,65	7,55	2,76
P VALUES (T-TEST):	**0.376**	**0.254**	**0.293**	**0.015**	**0.059**	**0.033**	**0.055**	**0.013**

APPENDIX B.

```
raw_data = xlsread('XXX.xlsx');

fs=5;
[M,N]=size(raw_data);
Mean_duration= 1; % Duration of data to calculate the mean for baseline
(first 2 seconds)
t=linspace(0,M/fs,M);
M_base=round(fs*Mean_duration); %Takes the first Mean_duration
seconds as the baseline calculation
mean_data=mean(raw_data(2:M_base,:),1); % Drop the first point in
baseline calculation

od730=zeros(M,8);
od850=zeros(M,8);

for k=0:7
   od730(1:580,k+1)=log10(mean_data(2*k+1)./raw_data(1:580,2*k+1));
   od850(1:580,k+1)=log10(mean_data(2*k+2)./raw_data(1:580,2*k+2));
end
%%%%%%%%%%%%%%CALCULATIONS BASED ON BEER-LAMBERT
LAW%%%%%%%%%%

eHB_730=1.1022;
eHBO2_730=0.390;
eHB_850=0.69132;
eHBO2_850=1.058;

HB=(od850*eHBO2_730-od730*eHBO2_850)/(eHBO2_730*eHB_850-
eHBO2_850*eHB_730)/0.015;
HBO2=(od730*eHB_850-od850*eHB_730)/(eHBO2_730*eHB_850-
eHBO2_850*eHB_730)/0.015;

[b,a]=butter(4,[0.003 0.08]/(fs/2));
```

```
%filt_ss1=filtfilt(b,a,ss1);
HBO2f=filtfilt(b,a,HBO2); % Filtering the low freq values and leaving only high freq data
HBO2fm=mean(HBO2f,2); % Major Regressor for the PC analysis

HBf=filtfilt(b,a,HB); % Filtering the low freq values and leaving only high freq data
HBfm=mean(HBf,2); % Major Regressor for the PC analysis

BV=HBO2f+HBf;

[b,a]=butter(4,[0.09 0.6]/(fs/2));

%filt_ss1=filtfilt(b,a,ss1);
HBO2h=filtfilt(b,a,HBO2); % Filtering the low freq values and leaving only high freq data
HBO2hm=mean(HBO2h,2); % Major Regressor for the PC analysis

HBh=filtfilt(b,a,HB); % Filtering the low freq values and leaving only high freq data
HBhm=mean(HBh,2); % Major Regressor for the PC analysis

BVh=HBO2h+HBh;
```

APPENDIX C.

ACIBADEM MEHMET ALİ AYDINLAR ÜNİVERSİTESİ

İnsan Araştırmaları Kurumsal Değerlendirme Başvuru Formu

I. Kişisel Bilgiler:

1. Başvuruyu yapan Proje Yöneticisi/Araştırmacının adı ve kurumsal bilgileri:

Adı, Soyadı, Ünvanı: Ata Akın, Prof. Dr.

Fakülte/Bölümü: Acıbadem Mehmet Ali Aydınlar Üniversitesi Fen Bilimleri Enstitüsü, Tıp Mühendisliği Programı

Araştırmadaki Sorumluluğu: Proje Yürütücüsü

Proje Ekibi:

Adı, Soyadı, Ünvanı: Serhat Ilgaz Yöner, Yüksek Lisans Öğrencisi

Fakülte/Bölümü: Acıbadem Mehmet Ali Aydınlar Üniversitesi Fen Bilimleri Enstitüsü, Tıp Mühendisliği Programı

Araştırmadaki Sorumluluğu: Yardımcı Araştırmacı

2. İletişim Bilgileri:

Ata Akın, Prof. Dr.

Adres: Acıbadem Mehmet Ali Aydınlar Üniversitesi Fen Bilimleri Enstitüsü

Telefon: (0216) 500 4144

E-posta: Ata.Akin@acibadem.edu.tr

Serhat Ilgaz Yöner

Adres: Acıbadem Mehmet Ali Aydınlar Üniversitesi Fen Bilimleri Enstitüsü

Telefon: (0539) 746 0155

E-posta: ilgazyoner@gmail.com

II. Önerilen Araştırma ile ilgili bilgiler

1. Projenin Adı:

Geliştirilmiş olan fNIRS sisteminin ölçüm doğruluğunun kanıtlanması.

2. Projenin Kısa Özeti (20 satırı geçmeyecek şekilde):

fNIRS (functional near infrared spectroscopy) son 30 yıldır geliştirilmekte olan, puls oksimetre prensibine benzer bir yaklaşımla çalışan bir nörogörüntüleme tekniğidir. Alına yerleştirilen bir prob, bir veri toplama ünitesi ve veri kaydı için bir yazılımdan oluşan bu sistem ile prefrontal korteksteki hemodinamik değişimler an be an gözlemlenebilmektedir. Günümüzde fNIRS teknolojileri kablosuz teknolojiye dönüştürülmektedir. Projenin temel amacı, Nöoroteknoloji Laboratuvarında geliştirilen çok kanallı kablosuz fNIRS sistemiyle beyin hemodinamiklerinin kafa eğme testi aracılığıyla ölçebilmek ve sigara içenlere göre kıyaslamaktır. Bu sayede özellikle beyin damarlarının esnekliği ve kişinin inme riskinin belirlenebileceğini düşünmekteyiz.

3. Projenin Yöntemi:

3.1 Uygulanacak Testler:

Bu proje kapsamında katılımcılara kafa eğme testi uygulanacaktır.

Kafa Eğme Testi: Geliştirilen fNIRS sistemlerinin temel verifikasyonuna dair uygulanan standart testidir. Denek, teste dik bir şekilde oturarak başlar. Denek, deney protokolünce belirlenen süre boyunca (20 sn) dik pozisyonda bekledikten sonra, boynunu sabit tutmak suretiyle öne doğru eğilir.Yine deney protokolünce belirlenen süre boyunca beklendikten sonra (30 sn) dik pozisyona yeniden dönülür ve belirli bir süre (75 sn) bu konumda beklenir. Bu sayede; öne eğilerek kafadaki atar damar kılcallarında kan göllenmesi gerçekleştirilip, geri kalkarak kan akışı düzenlenir. Bu göllenmenin yarattığı basınç artışı ile sağlıklı bireylerde atar damar kılcallarında genişleme gerçekleşir. Söz konusu değişimleri fNIRS sistemleri ile ölçmek mümkündür.

3.2 fNIRS kaydı ve analizi:

fNIRS kaydı için Acıbadem Mehmet Ali Aydınlar Üniversitesi Tıp Mühendisliği Bölümü Nöroteknoloji Laboratuvarında[1] geliştirilen sürekli dalga yakın kızılaltı spektroskopi cihazı kullanılacaktır. İki dalga boyunda (730 nm ve 850 nm) çok düşük enerjili (1 mW) ışık uygulanacaktır. Cihazın 2 adet ışık salan diyotu (light emitting diodes [LED]) ve 6 detektörü vardır ve aynı anda 8 alandan hemodinamik yanıt ölçümü yapılacaktır. Detektörler yakın ve uzak olmak üzere sırasıyla 1,5 ve 3 cm aralıkla yerleştirilecektir. Prob alın bölgesine yerleştirilerek testler sırasında prefrontal korteks bölgesinde oksi [HbO2] ve deoksihemoglobin [HbH] düzeylerindeki değişimler hesaplanacaktır.

4. Katılımcıların Özellikleri:

Projeye 20-35 yaşları arasında erkek ve kadın katılımcılar alınacaktır. Araştırma grubunun 12 sağlıklı kontrol grubu, 12 sigara tüketen olarak toplam 24 kişiden oluşturulması planlanmıştır. Katılımcılar, kardiyovasküler, nörolojik ve psikiyatrik hastalığı olmayan ve ilaç kullanmayan bireyler arasından seçilecektir.

5. Etik açıdan gözetilmesi gereken hususlar ve alınan önlemler:

Uygulanacak yöntemlerin sağlık üzerine olumsuz etki yapma riski yoktur. Çalışmada kullanılacak cihaz tam olarak izolasyonludur, kontrolleri yapılmıştır ve elektriksel açıdan hastane güvenlik standartlarına tamamen uymaktadır.

Katılımcılardan alınacak bilgilendirilmiş onam formları ektedir.

İsim: Prof. Dr. Ata Akın

İmza:

Tarih:

KATILIMCI BİLGİ ve ONAM FORMU

Proje yürütücüsü: Prof. Dr. Ata Akın

Proje başlığı: Geliştirilmiş olan fNIRS sisteminin ölçüm doğruluğunun kanıtlanması.

Proje konusu: fNIRS (functional near infrared spectroscopy) son 20 yıldır geliştirilmekte olan, puls oksimetre prensibine benzer bir yaklaşımla çalışan bir nörogörüntüleme tekniğidir. Alına yerleştirilen bir prob, bir veri toplama ünitesi ve veri kaydı için bir yazılımdan oluşan bu sistem ile prefrontal korteksteki hemodinamik değişimler an be an gözlemlenebilmektedir. Alın yüzeyinden gönderilen yakın kızılaltı rejiminde çalışan ışık, deri, kafatası katmanlarından geçtikten sonra korteks yüzeyindeki kılcal damarlarda kısmen soğurulur. Işığın soğurulmayan kısmı ise tekrar aynı katmanlardan yansır ve gene alın yüzeyindeki fotoalgılayıcı tarafından ölçülür. Projenin temel amacı, geliştirilen kablosuz fNIRS sistemi ile kafa eğme testi sırasında beyin hemodinamik etkinliğinin gözlemlenebilmesidir.

Onay:

Sizleri, Acıbadem Mehmet Ali Aydınlar Üniversitesi'nin yürüttüğü çalışmamıza davet ediyoruz. Bu çalışma ile Acıbadem Mehmet Ali Aydınlar Üniversitesi laboratuvarlarında geliştirilen fNIRS cihazının ölçüm doğruluğunun kanıtlanmasına yardımcı olacaksınız.

Çalışmada yer almayı kabul ettiğiniz takdirde, beyin işlevlerinizi değerlendiren bazı testler gerçekleştirirken fNIRS olarak adlandırılan cihazla alnınıza yerleştirilen bir bant aracılığıyla ölçümler alınacaktır. fNIRS ölçümü için, plastik kaplı küçük ışık kaynakları ve dedektörler bulunan bir malzeme elastik bandajla alın bölgesine tutturulacaktır. Düşük güçlü ışık kaynakları ile alın bölgesine ışık verilecektir. Kullanılacak ışığın parlaklığı çok düşüktür ve herhangi bir zararı yoktur.

Uygulanacak yöntemler, sağlığınız üzerine olumsuz etki yapma riski taşımamaktadır. Çalışmada kullanılan cihaz tam olarak izolasyonludur, kontrolleri yapılmıştır ve elektriksel açıdan hastane güvenlik standartlarına tamamen uymaktadır. Ancak,

herhangi bir sebeple rahatsızlık hissetmeniz halinde çalışmayı yürüten kişilerden birine durumu bildirip prosedürü hemen sonlandırabilirsiniz. Ayrıca çalışmayı yürüten araştırmacılar gerekli gördükleri zaman prosedürü sonlandırma hakkına sahiptirler.

Çalışmaya katılım tamamen isteğe bağlıdır. Herhangi bir ücret talep edilmeyecek ve size herhangi bir ödeme yapılmayacaktır. İsminiz tamamen gizli tutulacaktır. Çalışmaya katılmayı kabul ettiğiniz takdirde çalışmanın herhangi bir aşamasında herhangi bir sebep göstermeden onayınızı çekmek hakkına sahipsiniz.

Bu araştırma sonucunda elde edilen verilerin damar yapınıza dair önemli bilgiler sağlayacağını düşünüyoruz.

Bu formu imzalamadan önce, çalışmayla ilgili sorularınız varsa lütfen sorun. Daha sonra sorunuz olursa, Prof. Dr. Ata Akın'a (Tel: 0216 500 4144) sorabilirsiniz. Araştırmayla ilgili haklarınız konusunda yerel etik kurullarına da danışabilirsiniz.

Bana anlatılanları ve yukarıda yazılanları anladım. Bu formun bir kopyasını aldım.

Çalışmaya katılmayı kabul ediyorum.

Katılımcının adı/soyadı ve imzası Tarih

Araştırmacının adı/soyadı ve imzası

REFERENCES

1. Tuchin VV. Tissue optics: light scattering methods and instruments for medical diagnosis, 2nd ed. Bellingham, WA: SPIE Publications, 2007
2. Wang LV, Wu HI. Biomedical optics: principles and imaging, 1st ed. Hoboken, NJ: Wiley-Interscience, 2007
3. Berezin MY, Achilefu S. Fluorescence lifetime measurements and biological imaging. Chem Rev 2010; 110:2641–2684
4. Wang LV. Photoacoustic imaging and spectroscopy. Boca Raton, FL: CRC, 2009
5. Knappe V, Frank F, Rohde E. Principles of lasers and biophotonic effects. Photomed Laser Surg 2004; 22:411–417
6. https://maxfacts.uk/diagnosis/tests/ultrasound
7. Stuker F, Ripoll J, Rudin M. Fluorescence molecular tomography: principles and potential for pharmaceutical research. Pharmaceutics 2011; 3:229–274
8. Giovanni DL, Rubina MT, Tamar S, Francesco S. Optical imaging of the breast: basic principles and clinical applications. Ameican Journal of Roentgenology; 209, 2017
9. Sokolov K, Follen M, Richards-Kortum R. Optical spectroscopy for detection of neoplasia. Curr Opin Chem Biol 2002; 6:651–658
10. Kukreti S, Cerussi AE, Tanamai W, Hsiang D, Tromberg BJ, Gratton E. Characterization of metabolic differences between benign and malignant tumors: high-spectral-resolution diffuse optical spectroscopy. Radiology 2010; 254:277–284
11. Ramanujam N, Mitchell MF, Mahadevan A, Thomsen S, Silva E, Richards-Kortum R. Fluorescence spectroscopy: a diagnostic tool for cervical intraepithelial neoplasia (CIN). Gynecol Oncol 1994; 52:31–38
12. Richards-Kortum R, Sevick-Muraca E. Quantitative optical spectroscopy for tissue diagnosis. Annu Rev Phys Chem 1996; 47:555–606
13. Tromberg BJ, Pogue BW, Paulsen KD, Yodh AG, Boas DA, Cerussi AE. Assessing the future of diffuse optical imaging technologies for breast cancer management. Med Phys 2008; 35:2443–2451
14. Vishwanath K, Klein D, Chang K, Schroeder T, Dewhirst MW, Ramanujam N. Quantitative optical spectroscopy can identify long-term local tumor control in irradiated murine head and neck xenografts. J Biomed Opt 2009; 14:054051
15. Kukreti S, Cerussi A, Tromberg B, Gratton E. Intrinsic tumor biomarkers revealed by novel double-differential spectroscopic analysis of near-infrared spectra. J Biomed Opt 2007; 12:020509
16. http://bme240.eng.uci.edu/students/10s/nguyenjq/index_files/DOSI_data/Picture1.jpg
17. Moesta KT, Fantini S, Jess H, et al. Contrast features of breast cancer in frequency-domain laser scanning mammography. J Biomed Opt 1998; 3:129–136
18. Ntziachristos V, Ripoll J, Wang LV, Weissleder R. Looking and listening to light: the evolution of whole-body photonic imaging. *Nat Biotechnol* 2005; 23:313–320
19. Maslov K, Stoica G, Wang LV. In vivo dark-field reflection-mode photoacoustic microscopy. *Opt Lett* 2005; 30:625–627
20. Zhang HF, Maslov K, Wang LV. In vivo imaging of subcutaneous structures using functional photoacoustic microscopy. *Nat Protoc* 2007; 2:797–804
21. Li ML, Zhang HE, Maslov K, Stoica G, Wang LV. Improved in vivo photoacoustic microscopy based on a virtual-detector concept. *Opt Lett* 2006; 31:474–476
22. Kim C, Favazza C, Wang LV. In vivo photoacoustic tomography of chemicals: high-resolution functional and molecular optical imaging at new depths. *Chem Rev* 2010; 110:2756–2782
23. Deán-Ben XL, Razansky D. Portable spherical array probe for volumetric real-time optoacoustic imaging at centimeter-scale depths. *Opt Express* 2013; 21:28062–28071

24. Deán-Ben XL, Razansky D. Functional optoacoustic human angiography with handheld video rate three dimensional scanner. *Photoacoustics* 2013; 1:68–73

25. Daoudi K, van den Berg PJ, Rabot O, et al. Handheld probe integrating laser diode and ultrasound transducer array for ultrasound/photoacoustic dual modality imaging. *Opt Express* 2014; 22:26365–26374

26. Liu JM. (2005). Photonic Devices, Cambridge University Press, Cambridge

27. Strangman G, Boas, DA, Sutton JP. (2002). Non-invasive neuroimaging using nearinfrared light. Biol. Psychiatry 52 (7), 679–693.

28. Strangman G, Franceschini MA, Boas DA. (2003). Factors affecting the accuracy of near-infrared spectroscopy concentration calculations for focal changes in oxygenation parameters. Neuroimage 18 (4), 865–879.

29. Jobsis FF. (1977). Non-invasive, infrared monitoring of cerebral and myocardial oxygen sufficiency and circulatory parameters. Science, 198(4323), 1264–1267.

30. Gratton G, Goodman-Wood MR, Fabiani M. (2001). Comparison of neuronal and hemodynamic measures of the brain response to visual stimulation: An optical imaging study. Human Brain Mapping, 13(1), 13–25.

31. Fox PT, Raichle ME, Mintun MA, Dence C. (1988). Nonoxidative glucose consumption during focal physiologic neural activity. Science, 241(4864), 462–464.

32. Chance B, Zhuang Z, Unah, C, Alter C, Lipton L. (1993). Cognition-activated lowfrequency modulation of light absorption in human brain. Proceedings of the National Academy of Science USA, 90(8), 3770–3774.

33. Villringer A, Chance, B. (1997). Non-invasive optical spectroscopy and imaging of human brain function. Trends in Neurosciences, 20(10), 435–442.

34. Kobayashi H, Ogawa M, Alford R, Choyke PL, Urano Y. New Strategies for Fluorescent Probe Design in Medical Diagnostic Imaging. *Chem. Rev*. 2010, *110*, 2620–2640.

35. Gratton G, Maier JS, Fabiani M, Mantulin WW, Gratton E. (1994). Feasibility of intracranial near-infrared optical scanning. Psychophysiology, 31(2), 211–215.

36. http://www.frontiersin.org/files/Articles/124008/fnhum-09-00003-g002.jpg

37. Cope M. (1991). The development of a near-infrared spectroscopy system and its application for non-invasive monitoring of cerebral blood and tissue oxygenation in the newborn infant. London: University College London.

38. Cope M, Delpy DT. (1988). System for long-term measurement of cerebral blood and tissue oxygenation on newborn infants by near infra-red transillumination. Medical & Biological Engineering & Computing, 26(3), 289–294.

39. http://www.artinis.com/octamon

40. Chance B, Leigh JS, Miyake H, Smith DS, Nioka S, Greenfeld R, et al. (1988). Comparison of time-resolved and -unresolved measurements of deoxyhemoglobin in brain. Proceedings of the National Academy of Science USA, 85(14), 4971–4975.

41. Tamura, M, Hoshi Y, Hazeki O, Okada F. (1997). Cerebral oxygenation states as revealed by near-infrared spectrophotometry. Advances in Experimental Medicine & Biology, 413, 91–96.

42. Firbank M, Okada E, Delpy DT. (1998). A theoretical study of the signal contribution of regions of the adult head to near-infrared spectroscopy studies of visual evoked responses. Neuroimage, 8(1), 69–78.

43. Izzetoglu K, Bunce SB. O., Pourrezaei, K., & Chance, B. (2004). Functional optical brain imaging using NIR during cognitive tasks [special issue]. International Journal of Human – Computer Interaction, 17, 211–227.

44. Crowe JH, Rea PA, Wickramasinghe Y, Rolfe P. (1984). Towards non-invasive optical monitoring of cerebral metabolism. Paper presented at the Proceedings of the International Conference on Fetal and Neonatal Physiology, Meas, Oxford, UK.

45. Gurfinkel M, Ke S, Wen X, Li C, Sevick-Muraca EM. (2003). Near-infrared fluorescence optical imaging and tomography. Disease Markers, 19(2–3), 107–121.

46. Hawrysz DJ, Sevick-Muraca EM. (2000). Developments toward diagnostic breast cancer imaging using near-infrared optical measurements and fluorescent contrast agents. Neoplasia, 2(5), 388–417.

47. Madsen PL, Nielsen HB, Christiansen P. (2000). Well-being and cerebral oxygen saturation during acute heart failure in humans. Clinical Physiology, 20(2), 158–164.

48. Obrig H, Villringer A. (1997). Near-infrared spectroscopy in functional activation studies. Can NIRS demonstrate cortical activation? Advances in Experimental Medicine and Biology, 413, 113–127

49. Zabel TA, Chute DL. (2002). Educational neuroimaging: a proposed neuropsychological application of near-infrared spectroscopy (nIRS). Journal of Head Trauma Rehabilitation, 17(5), 477–488.

50. Chute DL. (2002). Neuropsychological technologies in rehabilitation. Journal of Head Trauma Rehabilitation, 17(5), 369–377.

51. Gore J. (2003). Out of the shadows—MRI and the Nobel Prize. New England Journal of Medicine, 349(24), 2290–2292.

52. Pauling L. (1977). Magnetic properties and structure of oxyhemoglobin. Proceedings of the National Academy of Science USA, 74(7), 2612–2613.

53. Ashburner J, Friston KJ. (1999). Nonlinear spatial normalization using basis functions. Human Brain Mapping, 7(4), 254–266.

54. Ashburner J, Friston KJ. (2005). Unified segmentation. Neuroimage, 26(3), 839–851.

55. Izzetoglu M, Devaraj A, Bunce S, Onaral B. (2005). Motion artifact cancellation in NIR spectroscopy using Wiener filtering. IEEE Transactions on Biomedical Engineering, 52(5), 934–938.

56. http://www.artinis.com/nirs-eeg-package/

57. Obrig H, Wenzel R, Kohl M, Horst S, Wobst P, Steinbrink J, et al. (2000). Near-infrared spectroscopy: Does it function in functional activation studies of the adult brain? International Journal of Psychophysiology, 35(2–3), 125–142.

58. Toronov V, Webb A, Choi JH, Wolf M, Michalos A, Gratton E, Hueber D. (2001). Investigation of human brain hemodynamics by simultaneous near-infrared spectroscopy and functional magnetic resonance imaging. Medical Physics, 28, 521–527.

59. Kato H, Izumiyama M, Koizumi H, Takahashi A, Itoyama Y. (2002). Near-infrared spectroscopic topography as a tool to monitor motor reorganization after hemiparetic stroke: A comparison with functional MRI. Stroke, 33(8), 2032–2036.

60. Murata Y, Sakatani K, Katayama Y, Fukaya C. (2002). Increase in focal concentration of deoxyhaemoglobin during neuronal activity in cerebral ischaemic patients. Journal of Neurology, Neurosurgery, and Psychiatry, 73(2), 182–184.

61. Mehagnoul-Schipper DJ, van der Kallen BF, Colier WN, van der Sluijs MC, van Erning LJ, Thijssen HO, et al. (2002). Simultaneous measurements of cerebral oxygenation changes during brain activation by near-infrared spectroscopy and functional magnetic resonance imaging in healthy young and elderly subjects. Human Brain Mapping, 16(1), 14–23.

62. Wobst P, Wenzel R, Kohl M, Obrig H, Villringer A. (2001). Linear aspects of changes in deoxygenated hemoglobin concentration and cytochrome oxidase oxidation during brain activation. Neuroimage, 13(3), 520–530.

63. Huppert TJ, Hoge RD, Diamond SG, Franceschini MA, Boas DA. (2006). A temporal comparison of BOLD, ASL, and NIRS hemodynamic responses to motor stimuli in adult humans. Neuroimage, 29, 368–382.

64. Schroeter ML, Kupka T, Mildner T, Uludag K, von Cramon DY. (2006). Investigating the post-stimulus undershoot of the BOLD signal: A simultaneous fMRI and fNIRS study. Neuroimage, 30, 349–358.

65. Plichta MM, Herrmann MJ, Ehlis AC, Baehne CG, Richter MM, Fallgatter AJ. (2006). Event-related visual versus blocked motor task: Detection of specific cortical activation patterns with functional near-infrared spectroscopy. Neuropsychobiology, 53, 77–82.

66. MacIntosh BJ, Klassen LM, Menon RS. (2003). Transient hemodynamics during a breath hold challenge in a two part functional imaging study with simultaneous nearinfrared spectroscopy in adult humans. Neuroimage, 20, 1246–1252.

67. Fonteyn L, Irani F, Ayaz HK I, Myers TE, Patel S, Chance B, et al. (2006). Neural correlates of self–other processing: A functional near infrared spectroscopy (fNIRS) study. Manuscript submitted for publication.

68. Platek S, Fonteyn L, Myers TE K I, Ayaz H, Li C, Chance B. (2005). Functional near infrared spectroscopy (fNIRS) reveals differences in self–other processing as a function of schizotypal personality traits. Schizophrenia Research, 73(1), 125–127.

69. Platek SM, Keenan JP, Gallup GG Jr, Mohamed FB. (2004). Where am I? The neurological correlates of self and other. Brain Research: Cognitive Brain Research, 19(2), 114–122.

70. Okamoto M, Dan H, Shimizu K, Takeo K, Amita T, Oda I, et al. (2004). Multimodal assessment of cortical activation during apple peeling by NIRS and fMRI. Neuroimage, 21(4), 1275–1288.

71. Platek S, Loughead J, Gur R, Busch S, Ruparel K, Phend N, et al. (2006). Neural substrates for functionally discriminating self-face from personally familiar faces. Human Brain Mapping, 27(2), 91–98.

72. Andrews, R. (2001). Monitoring for neuroprotection: New technologies for the new millennium. Annals of the New York Academy of Sciences, 939, 101–113.

73. Gopinath SP, Robertson CS, Grossman RG, Chance B. (1993). Near-infrared spectroscopic localization of intracranial hematomas. Journal of Neurosurgery, 79(1), 43–47.

74. Brawanski A, Faltermeier R, Rothoerl RD, Woertgen, C. (2002). Comparison of near-infrared spectroscopy and tissue p(O2) time series in patients after severe head injury and aneurysmal subarachnoid hemorrhage. Journal of Cerebral Blood Flow and Metabolism, 22(5), 605–611.

75. Kampfl A, Pfausler B, Denchev D, Jaring HP, Schmutzhard E. (1997). Near infrared spectroscopy (NIRS) in patients with severe brain injury and elevated intracranial pressure. A pilot study. Acta Neurochirurgica Supplement (Wein), 70, 112–114.

76. Adelson PD, Nemoto E, Colak A, Painter M. (1998). The use of near infrared spectroscopy (NIRS) in children after traumatic brain injury: A preliminary report. Acta Neurochirurgica Supplement (Wein), 71, 250–254.

77. Lewis SB, Myburgh JA, Thornton EL, Reilly PL. (1996). Cerebral oxygenation monitoring by near-infrared spectroscopy is not clinically useful in patients with severe closed-head injury: A comparison with jugular venous bulb oximetry. Critical Care Medicine, 24(8), 1334–1338.

78. Ter Minassian A, Poirier N, Pierrot M, Menei P, Granry JC, Ursino M, et al. (1999). Correlation between cerebral oxygen saturation measured by near-infrared spectroscopy and jugular oxygen saturation in patients with severe closed head injury. Anesthesiology, 91(4), 985–990.

79. Watanabe E, Maki A, Kawaguchi F, Yamashita Y, Koizumi H, Mayanagi Y. (2000). Non-invasive cerebral blood volume measurement during seizures using multichannel near infrared spectroscopic topography. Journal of Biomedical Optics, 5(3), 287–290.

80. Watanabe E, Nagahori Y, Mayanagi Y. (2002). Focus diagnosis of epilepsy using nearinfrared spectroscopy. Epilepsia, 43(Suppl. 9), 50–55.

81. Villringer A, Planck J, Stodieck S, Botzel K, Schleinkofer L, Dirnagl U. (1994). Noninvasive assessment of cerebral hemodynamics and tissue oxygenation during activation of brain cell function in human adults using near infrared spectroscopy. Advances in Experimental Medicine and Biology, 345, 559–565.

82. Sokol DK, Markand ON, Daly EC, Luerssen TG, Malkoff MD. (2000). Near infrared spectroscopy (NIRS) distinguishes seizure types. Seizure, 9(5), 323–327.

83. Steinhoff BJ, Herrendorf G, Kurth C. (1996). Ictal near infrared spectroscopy in temporal lobe epilepsy: A pilot study. Seizure, 5(2), 97–101.

84. Hock C, Villringer K, Muller-Spahn F, Hofmann M, Schuh-Hofer S, Heekeren H, et al. (1996). Near infrared spectroscopy in the diagnosis of Alzheimer's disease. Annals of the New York Academy of Sciences, 777, 22–29.

85. Fallgatter AJ, Roesler M, Sitzmann L, Heidrich A, Mueller TJ, Strik WK. (1997). Loss of functional hemispheric asymmetry in Alzheimer's dementia assessed with near-infrared spectroscopy. Brain Research: Cognitive Brain Research, 6(1), 67–72.

86. Murata Y, Katayama Y, Oshima H, Kawamata T, Yamamoto T, Sakatani K, et al. (2000). Changes in cerebral blood oxygenation induced by deep brain stimulation: Study by near-infrared spectroscopy (NIRS). The Keio Journal of Medicine, 49(Suppl. 1), A61–63.

87. Sakatani K, Katayama Y, Yamamoto T, Suzuki S. (1999). Changes in cerebral blood oxygenation of the frontal lobe induced by direct electrical stimulation of thalamus and globus pallidus: A near infrared spectroscopy study. Journal of Neurology, Neurosurgery and Psychiatry, 67(6), 769–773.

88. Okada F, Tokumitsu Y, Hoshi Y, Tamura M. (1994). Impaired interhemispheric integration in brain oxygenation and hemodynamics in schizophrenia. European Archives of Psychiatry and Clinical Neuroscience, 244(1), 17–25.

89. Fallgatter AJ, Strik, WK. (2000). Reduced frontal functional asymmetry in schizophrenia during a cued continuous performance test assessed with near-infrared spectroscopy. Schizophrenia Bulletin, 26(4), 913–919.

90. Shinba T, Nagano M, Kariya N, Ogawa K, Shinozaki T, Shimosato S, et al. (2004). Near-infrared spectroscopy analysis of frontal lobe dysfunction in schizophrenia. Biological Psychiatry, 55(2), 154–164.

91. Kubota Y, Toichi M, Shimizu M, Mason RA, Coconcea CM, Findling RL, et al. (2005). Prefrontal activation during verbal fluency tests in schizophrenia—a near-infrared spectroscopy (NIRS) study. Schizophrenia Research, 77(1), 65–73.

92. Okada F, Takahashi N, Tokumitsu Y. (1996). Dominance of the 'nondominant' hemisphere in depression. Journal of Affective Disorders, 37(1), 13–21.

93. Matsuo K, Kato T, Fukuda M, Kato N. (2000). Alteration of hemoglobin oxygenation in the frontal region in elderly depressed patients as measured by near-infrared spectroscopy. Journal of Neuropsychiatry and Clinical Neurosciences, 12(4), 465–471.

94. Matsuo K, Kato N, Kato T. (2002). Decreased cerebral haemodynamic response to cognitive and physiological tasks in mood disorders as shown by near-infrared spectroscopy. Psychological Medicine, 32(6), 1029–1037.

95. Eschweiler GW, Wegerer C, Schlotter W, Spandl C, Stevens A, Bartels M, et al. (2000). Left prefrontal activation predicts therapeutic effects of repetitive transcranial magnetic stimulation (rTMS) in major depression. Psychiatry Research, 99(3), 161–172.

96. Akiyoshi J, Hieda K, Aoki Y, Nagayama H. (2003). Frontal brain hypoactivity as a biological substrate of anxiety in patients with panic disorders. Neuropsychobiology, 47(3), 165–170.

97. Matsuo K, Kato T, Taneichi K, Matsumoto A, Ohtani T, Hamamoto T, et al. (2003). Activation of the prefrontal cortex to trauma-related stimuli measured by near-infrared spectroscopy in posttraumatic stress disorder due to terrorism. Psychophysiology, 40(4), 492–500.

98. Wolpaw JR, Birbaumer N, McFarland DJ, Pfurtscheller G, Vaughan TM. (2002). Brain-computer interfaces for communication and control. Clin. Neurophysiol. 113, 767–791.

99. https://static1.squarespace.com/static/54ddd9b0e4b0e11f3685f546/t/5979e369a803bb7c43cf819b/1501160299464/OctaMon+Leaflet.pdf

100. https://www.biopac.com/wp-content/uploads/fNIR-Systems.pdf

101. https://www.biopac.com/product/wireless-fnir-optical-brain-imaging-system

102. http://www.hamamatsu.com/resources/pdf/sys/e_niro200nx.pdf?_ga=2.45001315.694672929.1520936551-835045610.1511986497&_gac=1.258799992.1520936551.Cj0KCQjw7Z3VBRC-ARIsAEQifZTxNCtPfLJLPtY-c5nVrZr-vG3ryl3omLQUBEEiDASPtA7B_TlvMHAaAuAPEALw_wcB

103. https://www.hamamatsu-news.de/issues/hamamatsu_news_01_2016/files/assets/basic-html/page42.html

104. http://www.hitachi.com/businesses/healthcare/products-support/opt/etg4000/contents2.html

105. http://www.hitachi.com/businesses/healthcare/products-support/opt/etg4000/index.html

106. http://www.medicalexpo.com/prod/hitachi-medical-systems-europe/product-70725-435711.html

107. Yöner SI, Ertaş G (2016) Development of a microcontroller controlled transistor based current source for pulse oximeter devices. Biomedical Engineering Meeting (BIYOMUT), 2016 20th National

108. http://www.analog.com/media/en/technical-documentation/data-sheets/AD5241_5242.pdf

109. https://www.olimex.com/Products/Components/RF/BLUETOOTH-SERIAL-HC-06/resources/hc06.pdf

110. http://akizukidenshi.com/download/pic16f1827.pdf

111. http://www.ti.com/lit/ds/symlink/opt101.pdf

112. Becker CG, Hajjar DP, Hefton JM. Tobacco constituents are mitogenic for arterial smooth-muscle cells 1985 Jul; 120(1): 1–5.

113. Gerzanich V, Zhang F, West GA, Simard JM. Chronic nicotine alters NO signaling of Ca2+ channels in cerebral arterioles. Circ Res 2001; 88: 359-65.

114. Zhang, J. Y., Cao, Y. X., Xu, C. B., and Edvinsson, L. (2006). Lipid-soluble smoke particles damage endothelial cells and reduce endothelium-dependent dilatation in rat and man. BMC Cardiovasc. Disord. 6, 3.

115. Guo X, Oldham MJ, Kleinman M, Phalen RF, Kassab GS. Effect of Cigarette Smoking on Nitric Oxide, Structural and Mechanical Properties of Mouse Arteries. Am J Physiol Heart Circ Physiol 2006; 291: H2354-61.

116. Panerai RB. Assessment of cerebral pressure autoregulation in humans-a review of measurement methods. Physiol Meas. 1998 Aug;19(3):305-38.

117. Greenfield J C, Rembert J C and Tindall G T 1984 Transient changes in cerebral vascular resistance during the Valsalva maneuver in man *Stroke* **15** 76–9 [24].

118. Edlow BL, Kim MN, Durduran T, Zhou C, Putt ME, Yodh AG, Greenberg JH, Detre JA. The effects of healthy aging on cerebral hemodynamic responses to posture change Physol Meas. 2010 Apr;31(4):477-95.